ALMA MATER STUDIORUM - UNIVERSITY OF BOLOGNA

FACULTY OF ENGINEERING

INTERNATIONAL MASTER COURSE IN CIVIL ENGINEERING

D I C A M

Civil, Environmental and Materials Engineering

THESIS IN

Advanced Design of Structures

TIME-DEPENDENT BEHAVIOUR OF REINFORCED CONCRETE SLABS

CANDIDATE   **SUPERVISOR**

Stefano De Vittorio   **Chiar.mo Prof. Marco Savoia**

                                                Chiar.mo Prof Gianluca Ranzi

                                                COSUPERVISOR

                                                Chiar.mo Prof. Claudio Mazzotti

Academic Year 2010 – 2011
Session III

THE UNIVERSITY OF SYDNEY

FACULTY OF ENGINEERING

MASTER DEGREE IN CIVIL ENGINEERING

School of Civil Engineering

EXCHANGE STUDENT PROGRAM

TIME-DEPENDENT BEHAVIOUR OF REINFORCED CONCRETE SLABS

CANDIDATE   **SUPERVISOR**

Stefano De Vittorio   **Chiar.mo Prof. Marco Savoia**

Chiar.mo Prof Gianluca Ranzi

COSUPERVISOR

Chiar.mo Prof. Claudio Mazzotti

Academic Year 2010 – 2011

To my parents…

Abstract

In this thesis is studied the long-term behaviour of steel reinforced slabs paying particular attention to the effects due to shrinkage and creep. Despite the universal popularity of using this kind of slabs for simply construction floors, the major world codes focus their attention in a design based on the ultimate limit state, restraining the exercise limit state to a simply verification after the design. For Australia, on the contrary, this is not true. In fact, since this country is not subjected to seismic effects, the main concern is related to the long-term behaviour of the structure.

Even if there are a lot of studies about long-term effects of shrinkage and creep, up to date, there are not so many studies concerning the behaviour of slabs with a cracked cross section and how shrinkage and creep influence it. For this reason, a series of ten full scale reinforced slabs was prepared and monitored under laboratory conditions to investigate this behaviour. A wide range of situations is studied in order to cover as many cases as possible, as for example the use of a fog room able to reproduce an environment of 100% humidity.

The results show how there is a huge difference in terms of deflections between the case of slabs which are subjected to both shrinkage and creep effects soon after the partial cracking of the cross section, and the case of slabs which have already experienced shrinkage effects for several weeks, when the section has not still cracked, and creep effects only after the cracking.

Table of Contents

Chapter 1

Introduction

"Engineering is a great profession. There is the satisfaction of watching a figment of the imagination emerge through the aid of science to a plan on paper. Then it moves to realisation in stone or metal or energy. Then it brings homes to men or women. Then it elevates the standard of living and adds to the comforts of life. This is the engineer's high privilege."
  [Herbert Hoover]

1.1   Background

The construction techniques and the materials used for building are constantly improving in the last years, but concrete and steel remain the two main ingredients to build any kind of civil construction. They are the best ones, up to now, to provide, respectively, the required resistance in compression and in tension.

A structure is usually designed based on the ultimate limit state requirements given by the national building code of practice. These requirements are relative to the strength of the structure, i.e. the ability of the structure to carry the design ultimate loads without collapsing. But these are not the unique requirements that a structure must satisfy. There are also the so called serviceability limit states. Serviceability requirements refer to the behaviour of structures at working loads and they are satisfied when the structure does not deflect or crack more than certain limits provided by the building codes. Both cracking and deflection are primarily dependent on the properties and behaviour of the concrete, but are more difficult to predict because of the non-linear, inelastic and time-dependent nature of the concrete. In this thesis, the attention is focused on the serviceability issues related to the time-dependency nature of concrete and thus on shrinkage and creep effects and their fundamental role in the design procedure. In this view, the long-term effects of the materials composing the structure become a critical factor which must be taken into account in the design procedure.

The aim of the serviceability limit state is to provide an indication about the admissible deflection that a concrete structure can support over a period of time. Design a structure which complies with these limits is a considerable challenge for a structural engineer, since the properties of concrete, without any doubt the most common construction material in the world, are not predictable with certainty. The uncertainties related to the long-term behaviour of concrete are mostly related to its propensity to crack under tensile stresses and to the predictability of time-dependent properties that characterize it. Gilbert (1), in one of his numerous publications regarding the topic, refers that the serviceability failure of a structure in Australia is quite common, even if most of these structures satisfy the requirements provided by the relevant code of practice.

Nowadays concrete structures are becoming always more elaborated, due to the higher architectonical complexity and due to the developed construction

techniques involved. Always more often, a structure is a combination of conventional reinforced concrete, post tensioning or composite member and so on. In this view, appears evident the necessity to have a better understanding of the main concrete properties and their influence on the general behaviour. This is extremely valid for time-dependent comportment. As a matter of facts, creep and shrinkage, the time-dependent characteristics of concrete, are really uncertainty to quantify. Always Gilbert (1) believes that shrinkage is the most problematic factor to be determined. In addition, in this project, the presence of a cracked cross section should not be forgotten, because it influence decisively all the other factors.

How creep and shrinkage develop in time is quite difficult to be predicted and quantified, since they verify as rather chaotic event. Usually shrinkage of concrete is mainly caused by the evaporation of moisture from the concrete to the outside environment (drying shrinkage); the consequence is a reduction of the concrete volume if there are no restrains, or, in presence of it, the consequence will be a change in the build-up of stresses. Creep starts only after the application of a load on the specimen, and thus, many times, the main difficulty is to differentiate it from the shrinkage component, since experimental measurements take into consideration both of them together.

Several parameters influence the development of creep and shrinkage. Just to name a few of them, let's consider the specimen condition of exposure and the environmental conditions themselves (e.g. temperature and relative humidity). For example, the sealing condition of the sample can strongly influence how long-term effects develop. Usually building codes, as the Australian Standards (2) or the Eurocode (3), do not take into consideration this, and therefore, the actual results can be significantly different from the theoretical ones.

In this test, in addition to long-term effects, there are some more uncertainties in the general behaviour related to the presence of a cross section partially cracked. As this study will demonstrate, the final deflection is considerably affected by these openings.

This thesis presents an original study on the behaviour of reinforced slabs under service loading conditions. The project involved the preparation of a series of full scale reinforced slabs and the fundamental factors affecting the long-term behaviour of these structures were identified and studied. The results have shown

that shrinkage and creep are the main factors affecting the long-term behaviour of such structures and that the cracked cross section plays a fundamental role in the final deflection value.

1.2   Aims and objectives

The main task of this project is to investigate the time-dependent comportment of reinforced concrete slabs. Particular attention is paid to understand how creep and shrinkage behave and develop in the case of a partially cracked cross section. The aim is to improve the serviceability design of these reinforced concrete slabs.

Furthermore a theoretical model is developed to account for the concrete time-dependent behaviour when dealing with building floors. The adequacy of the proposed model for the long-term prediction of reinforced concrete slabs must be evaluated as additional aim of the project. To finalize this objective, a numerical comparison is developed with a previous test on composite post-tensioned slab.

The role that a crack has in regard to creep and shrinkage is one of the key points that this test wants to investigate. The crack modifies the tensile concrete reacting part and consequently it modifies the distribution of stresses between steel and concrete. In addition, different values of loads are used to investigate more deeply which is the contribution of creep and how it influences the overall comportment. Furthermore, regarding shrinkage, part of the slabs prepared are stored in a "fog room", a constant 100% relative humidity room, to avoid that shrinkage start before than creep. For these samples, the long-term effects develop simultaneously starting from the cracking operation day.

Since the analytical models provided by the standards for the calculation of creep and shrinkage can be misleading and since they differ quite a lot from the actual case studied, this projects is based on experimental measures of these two effects. It is a quite time-consuming work, but it allows for the use of exact parameters, the best ones that can fit the problem. In addition, in this way, it can be obtained some laboratory controlled data to calibrate, validate and extent analytical models that are being developed concurrently with the experimental program.

In order to achieve these objectives, the work has been subdivided into a number of discrete tasks which are summarized as follow:

8

Six fully-supported slab specimens with two different reinforcement layouts were casted, cured for a period of 8 days and then monitored, through the use prismatic and cylindrical samples subjected to the same environmental condition, for a period of about 60 days to measure the effects of drying shrinkage.

Four fully supported slab specimens with a single reinforcement layout were casted and stored in a "fog room", to avoid shrinkage effects. Also in this case a monitoring process was held with the use of prismatic and cylindrical samples for a period of about 60 days.

After this initial period all the ten specimens were partially cracked and then subjected to three different load conditions. The effects of varying the quantity of reinforcing steel, the bar spacing and the load conditions were studied.

Two analytical models were developed and used to study the creep and shrinkage effects. In addition, these models were also validated through the comparison with a previous experimental test performed some time before in the same University of Sydney.

A series of test were also conducted to obtain the creep and shrinkage characteristics of the concrete, and other properties such as compressive strength, tensile strength and elastic modulus, to provide accurate data for analyzing the specimens

1.3   Layout of the thesis

The thesis is structured in seven chapters and three appendices. An Introduction and the literature review of previous work published in the open literature is presented in Chapter 1. The fundamental concepts related to the time-dependent behaviour of the concrete are outlined in Chapter 2. This is followed, in Chapter 3, by the description of the theoretical model able to predict the time-dependent behaviour of the reinforced concrete and composite steel-concrete members. In addition, this chapter presents how to calculate the deflections at the mid span once the curvature is known at the two supports and at the mid span of a simply-supported slab. The ability of the proposed theoretical approach to predict the long-term response of composite post-tensioned slabs is outlined in Chapter 4 using experimental results recently collected at the University of Sydney. Chapter 5 presents the complete experimental program. It explains in detail the description of the specimen, the experimental procedure and the instrumentation used. It also contains the design

procedure adopted to decide the dimension of the load blocks used in the sustained load phase. Chapter 6 contains the experimental test results and a brief discussion on what obtained. More in detail, a comparison between experimental and numerical results is held in order to determine how much they differ among them. Finally, Chapter 7 presents the conclusions and gives general recommendations regarding the serviceability design of steel reinforced concrete slabs.

APPENDIX A contains more detailed and complete drawings related to the test. APPENDIX B contains a detailed explanation of the procedure used for the installation of the strain gauges on the steel bars. In the end, in APPENDIX C, there are some photos regarding the test.

1.4   Literature review

1.4.1   Introduction

The comportment of structures at service load is a fundamental design consideration. If a slab system is designed according to the strength requirements, the degree of safety against collapse may be adequate, but the performance at service loads may be not. For this reason, the design procedure should follow three main concepts and satisfy them: strength at overloads, deflections at service loads and crack widths at service loads. The aim of designing must be to ensure an adequate margin of safety against collapse and against the possibility that the structure becomes unsatisfactory for use at service loads.

The Eurocode (3) and the ACI Code (4) emphasize a design based on the ultimate limit state (strength) with additional checks on the exercise limit state. Deflections are controlled imposing a maximum admissible limit value, or alternatively, specifying a minimum allowable slab thickness in order to ensure an adequate stiffness. Regarding cracking in one-way slabs, the design should be revised in the case of reinforcement yield strength larger than 300 N/mm^2.

1.4.2   Deflections

The deflection prediction is a challenge in case of reinforced concrete structures and it is even more problematic for slabs. Two main problems are related to this prediction. The first is to find a function able to describe the deflection, as the familiar $\delta = wl^4/384EI$ used for prismatic beam of span l

with fixed ends carrying a uniform load per unit length w. The second is to determinate the appropriate flexural rigidity EI to use in the deflection function, once it has been found.

The elastic theory analysis of a slab is quite complicated, but the availability in the last ten years of always more powerful computers and softwares based on finite element analysis is easing the problem to some extent. Considering also that the deflection functions have been calculated and tabulated for many cases, the more serious problem is nowadays related to the calculation of the flexural rigidity EI. The determination of this quantity is more difficult for a slab than a beam, largely because the reinforcement ratios in slabs are usually quite slow, due to relative low bending moment. Quite often the reinforcement ratio is governed by maximum bar spacing or minimum steel area requirements. A direct consequence of the low steel ratios is a large value of the ratio between uncracked and cracked flexural rigidity EI_g / EI_{cr}; thus also cracking amount has an influence on the deflection.

Assuming, as it is in reality, a spreading of cracking with time, the long-term deflections may be larger than the initial ones. According to the ACI Code (4), if there is no compression steel, the total long-term deflection is 3 times the initial deflection. But a series of experimental tests demonstrates that this provision may be unsafe in some cases. For example, Taylor and Heiman (5) (6) reported long-term experimental results on flat slabs which, after 2.3 years from loading, the time-dependent deflections were about 6.5-7.5 greater than the initial ones.

It is also challenging to define acceptable deflections. The last ones depend on the use of the structure and the nature of the other components, structural and no structural, of the building. Excessive deflections interfere with the function of some non-structural components. For example, if the floor deflects too much, rigid masonry walls may crack and doors and windows may no longer fit properly.

Blakey (7) studied the deflection of flat plate structures and suggested that if cracking of masonry partitions is to be avoided, initial deflections may have to be limited to about span/1500. In addition, he suggested that the minimum plate thickness should be span/32, using, as reference span, the long-span center to center of columns.

As it seems from the previous discussion, cracking is a fundamental factor for

long-term excessive deflection. Thus it is important to reduce it as much as possible. Shrinkage strain is sometimes also responsible for cracking after the completion of the slab. In turn, shrinkage is restrained by the reinforcement in the concrete and also by other elements in the structure such as beams, columns and walls. The tensile stress caused by the restraint of the shrinkage strains, combined with the stresses caused by loads, may produce some cracks at a lower load level than otherwise expected. For this reason, any measure that reduces the shrinkage is a benefit in maintaining deflections as lower as possible.

1.4.2.1 Computation of deflections

A common deflection expression is expressed in the form

$$\delta = C \frac{wl_1^4}{D} = C_1 \frac{wl_1^4}{Eh^3} \tag{1.1}$$

where w is the uniformly distributed load per unit area; C and C_1 are constants depending on the panel shape, support conditions, and Poisson's ratio; l_1 the long span, either as clear span, center-to-center span or some average span; $D = Eh^3 / \left[12\left(1 - \mu^2\right)\right]$, the slab stiffness per unit width; E the Young's modulus; and h the slab thickness. For the same reasons mentioned above, there are significant difficulties in determining the values of C and C_1 for the uncertainty related to the realistic support conditions, and in determining the effective value of D when time-dependent effects and cracking must be taken into account.

The most comprehensive studies of deflections of reinforced concrete slabs structures available are those by Vanderbilt et al, (8) and (9), Chang and Hwang, (10) and (11), and Jofriet (12).

The work done by Vanderbilt and Chang and Hwang is directed to the general problem of slabs with and without beams, while Jofriet's concerns flat plate structures that may have spandrel beams. All considered both the effects of cracking and the elastic theory analysis for deflections. The elastic theory deflection values are considered first.

Vanderbilt's work can be summarized as an extensive table of elastic deflection coefficients, the ones reported as C in equation (1.1), for typical interior panels supported on square columns considering the beam relative

stiffnesses, support size and panel shape. Chang and Hwang (10) analysed a group of slabs similar to the Vanderbilt's ones, but using the finite element method. The deflection results match quite perfectly for similar slabs. In a second moment, they extend the formulation to take into account cracking and the different restraint conditions existing in the ends span and successively they altered it to account for creep effects. Their formulation for short-term deflection is

$$\delta_s = K_a K_b K_c \frac{w l_{n1}^4}{D} \tag{1.2}$$

where K_a is the elastic deflection coefficient, K_b the coefficient accounting for the state of cracking, K_c the coefficient accounting for reduced restraint in an end span, and l_{n1} the clear span in the long-span direction. Each of the K values derives from a semi empirical formulation. To take into consideration long-term deflections, the applied load w is substituted by $(w_v + i w_s)$, where w_v is the variable part of the load that is assumed to cause no creep, w_s the sustained load consisting of the self-weight plus the sustained part of the live load, and $i = 1 + \lambda$, where λ is a creep multiplier.

According to Jofriet's research (12), the mid span deflection of a typical interior panel of a beamless slab is

$$\delta_{\max}^i = C_i \frac{w l_l^4}{E h^3} \tag{1.3}$$

where C_i is a coefficient depending on the support shape and panel shape, E the concrete modulus of elasticity, h the slab thickness, w the uniformly distributed load per unit area, and l_l a weighted average of the long clear span l_n and the long center-to-center span l, where

$$l_l = \frac{l + 3 l_n}{4} \tag{1.4}$$

$$C_i = 0.0285 + 0.0375 \left(\frac{l_s}{l_l} \right)^3 \tag{1.5}$$

The short-span l_s is also a weighted average. The results obtained through these equations do not match exactly with the Vanderbilt's ones, but they are

sufficiently close. This is due to the fact that the results were obtained from a study of deflection computed by finite element and other solution of slabs.

Elastic deflection coefficients for additional cases are given by Timoshenko and WoinoWsky-Krieger (13) and by Brotchie and Wynn (14).

Regarding the choice of the flexural rigidity, Vanderbilt et al (8) (9) suggested two empirical approaches. In the case of low loads, up to the one causing the initial mid span cracks, deflections should be computed with the gross flexural rigidity EI. For higher values of load, the suggestion is to use the fully cracked section value EI_{cr}. In addition, for intermediate loads, two different transitions were suggested to compute deflection. These transitions are based on the observed load-deflection curves. Jofriet (12), instead, suggested a simple equation providing a reduction in stiffness as the moment exceeded the cracking moments.

Chapter 2

Time-dependent behaviour of concrete

"Research is what I'm doing when I don't know what I'm doing."
[Wernher von Braun]

2.1   Overview

When a concrete member is subjected to a sustained applied load it undergoes an instantaneous deformation at the time of loading followed by a time-dependent one over time. In most of the cases, the time-dependent component is greater than the instantaneous one. This behaviour of the concrete should be considered in the checks related to serviceability limit state. Under the hypothesis of constant stress and temperature, the time-dependent response is due to the creep and the shrinkage of the concrete.

The total strain developed by concrete over time can be defined as the sum of an instantaneous strain, a creep strain, a shrinkage strain and a temperature strain. Assuming a constant temperature, the total strain results:

$$\varepsilon(t) = \varepsilon_e(t) + \varepsilon_{cr}(t) + \varepsilon_{sh}(t) \tag{2.1}$$

As represented in Figure 2.1, the shrinkage component does not depend on the load history, while, the other two depend on the applied stress. Shrinkage starts soon after the concrete has been poured, as the latter begins to harden, while creep occurs when the concrete is subjected to an sustained load.
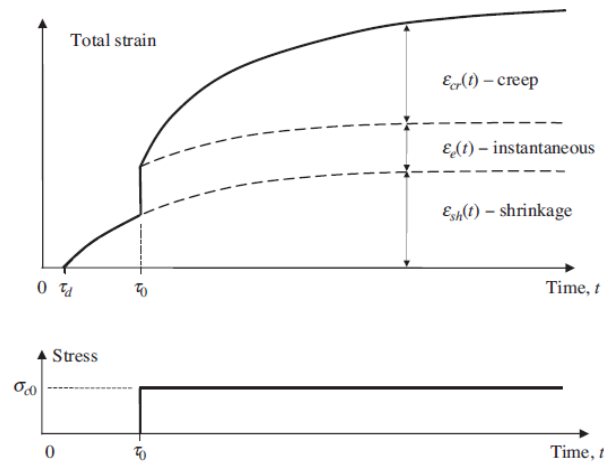

Figure 2.1 – Concrete strain components in a specimen subjected to a sustained load (15)

Creep and shrinkage tend to increase with a decreasing rate over time. As suggested by Gilbert (15), about 50% of the final creep develops in the first 2-3 months and about 90% after 2-3 years. Similarly, 30% of the final shrinkage is developed in the first 2-3 weeks.

2.2 Creep

As defined in (16), in materials science, creep is the tendency of a solid material to slowly move or deform permanently under the influence of stresses. It occurs as a result of long-term exposure to high levels of stress that are below the yield strength of the material. Creep is more severe in materials that are subjected to heat for long periods, and near melting point. Creep always increases with temperature.

Creep of concrete develops in the cement paste, after its hardening; this paste is composed by a cement gel and a series of included capillaries, and it is made of colloidal sheets formed by calcium silicate hydrates and evaporable water. The mechanism through which creep occurs has always been a cause of controversy among the scientific community and until now there is not a satisfactory theory able to describe the formation of creep. Bazant (17) explains that it is generally believed that creep is due to the disorder and instability that characterize the bond between the colloidal sheets.

Creep is affected by numerous factors which include, among the others, concrete mix, environmental and loading conditions. Generally, for increasing concrete strength, the concrete capacity to creep decreases. In addition, the creep capacity decreases for either an increasing maximum aggregate size or aggregate content and for a reduction of water/cement ratio. As previously mentioned, creep is also influenced by environment: it increases in thin members with large surface-area-to-volume ratios, such as slabs, and it also increases for reducing humidity and increasing temperature. Finally, creep depends on the magnitude and duration of the stress and on the age of the concrete at which the stress was applied for the first time. In particular, concrete creeps more when loaded at an early stage.

Usually, creep strain is formed by two main components: recoverable creep and irrecoverable creep. When subjected to a sustained stress σ_0, creep increases at a decreasing rate. Removing this load at a time τ_1, creep tends to decrease gradually, as reported in Figure 2.2. At this time, a sudden change in the total strain occurs, due to the elimination of the instantaneous strain. Thus, a smaller part of the creep strain is recoverable, while a bigger part of it is irrecoverable.
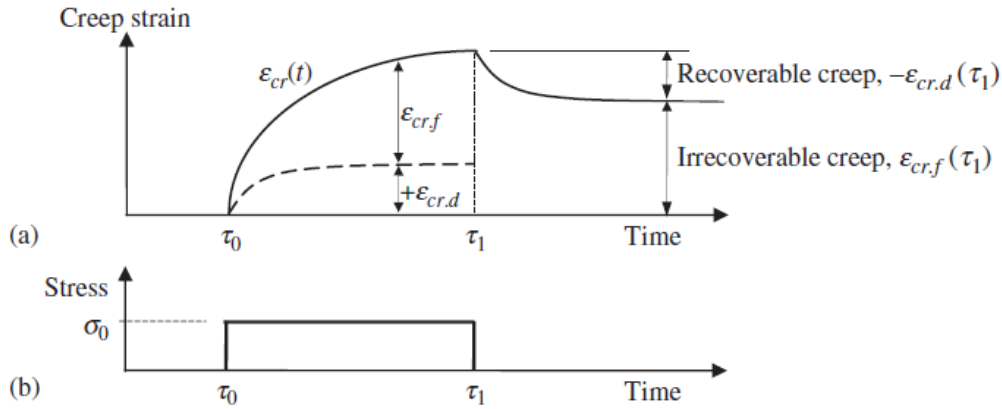
Figure 2.2 – Recoverable and irrecoverable creep components. (15)

During the last century, several analytical methods were developed to take creep into consideration. Most of them are based on the calculation of the creep coefficient φ, defined as the ratio of the creep deformation over the instantaneous one. It quantifies the capacity of concrete to creep. The simplest analytical method available to account for creep is Faber's Effective Modulus Method (EMM) (18). The basic idea of this model is to modify the elastic modulus of the concrete to account for creep. A slightly more complex model is the Age-adjusted Effective Modulus Method (AEMM). A more refined model is represented by the Step by Step Model (SSM) which enables a more accurate prediction of the changes in the concrete stresses taking place over time.

2.3   Shrinkage

Shrinkage is commonly defined as the time-dependent change in volume of a non-stressed concrete specimen at constant temperature and it affects every concrete structure during its service life.

Shrinkage is larger on the external surface of a member, i.e. the one exposed to drying, while it decreases when moving towards its inner part. Figure 2.3a depicts the shrinkage distribution through the thickness of the cross section in which ε_{sh} is the mean shrinkage strain value. $\Delta\varepsilon_{sh}$ is the strain required to restore the compatibility, and thus the hypothesis of plane section. A typical distribution of the instantaneous and creep strain distributions are shown in Figure 2.3b and this is equal and opposite to $\Delta\varepsilon_{sh}$. Based on this, the total strain caused by shrinkage, obtained from the sum of elastic, creep and shrinkage components, is linear, as shown in Figure 2.3c. In this way compatibility is
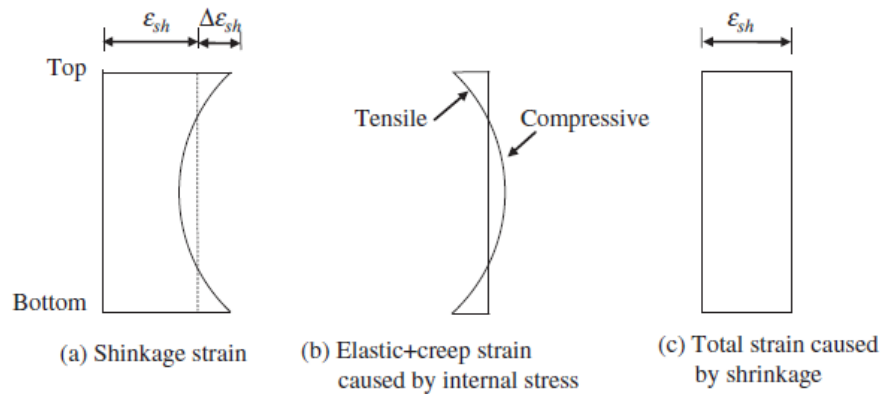
satisfied.

Figure 2.3 – Strain components caused by shrinkage in plain concrete (15)

For a specimen with the complete perimeter exposed to air, the shrinkage deformation in it longitudinal direction can be defined as

$$\varepsilon_{sh}\left(\tau_0,\tau_i\right)=\frac{l_i-l_0}{l_0} \tag{2.2}$$

where l_0 represents the initial longitudinal length at time $t=\tau_0$ and l_i the longitudinal length after shrinkage has developed at $t=\tau_i$.

For typical structural engineering applications, the design values of shrinkage deformations is of the order of 500 – 800 microstrains.

When concrete is exposed to air it tends to shrink, while, when it is subjected to water, it tends to swells (19). When shrinkage or swelling is restrained some stresses develop. In reinforced concrete structures, examples of restrain are the supports or the reinforcing bars. Usually, in concrete members, the shrinkage effects are larger in absolute value than the swelling effects and they verify frequently. For this reasons, in most of the analysis, only shrinkage effects are taken into consideration, even if the analytical procedure is exactly the same, except for the sign of the term representing the amount of volume change.

Usually, shrinkage is divided into four components: plastic shrinkage, chemical shrinkage, thermal shrinkage and drying shrinkage. Plastic shrinkage develops before the concrete has hardened and is associated with the evaporation of the surface water of the mix. Thermal shrinkage is a consequence of the heat induced during the hydration process and does not last more than a few days. Chemical shrinkage (or autogenous shrinkage) is caused by the chemical reaction taking place in the cement paste. Unlike drying shrinkage, it is an intrinsic

characteristic of the material, less dependent on the size and the shape of the specimen of concrete. Except at extremely low water-cement ratios, autogenous shrinkage is generally small, about 5% of the maximum drying shrinkage (17).

Usually, the major component is represented by the drying shrinkage. The main difference between drying shrinkage and autogenous shrinkage is that the first one is concerned with the water which has not been used during the cement reactions and that is able to find its way our of the sample. The drying shrinkage process starts as soon as the water contained in the concrete paste evaporates in the surrounding environment and, as previously mentioned, it increases in time with a decreasing rate. Since the drying shrinkage strictly depends on the initial water quantity contained in the concrete mix, it is higher for larger values of initial water-cement ratio of the concrete. Drying shrinkage is very difficult to predict because of the large number of factors that can affect its value: concrete mix characteristics, relative humidity and specimen shape, size and exposure. These are some of all the possible factors that affect this difficult evaluation.

It is important to underline how the sealing condition of the specimen can affect the general behaviour. Usually shrinkage happens faster on the free side of the sample where the evaporation is not restrained and slower in the core of it, as much as it is further from the drying surface. The quick contraction on the surface is restrained by the lower shrinkage rate occurring inside the specimen; this differential shrinkage within the member develops some internal stresses and these may lead to a premature cracking of the external surface. Because of the same reason, a non-symmetric drying exposure may induce warping in the concrete member or shrinkage induced curvatures. Since the drying process is based on the way in which moisture abandons the sample, a non-symmetrical moisture migration can cause the development of a gradient in the shrinkage deformation.

Chapter 3

Theoretical model

"Engineers are not superhuman. They make mistakes in their assumptions, in their calculations, in their conclusions. That they make mistakes is forgivable; that they catch them is imperative. Thus it is the essence of modern engineering not only to be able to check one's own work but also to have one's work checked and to be able to check the work of others."
 [Henry Petroski]

3.1   Introduction

As part of this project an analytical model was derived aimed at predicting the long-term response of concrete members considering different degrees of refinement in the representation of the concrete behaviour. The numerical models were implemented in MATLAB and were used to predict the results measured in previous long-term experiments carried out on post-tensioned composite slabs and on the long-term reinforced concrete slabs tested as part of this project.

The software used to run these analyses is MATLAB. The general idea is that, for a single span beam element, once the curvature is known at three different points, the deflection shape can be interpolated with a 4th order parabola (for detailed calculation refer to paragraph 3.4), while to estimate the curvature of a prismatic element at a given cross section, a cross sectional analysis can be performed. Finally, once the models provide the required deflections, they can be compared with the experimental values.

3.2   Theoretical methodology

3.2.1   Cross Sectional Analysis (CSA)

A cross-sectional analysis (CSA) is a useful tool for the determination of stress and strain distributions at particular locations along a member. The complexity of the analysis and accuracy of the results depend on the assumptions of the formulation and the constitutive models adopted for the materials forming the cross-section.

The CSA is based on the classical Euler-Bernoulli beam assumptions in which plane sections remain plane and perpendicular to the beam axis before and after deformations.

The cross-sectional analysis is formulated with the strain value at the level of the reference axis ε_r and the curvature κ as the unknowns of the problems. These are calculated enforcing horizontal and rotational equilibrium at the cross-section as follows:

$$N_{ext} = \int_A \sigma \, dA \qquad\qquad (3.1)$$

and

$$M_{x,ext} = \int_A \sigma \, y \, dA \tag{3.2}$$

where A represents the cross section, σ depicts the internal stress, N_{ext} and $M_{x,ext}$ are the external axial force and bending moment calculated with respect to the x-axis, respectively.

The calculation of the internal stress is based on the constitutive models specified for the different materials forming the cross-section. These are linear-elastic for the steel reinforcement and profiled sheeting, while for the concrete account for its time-dependent behaviour. Compatibility is enforced calculating the strain for the different material forming the cross-section with the following expression:

$$\varepsilon(y) = \varepsilon_r + \kappa y \tag{3.3}$$

where y represents the vertical axis of the cross section.

When adopting the proposed method of analysis one analysis needs to be carried out to evaluate the instantaneous deformations, expressed in terms of the strain at the level of the reference axis and the curvature, while the number of simulations to be performed with time depends on the time-dependent representation adopted for the concrete.

3.2.2 Time-dependent behaviour of concrete

As already described in Chapter 3, creep and shrinkage take place in the concrete over time and different expressions can be adopted for their representation.

The total deformation at time t of a concrete specimen loaded at time τ_0 can be decomposed in instantaneous, creep and shrinkage components

$$\varepsilon(t,\tau_0) = \varepsilon_e(\tau_0) + \varepsilon_{cr}(t,\tau_0) + \varepsilon_{sh}(t,\tau_0) \tag{3.4}$$

The instantaneous and the creep components, $\varepsilon_e(\tau_0)$ and $\varepsilon_{cr}(t,\tau_0)$, are stress dependent, while the shrinkage component $\varepsilon_{sh}(t,\tau_0)$ is not.

3.2.2.1 Constant and non uniform shrinkage deformations

The shrinkage deformation can be calculated using some analytical models, but, usually, these kinds of models lead to an excessive simplification of the problem. For this reason, during experimental tests, the shrinkage data is taken

directly from the samples, because it represents better the real condition of the main test. But in design, usually, this is not possible and thus the shrinkage is calculated through the formulation provided by the codes. More in detail, in this experiment, shrinkage data is taken from some cylinders and prisms poured the same day of the main test and with the same concrete mix. In addition, these cylindrical and prismatic samples are taken in the same environment of the main specimen and thus also the boundary conditions are exactly the same for both of them. Obviously, this precision cannot be reached using a certain analytical model provided by codes or other experimental tests. Moreover, as obtained from other experimental data collected in the laboratory, shrinkage can occur with different velocities in different parts of the concrete sample, depending on the boundary conditions. For this reason the model should allow for a non-uniform profile input in the cross section of the analysed member. Consequently the shrinkage expression used in this model depends also from the position y in the vertical axis of the cross section, and thus it can be written as

$$\varepsilon_{sh} = \varepsilon_{sh}\left(t, \tau_0, y\right) \tag{3.5}$$

More in detail, to take into consideration a different shrinkage throughout the depth of the cross section, the general shrinkage deformation is defined as

$$\varepsilon_{sh} = \varepsilon_{r,sh} + \kappa_{sh} y \tag{3.6}$$

where $\varepsilon_{r,sh}$ and κ_{sh} are respectively the shrinkage strain at the depth position $y = 0$ and the curvature of the shrinkage profile. An illustration of the general shape of a shrinkage strain profile throughout the depth of a cross section is reported in Figure 3.1.
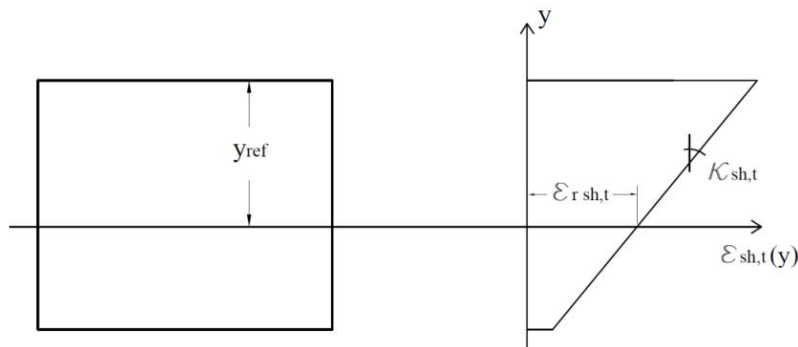

Figure 3.1 – General shrinkage profile along the depth of the cross section

At present there are no expressions for the determination of the value for $\varepsilon_{r,sh}$ and κ_{sh}, and their calculation is based on the limited experimental measurements carried out at the University of Sydney (20). In the laboratory environment readings of free shrinkage were taken on the outside faces and within the thickness of unreinforced concrete samples. Considering the linear distribution measured for the total deformations, the outside face measurements have been used to calculate $\varepsilon_{r,sh}$ and κ_{sh} as follows:

$$\varepsilon_{r,sh} = \frac{\left(\varepsilon_{sh,btm} - \varepsilon_{sh,top}\right) y_{ref}}{D} + \varepsilon_{sh,top} \tag{3.7}$$

$$\kappa_{sh} = \frac{\varepsilon_{sh,btm} - \varepsilon_{sh,top}}{D} \tag{3.8}$$

where $\varepsilon_{sh,btm}$ and $\varepsilon_{sh,top}$ represent the shrinkage at the bottom and the top surfaces of the samples.

3.2.2.2 *Principle of superposition - the Step-by-Step Method (SSM)*

The SSM is based on the principle of superposition. As represented in Figure 3.2, the time period of sustained stress is subdivided into k intervals: at τ_0 corresponds the first loading after the pour and at τ_k corresponds the end of the time period.
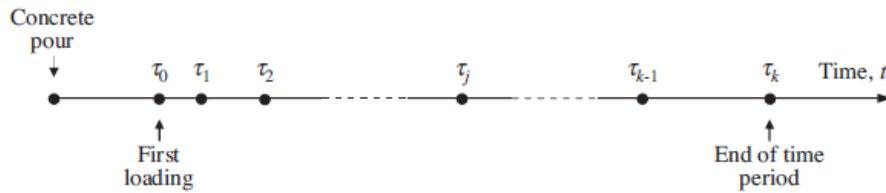

Figure 3.2 – Time discretisation

The general idea is the concrete stress varies between time steps at an increment $\Delta\sigma_c\left(\tau_j\right)$. Analytically, the constitutive relation for the concrete at any τ_j time step becomes:

$$\sigma_{c,j} = E_{c,j}\left(\varepsilon_j - \varepsilon_{sh,j}\right) + \sum_{i=0}^{j-1} F_{e,j,i}\sigma_{c,i} \tag{3.9}$$

where $E_{c,j}$ is the *instantaneous elastic modulus* of concrete and $F_{e,j,i}$ is the *stress modification factor*; these terms are defined as

$$E_{c,j} = \frac{1}{J_{j,j}}$$

(3.10)

$$F_{e,j,i} = \frac{J_{j,i+1} - J_{j,i}}{J_{j,j}}$$

(3.11)

3.2.2.3   Age-adjusted Effective Modulus Method (AEMM)

The AEMM was developed by Trost (21) and its formulation can be expressed as:

$$\sigma_c(t) = \bar{E}_e(t, \tau_0)\left[\varepsilon(t) - \varepsilon_{sh}(t)\right] + \sigma_c(\tau_0)\bar{F}_{e,0}$$

(3.12)

where the *age-adjusted effective modulus* $\bar{E}_e(t, \tau_0)$ and the coefficient $\bar{F}_{e,0}$ are given by the expressions

$$\bar{E}_e(t, \tau_0) = \frac{E_c(\tau_0)}{1 + \chi(t, \tau_0)\varphi(t, \tau_0)}$$

(3.13)

$$\bar{F}_{e,0} = \varphi(t, \tau_0)\frac{\chi(t, \tau_0) - 1}{1 + \chi(t, \tau_0)\varphi(t, \tau_0)}$$

(3.14)

The function $\chi(t, \tau_0)$ is defined as the *ageing coefficient* and, as suggested by Gilbert and Ranzi (15), for concrete loaded at early ages $(\tau_0 < 20 days)$ it can be approximated to 0.65 while a value of 0.75 is suggested for concrete loaded at later ages $(\tau_0 > 28 days)$.

3.3   Detailed expressions of the numerical formulation for a cracked section

The cross analysis used and developed in this thesis follows the procedure presented in Gilbert and Ranzi's book *Time-dependent behaviour of concrete structures* (15). In this thesis, only the main analytical expressions regarding steel and tendon will be showed in the following pages, but take into consideration that the MATLAB scripts are developed including a top and a bottom reinforcement layer, a tendon layer and a deck layer. Thus, the last ones are more complete and useful for a more complex situation. The cross section shape is rectangular. An example of the generic cross section discussed in this numerical formulation is reported in Figure 3.3; but remember that the slabs under examination have a single layer of ordinary steel reinforcement and no
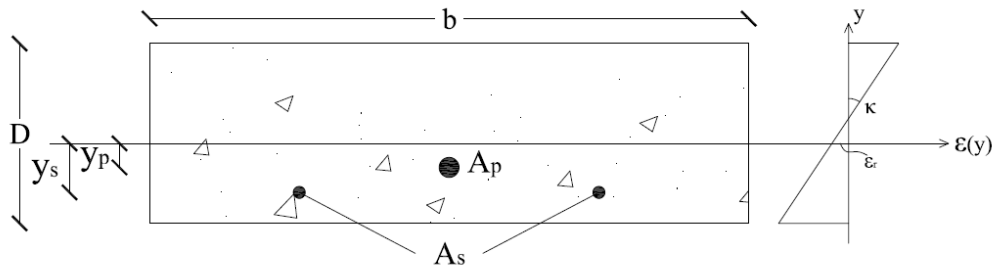
prestressed reinforcement layer.

Figure 3.3 – General cross section

The section is crossed by a couple of Cartesian axis located at a distance y_{ref} from the top concrete fibre. There is a bottom ordinary steel reinforcing layer of area A_s at a distance y_s from the reference axis and a post-tensioned strand layer at a distance y_p. Based on the Bernoulli's hypothesis, the deformation should be a linear function of the vertical axis y. Therefore the general expression of the total deformation can be written as

$$\varepsilon(y) = \kappa y + \varepsilon_r \tag{3.15}$$

where κ and ε_r are respectively the curvature and the strain at the reference axis level, both of them dependent on time. They are the main unknowns to solve in order to calculate the following stresses in all the structural elements.

The analysis can be divided in two main parts: instantaneous analysis and long-term analysis. In this specific thesis the analysis to carry out is that for a cracked cross section. This case is slightly more complicated than the uncracked cross section case, because the position of the neutral axis moves towards the compressive part of the section every time that part of the section itself cracks in the tensile part.

3.3.1 Age-adjusted Effective Modulus Method

3.3.1.1 *Short-term analysis*

Assuming an axial force $N_{e,0}$ and a bending moment $M_{e,0}$ about the x-axis sufficiently high to cause a tension stress able to produce the cracking of the bottom fibres and compression in the top ones, the strain at any y depth below the reference x-axis at time τ_0 is given by:

$$\varepsilon_0 = \varepsilon_{r,0} + y\kappa_0 \tag{3.16}$$

Once the curvature κ_0 and the strain at the reference axis level $\varepsilon_{r,0}$ are found, through the following constitutive relations it is possible to evaluate the stresses in the concrete, in the steel and in the tendon:

$$\sigma_{c,0} = E_{c,0}\varepsilon_0 = E_{c,0}\left(\varepsilon_{r,0} + y\kappa_0\right) \qquad \text{for } y \le y_{n,0}$$
$$\sigma_{c,0} = 0 \qquad \text{for } y > y_{n,0} \tag{3.17}$$

$$\sigma_{s,0} = E_s\varepsilon_0 = E_s\left(\varepsilon_{r,0} + y_s\kappa_0\right) \tag{3.18}$$

$$\sigma_{p,0} = E_p\left(\varepsilon_0 + \varepsilon_{p,init}\right) = E_p\left(\varepsilon_{r,0} + y_p\kappa_0 + \varepsilon_{p,init}\right) \tag{3.19}$$

where $E_{c,0}$, E_s and E_p are respectively the concrete Young modulus, the steel and the tendon elastic modulus at the time in which the load is applied (i.e. $t = 0$), while $\varepsilon_{p,init}$ is the strain in the prestressed steel immediately before the transfer of prestress to the concrete, expressed as

$$\varepsilon_{p,init} = \frac{P_{p,init}}{A_p E_p} \tag{3.20}$$

The first step in order to find the unknown κ_0 and $\varepsilon_{r,0}$ is enforcing equilibrium between the internal and the external axial forces:

$$N_{e,0} = N_{i,0}$$
$$M_{e,0} = M_{i,0} \tag{3.21}$$

The internal axial force can be expressed as

$$N_{i,0} = N_{c,0} + N_{s,0} + N_{p,0} \tag{3.22}$$

where $N_{c,0}$, $N_{s,0}$ and $N_{p,0}$ represent the axial forces resisted by the concrete, the ordinary steel and the prestressed steel and they can be calculated as

$$N_{c,0} = \int_{A_c} \sigma_{c,0}dA = \int_{A_c} E_{c,0}\left(\varepsilon_{r,0} + y\kappa_0\right)dA \tag{3.23}$$

$$\begin{aligned}
N_{s,0} = A_s\sigma_s &= A_s E_s\left(\varepsilon_{r,0} + y_s\kappa_0\right) = \\
&= A_s E_s\varepsilon_{r,0} + y_s A_s E_s\kappa_0 = \\
&= R_{A,s}\varepsilon_{r,0} + R_{B,s}\kappa_0
\end{aligned} \tag{3.24}$$

$$\begin{aligned}
N_{p,0} = A_p\sigma_p &= A_p E_p\left(\varepsilon_{r,0} + y_p\kappa_0 + \varepsilon_{p,init}\right) = \\
&= A_p E_p\varepsilon_{r,0} + y_p A_p E_p\kappa_0 + A_p E_p\varepsilon_{p,init} = \\
&= R_{A,p}\varepsilon_{r,0} + R_{B,p}\kappa_0 + A_p E_p\varepsilon_{p,init}
\end{aligned} \tag{3.25}$$

28

Substituting equations (3.23), (3.24) and (3.25) in equation (3.22) and rearranging the expression, it becomes

$$N_{i,0} = \int_{A_c} E_{c,0}\left(\varepsilon_{r,0} + y\kappa_0\right)dA + \left(R_{A,s} + R_{A,p}\right)\varepsilon_{r,0} + \left(R_{B,s} + R_{B,p}\right)\kappa_0 + A_p E_p \varepsilon_{p,init}$$

(3.26)

Thus, using the axial equilibrium condition (Equation (3.21)) and rearranging it, it becomes

$$N_{e,0} - A_p E_p \varepsilon_{p,init} = \int_{A_c} E_{c,0}\left(\varepsilon_{r,0} + y\kappa_0\right)dA + \left(R_{A,s} + R_{A,p}\right)\varepsilon_{r,0} + \left(R_{B,s} + R_{B,p}\right)\kappa_0$$

(3.27)

Following the exact same procedure, the expression below based on the moment equilibrium can be derived

$$M_{e,0} - y_p A_p E_p \varepsilon_{p,init} = \int_{A_c} E_{c,0}\left(\varepsilon_{r,0} + y\kappa_0\right)y\,dA + \left(R_{B,s} + R_{B,p}\right)\varepsilon_{r,0} + \left(R_{I,s} + R_{I,p}\right)\kappa_0$$

(3.28)

At this point, two possible solutions are available according to the initial load condition. In the case of a pure bending load $N_{e,0} = N_{i,0} = 0$ and no prestress, expression (3.27) becomes a quadratic equation that can be solved to obtain the location of the neutral axis $y_{n,0}$. Otherwise, in the case of external axial load different from zero or in presence of prestress, the solution can be found dividing equation (3.28) by equation (3.27); in this way, after some analytical passages and recognising that, at the axis of zero strain, $y = y_{n,0} = -\varepsilon_{r,0}/\kappa_0$, the expression becomes:

$$\frac{M_{e,0} - y_p A_p E_p \varepsilon_{p,init}}{N_{e,0} - A_p E_p \varepsilon_{p,init}} = \frac{\displaystyle\int_{y=-d_{ref}}^{y=y_{n,0}} E_{c,0}\left(-y_{n,0} + y\right)y\,dA - \left(R_{B,s} + R_{B,p}\right)y_{n,0} + \left(R_{I,s} + R_{I,p}\right)}{\displaystyle\int_{y=-d_{ref}}^{y=y_{n,0}} E_{c,0}\left(-y_{n,0} + y\right)dA - \left(R_{A,s} + R_{A,p}\right)y_{n,0} + \left(R_{B,s} + R_{B,p}\right)}$$

(3.29)

Finally equation (3.29) can be solved with a trial and error search and the value $y_{n,0}$ can be found. Once the portion of uncracked concrete section is known, the properties of the compressive concrete (A_c, B_c and I_c) can be

calculated with respect to the reference axis. Now it is possible to write once again the expressions for $N_{i,0}$ and $M_{i,0}$ as:

$$N_{i,0} = R_{A,0}\varepsilon_{r,0} + R_{B,0}\kappa_0 + A_p E_p \varepsilon_{p,init} \tag{3.30}$$

$$M_{i,0} = R_{B,0}\varepsilon_{r,0} + R_{I,0}\kappa_0 + y_p A_p E_p \varepsilon_{p,init} \tag{3.31}$$

where $R_{A,0}$, $R_{B,0}$ and $R_{I,0}$ are the axial rigidity and the stiffness respectively related to the first and second moment of area of the cracked section about the reference axis calculated at time τ_0 and given by:

$$R_{A,0} = A_c E_{c,0} + A_s E_s + A_p E_p = A_c E_{c,0} + R_{A,s} + R_{A,p} \tag{3.32}$$

$$R_{B,0} = B_c E_{c,0} + y_s A_s E_s + y_p A_p E_p = B_c E_{c,0} + R_{B,s} + R_{B,p} \tag{3.33}$$

$$R_{I,0} = I_c E_{c,0} + y_s^2 A_s E_s + y_p^2 A_p E_p = I_c E_{c,0} + R_{I,s} + R_{I,p} \tag{3.34}$$

Substituting the expression for $N_{i,0}$ and $M_{i,0}$ (equations (3.30) and (3.31)) into equations (3.21) and (3.22) produces the system of equilibrium equations that may be written in compact form as

$$r_{e,0} = D_0 \varepsilon_0 + f_{p,init} \tag{3.35}$$

and solved as

$$\varepsilon_0 = D_0^{-1}\left(r_{e,0} - f_{p,init}\right) = F_0\left(r_{e,0} - f_{p,init}\right) \tag{3.36}$$

The quantities used in the previous expression are defined as

$$r_{e,0} = \begin{bmatrix} N_{e,0} \\ M_{e,0} \end{bmatrix} \tag{3.37}$$

$$D_0 = \begin{bmatrix} R_{A,0} & R_{B,0} \\ R_{B,0} & R_{I,0} \end{bmatrix} \tag{3.38}$$

$$\varepsilon_0 = \begin{bmatrix} \varepsilon_{r,0} \\ \kappa_0 \end{bmatrix} \tag{3.39}$$

$$f_{p,init} = \begin{bmatrix} A_p E_p \varepsilon_{p,init} \\ y_p A_p E_p \varepsilon_{p,init} \end{bmatrix} \tag{3.40}$$

$$F_0 = \frac{1}{R_{A,0}R_{I,0} - R_{B,0}^2}\begin{bmatrix} R_{I,0} & -R_{B,0} \\ -R_{B,0} & R_{A,0} \end{bmatrix} \tag{3.41}$$

Finally the stress distribution in the concrete and in the steel reinforcement

30

can be calculated through equations (3.17), (3.18) and (3.19).

3.3.1.2 *Long-term analysis*

Before starting developing the analytical calculation of this part, it is important to underline the strong assumption at the base of AEMM necessary for a cracked section. It is assumed that the size of the uncracked concrete compressive zone remains constant in time, even if, for the presence of the sustained load, creep induces a movement of the neutral axis position. However, since the assumption simplifies considerably the calculation and since the corresponding error is little it will be used in the AEMM analysis.

In the case of axial force and uniaxial bending, the analytical calculations used for a cracked section are very similar to those used for an uncracked section. For long-term analysis, the steps to follow in order to find the unknowns are almost the same of the instantaneous analysis, except for some details; first of all, the Young modulus of the concrete should be substituted with the effective modulus and then the terms related to shrinkage, creep and relaxation of strands should be added. These last three terms are responsible for the time dependency. Analytically, each of them will give an additional contribution to equation (3.35) at the end of all the analytical passages.

Assuming a linear-elastic behaviour (as for the short-term analysis) of the steel reinforcement and the prestressing tendons (if any) and a constitutive relationship similar to equation (3.12) for concrete, the new constitutive relationships become

$$
\begin{aligned}
\sigma_{c,k} &= \bar{E}_{e,k}\left(\varepsilon_k - \varepsilon_{sh,k}\right) + \bar{F}_{e,0}\sigma_{c,0} && \text{for } y \leq y_{n,0} \\
\sigma_{c,k} &= 0 && \text{for } y > y_{n,0}
\end{aligned}
\tag{3.42}
$$

$$
\sigma_{s,k} = E_s \varepsilon_k
\tag{3.43}
$$

$$
\sigma_{p,k} = E_p\left(\varepsilon_k + \varepsilon_{p,init} - \varepsilon_{p,rel,k}\right)
\tag{3.44}
$$

where $\bar{E}_{e,k}$ and $\bar{F}_{e,0}$ are as defined previously (equations (3.13) and (3.14)) and the tensile creep strain $\varepsilon_{p,rel,k}$, also referred as *relaxation strain*, is calculated as the product between a design relaxation coefficient R (clause 3.3.4 of the Australian Standard (2)) and the initial strain in the prestressing steel before transfer:

$$
\varepsilon_{p,rel,k} = \varepsilon_{p,init} R
\tag{3.45}
$$

Once again, as in the instantaneous analysis, to solve the problem it is necessary to impose equilibrium between internal and external forces at time τ_k:

$$
\begin{aligned}
N_{e,k} &= N_{i,k} \\
M_{e,k} &= M_{i,k}
\end{aligned}
$$

(3.46)

As before, the axial force $N_{i,k}$ is

$$
N_{i,k} = N_{c,k} + N_{s,k} + N_{p,k}
$$

(3.47)

and the three components are

$$
\begin{aligned}
N_{c,k} &= \int_{A_c} \sigma_{c,k} dA = \int_{A_c} \left[\bar{E}_{e,k} \left(\varepsilon_{r,k} + y\kappa_k - \varepsilon_{sh,k} \right) + \bar{F}_{e,0}\sigma_{c,0} \right] dA = \\
&= A_c \bar{E}_{e,k}\varepsilon_{r,k} + B_c \bar{E}_{e,k}\kappa_k - A_c \bar{E}_{e,k}\varepsilon_{sh,k} + \bar{F}_{e,0}N_{c,0} \\
&= R_{A,c}\varepsilon_{r,k} + R_{B,c}\kappa_k - R_{A,c}\varepsilon_{sh,k} + \bar{F}_{e,0}N_{c,0}
\end{aligned}
$$

(3.48)

$$
\begin{aligned}
N_{s,k} &= A_s E_s \varepsilon_{r,k} + y_s A_s E_s \kappa_k = \\
&= R_{A,s}\varepsilon_{r,k} + R_{B,s}\kappa_k
\end{aligned}
$$

(3.49)

$$
\begin{aligned}
N_{p,0} &= A_p E_p \varepsilon_{r,k} + y_p A_p E_p \kappa_k + A_p E_p \left(\varepsilon_{p,init} - \varepsilon_{p,rel,k} \right) = \\
&= R_{A,p}\varepsilon_{r,k} + R_{B,p}\kappa_k + R_{A,p} \left(\varepsilon_{p,init} - \varepsilon_{p,rel,k} \right)
\end{aligned}
$$

(3.50)

Defining the axial rigidity $R_{A,k}$ and the stiffness related to the first moment of area $R_{B,k}$ at time τ_k as

$$
R_{A,k} = R_{A,c} + R_{A,s} + R_{A,p}
$$

(3.51)

$$
R_{B,k} = R_{B,c} + R_{B,s} + R_{B,p}
$$

(3.52)

equation (3.47), after some substitutions can be rewritten as

$$
N_{i,k} = R_{A,k}\varepsilon_{r,k} + R_{B,k}\kappa_k - R_{A,c}\varepsilon_{sh,k} + \bar{F}_{e,0}N_{c,0} + R_{A,p} \left(\varepsilon_{p,init} - \varepsilon_{p,rel,k} \right)
$$

(3.53)

Using the same procedure, the internal moment $M_{i,k}$ resisted by the cross section at time τ_k can be expressed as:

$$
M_{i,k} = R_{B,k}\varepsilon_{r,k} + R_{I,k}\kappa_k - R_{B,c}\varepsilon_{sh,k} + \bar{F}_{e,0}M_{c,0} + R_{B,p} \left(\varepsilon_{p,init} - \varepsilon_{p,rel,k} \right)
$$

(3.54)

with the stiffness related to the second moment of area $R_{I,k}$ at time τ_k equal to

$$R_{I,k} = R_{I,c} + R_{I,s} + R_{I,p} \tag{3.55}$$

Note that the quantities $N_{c,0}$ and $M_{c,0}$ present in equations (3.53) and (3.54) are known from the instantaneous analysis.

Substituting equations (3.53) and (3.54) into equation (3.46), the following compact form can be written

$$r_{e,k} = D_k \varepsilon_k + f_{cr,k} - f_{sh,k} + f_{p,init} - f_{p,rel,k} \tag{3.56}$$

where

$$r_{e,k} = \begin{bmatrix} N_{e,k} \\ M_{e,k} \end{bmatrix} \tag{3.57}$$

$$\varepsilon_k = \begin{bmatrix} \varepsilon_{r,k} \\ \kappa_k \end{bmatrix} \tag{3.58}$$

$$D_k = \begin{bmatrix} R_{A,k} & R_{B,k} \\ R_{B,k} & R_{I,k} \end{bmatrix} \tag{3.59}$$

The creep effect produced by the stress $\sigma_{c,0}$ resisted by the concrete at time τ_0 is represented by the vector

$$f_{cr,k} = \bar{F}_{e,0} \begin{bmatrix} N_{c,0} \\ M_{c,0} \end{bmatrix} = \bar{F}_{e,0} E_{c,0} \begin{bmatrix} A_c \varepsilon_{r,0} + B_c \kappa_0 \\ B_c \varepsilon_{r,0} + I_c \kappa_0 \end{bmatrix} \tag{3.60}$$

while the shrinkage strain vector $f_{sh,k}$ can be calculated as

$$f_{sh,k} = \begin{bmatrix} A_c & B_c \\ B_c & I_c \end{bmatrix} \bar{E}_{e,k} \varepsilon_{sh,k} = \begin{bmatrix} A_c & B_c \\ B_c & I_c \end{bmatrix} \bar{E}_{e,k} \begin{bmatrix} \varepsilon_{r,sh,k} & \kappa_k \end{bmatrix} \tag{3.61}$$

The vectors $f_{p,init}$ and $f_{p,rel,k}$ account respectively for the initial prestress and for the resultant actions caused by the loss of prestress in the tendon due to relaxation. They are given by:

$$f_{p,init} = \begin{bmatrix} A_p E_p \varepsilon_{p,init} \\ y_p A_p E_p \varepsilon_{p,init} \end{bmatrix} \tag{3.62}$$

and

$$f_{p,rel,k} = f_{p,init} R \tag{3.63}$$

Solving equation (3.56):

$$\varepsilon_k = D_k^{-1}\left(r_{e,k} - f_{cr,k} + f_{sh,k} - f_{p,init} + f_{p,rel,k}\right) =$$
$$= F_k\left(r_{e,k} - f_{cr,k} + f_{sh,k} - f_{p,init} + f_{p,rel,k}\right) \tag{3.64}$$

where

$$F_k = \frac{1}{R_{A,k}R_{I,k} - R_{B,k}^2}\begin{bmatrix} R_{I,k} & -R_{B,k} \\ -R_{B,k} & R_{A,k} \end{bmatrix} \tag{3.65}$$

Finally, the stress distribution at time τ_k

$$\sigma_{c,k} = \bar{E}_{e,k}\left(\varepsilon_k - \varepsilon_{sh,k}\right) + \bar{F}_{e,0}\sigma_{c,0} = \bar{E}_{e,k}\left\{\begin{bmatrix} 1 & y \end{bmatrix}\varepsilon_k - \varepsilon_{sh,k}\right\} + \bar{F}_{e,0}\sigma_{c,0} \tag{3.66}$$

$$\sigma_{s,k} = E_s\varepsilon_k = E_s\begin{bmatrix} 1 & y_s \end{bmatrix}\varepsilon_k \tag{3.67}$$

$$\sigma_{p,k} = E_p\left(\varepsilon_k + \varepsilon_{p,init} - \varepsilon_{p,rel,k}\right) = E_p\begin{bmatrix} 1 & y_p \end{bmatrix}\varepsilon_k + E_p\varepsilon_{p,init} - E_p\varepsilon_{p,rel,k} \tag{3.68}$$

3.3.2 Step-by-Step Method

Sometimes performing a time analysis for cracked sections with the AEMM may be not appropriate. An example could be the case of a complex load history. In these cases, is recommended to use some more refined method, as the one presented below.

Starting from the idea that the neutral axis change position every time part of the concrete cross section cracks due to excessive tensile force, it may be convenient to subdivide the concrete into layers, as shown in Figure 3.4. For the calculation of the internal actions, they can be obtained simply summing the contribution of each single layer.
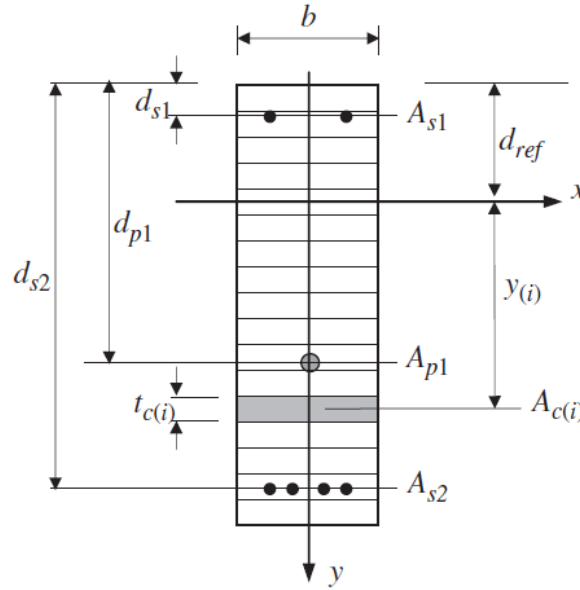
Figure 3.4 – Layered cross-section (15)

In the case of axial force and uniaxial bending, assuming m_c concrete layers, each of them uncracked in the initial configuration, the concrete contribution to the internal axial force $N_{i,0}$ can be calculated as follows:

$$N_{c,0} = \sum_{i=1}^{m_c} A_{c(i)} \sigma_{c,0} = \sum_{i=1}^{m_c} A_{c(i)} E_{c(i),0} \left(\varepsilon_{r,0} + y_{(i)} \kappa_0 \right) =$$
$$= \sum_{i=1}^{m_c} \left(A_{c(i)} E_{c(i),0} \right) \varepsilon_{r,0} + \sum_{i=1}^{m_c} \left(B_{c(i)} E_{c(i),0} \right) \kappa_0 \tag{3.69}$$

where $A_{c(i)}$ and $B_{c(i)}$ are the area and the first moment of area of the i-th concrete layer about the x-axis and where $y_{(i)}$ is the distance between the reference axis and the centroid of the i-th concrete layer. By using this approach it is assumed a constant value of the stress along the thickness of the layer; it is an approximation quite reasonable for our research, but it is also quite easy to implement a linear variation of it. To minimize as much as possible the errors due to this approximation it is suggested to take a high number of layers during the analysis without compromising the efficiency and the velocity of the model.

In the same way can be derived the contribution of the concrete to the internal moment $M_{i,0}$:

$$M_{c,0} = \sum_{i=1}^{m_c} y_{(i)} A_{c(i)} \sigma_{c,0} = \sum_{i=1}^{m_c} A_{c(i)} E_{c(i),0} \left(y_{(i)} \varepsilon_{r,0} + y_{(i)}^2 \kappa_0 \right) =$$

$$= \sum_{i=1}^{m_c} \left(B_{c(i)} E_{c(i),0} \right) \varepsilon_{r,0} + \sum_{i=1}^{m_c} \left(I_{c(i)} E_{c(i),0} \right) \kappa_0$$

(3.70)

where $I_{c(i)}$ is the second moment of area of the i-th concrete layer about the x-axis.

After writing the concrete rigidities for the cross section as

$$R_{A,c} = \sum_{i=1}^{m_c} A_{c(i)} E_{c(i),0}$$

$$R_{B,c} = \sum_{i=1}^{m_c} y_{(i)} A_{c(i)} E_{c(i),0}$$

(3.71)

$$R_{I,c} = \sum_{i=1}^{m_c} y_{(i)}^2 A_{c(i)} E_{c(i),0}$$

the axial force and the moment carried by the concrete might be rewritten as

$$N_{c,0} = R_{A,c} \varepsilon_{r,0} + R_{B,c} \kappa_0$$

$$M_{c,0} = R_{B,c} \varepsilon_{r,0} + R_{I,c} \kappa_0$$

(3.72)

According to the level of precision required in the analysis, in the determination of the properties $A_{c(i)}$, $B_{c(i)}$ and $I_{c(i)}$ of each concrete layer, it can be neglected that in some layers there could be the steel reinforcements or the tendon. In my MATLAB model, there are some parameters called *variable_s*, *variable_p* and *variable_d* which can be switched between 0 and 1 in order to give the chance to decide to calculate respectively the approximate area or the actual area excluding the non concrete material.

Including also the effects of ordinary and prestress steel reinforcements (which remain equal to the already discussed AEMM), for a general cross section, the governing equilibrium equations are:

$$N_{i,0} = \left(R_{A,c} + R_{A,s} + R_{A,p} \right) \varepsilon_{r,0} + \left(R_{B,c} + R_{B,s} + R_{B,p} \right) \kappa_0 + A_p E_p \varepsilon_{p,init} = N_{e,0}$$

$$M_{i,0} = \left(R_{B,c} + R_{B,s} + R_{B,p} \right) \varepsilon_{r,0} + \left(R_{I,c} + R_{I,s} + R_{I,p} \right) \kappa_0 + y_p A_p E_p \varepsilon_{p,init} = M_{e,0}$$

(3.73)

Solving this system of two equations, the unknown $\varepsilon_{r,0}$ and κ_0 can be found and from those ones all the stresses can be calculated.

To take into account cracking, the SSM need an iterative method: at the first

iteration, the cross section is supposed uncracked and the stress at the centroid of each concrete layer should be calculated as usual. At the second iteration, if one or more concrete layers have a tensile stress higher than the allowed tensile strength of concrete, then the model should set the value of the elastic modulus $E_{c(i),0}$ of those concrete layers equal to zero, in order to null the next stress calculation. Iterations must go on until all the reacting layers have a tensile stress lower than the admissible concrete tensile strength and no additional cracking is detected.

Long-term analysis for cracked sections is very similar to that required for uncracked sections. The only and fundamental difference is that when a concrete layer is cracked, it is not able to carry any tension stress anymore. Referring to the layered section of Figure 3.4, the axial force and moment carried by the concrete are:

$$
\begin{aligned}
N_{c,j} &= \sum_{i=1}^{m_c} A_{c(i)}\sigma_{c(i),j} = \\
&= \sum_{i=1}^{m_c}\left(A_{c(i)}E_{c(i),j}\left(\varepsilon_{(i),j}-\varepsilon_{sh,j}\right)+\sum_{n=0}^{j-1}F_{e,j,n}\sigma_{c(i),n}A_{c(i)}\right) = \\
&= \sum_{i=1}^{m_c}\left(A_{c(i)}E_{c(i),j}\varepsilon_{r,j}+B_{c(i)}E_{c(i),j}\kappa_j-A_{c(i)}E_{c(i),j}\varepsilon_{sh,j}+\sum_{n=0}^{j-1}F_{e,j,n}\sigma_{c(i),n}A_{c(i)}\right)
\end{aligned}
$$

(3.74)

$$
\begin{aligned}
M_{c,j} &= \sum_{i=1}^{m_c} y_{(i)}A_{c(i)}\sigma_{c(i),j} = \\
&= \sum_{i=1}^{m_c}\left(y_{(i)}A_{c(i)}E_{c(i),j}\left(\varepsilon_{(i),j}-\varepsilon_{sh,j}\right)+\sum_{n=0}^{j-1}F_{e,j,n}\sigma_{c(i),n}y_{(i)}A_{c(i)}\right) = \\
&= \sum_{i=1}^{m_c}\left(B_{c(i)}E_{c(i),j}\varepsilon_{r,j}+I_{c(i)}E_{c(i),j}\kappa_j-B_{c(i)}E_{c(i),j}\varepsilon_{sh,j}+\sum_{n=0}^{j-1}F_{e,j,n}\sigma_{c(i),n}B_{c(i)}\right)
\end{aligned}
$$

(3.75)

The axial force and the moment carried by the steel and the prestress reinforcements are:

$$
\begin{aligned}
N_{s,j} &= A_s E_s \varepsilon_{r,j} + y_s A_s E_s \kappa_j = \\
&= R_{A,s}\varepsilon_{r,j} + R_{B,s}\kappa_j
\end{aligned}
$$

(3.76)

$$
\begin{aligned}
M_{s,j} &= y_s A_s E_s \varepsilon_{r,j} + y_s^2 A_s E_s \kappa_j = \\
&= R_{B,s}\varepsilon_{r,j} + R_{I,s}\kappa_j
\end{aligned}
$$

(3.77)

$$N_{p,j} = A_p E_p \varepsilon_{r,j} + y_p A_p E_p \kappa_j =$$
$$= R_{A,p} \varepsilon_{r,j} + R_{B,p} \kappa_j$$

(3.78)

$$M_{p,j} = y_p A_p E_p \varepsilon_{r,j} + y_p^2 A_p E_p \kappa_j =$$
$$= R_{B,p} \varepsilon_{r,j} + R_{I,p} \kappa_j$$

(3.79)

Substituting all those quantities in the expressions

$$N_{i,j} = N_{c,j} + N_{s,j} + N_{p,j}$$
$$M_{i,j} = M_{c,j} + M_{s,j} + M_{p,j}$$

(3.80)

and after solving the equilibrium equations and rearranging the expressions, it becomes:

$$r_{e,j} = D_j \varepsilon_j + f_{cr,j} - f_{sh,j} + f_{p,init} - f_{p,rel,j}$$

(3.81)

where

$$r_{e,j} = \begin{bmatrix} N_{e,j} \\ M_{e,j} \end{bmatrix}$$

$$\varepsilon_j = \begin{bmatrix} \varepsilon_{r,j} \\ \kappa_j \end{bmatrix}$$

$$D_j = \begin{bmatrix} R_{A,j} & R_{B,j} \\ R_{B,j} & R_{I,j} \end{bmatrix}$$

$$f_{cr,j} = \sum_{i=0}^{j-1} F_{e,j,i} r_{c,i}$$

(3.82)

$$f_{sh,j} = \begin{bmatrix} A_c & B_c \\ B_c & I_c \end{bmatrix} E_{c,j} \varepsilon_{sh,j} = \begin{bmatrix} A_c & B_c \\ B_c & I_c \end{bmatrix} E_{c,j} \begin{bmatrix} \varepsilon_{r,sh,j} & \kappa_j \end{bmatrix}$$

$$f_{p,init} = \begin{bmatrix} A_p E_p \varepsilon_{p,init} \\ y_p A_p E_p \varepsilon_{p,init} \end{bmatrix}$$

$$f_{p,rel,j} = f_{p,init} R$$

Only to simplify the notation, the internal actions resisted by the concrete at a previous time instant τ_i are collected in a vector called $r_{c,i}$ and expressed as:

$$r_{c,i} = \begin{bmatrix} N_{c,i} \\ M_{c,i} \end{bmatrix} = D_c \varepsilon_i + \sum_{n=0}^{j-1} F_{e,i,n} r_{c,n} - \begin{bmatrix} A_c E_{c,i} \\ B_c E_{c,i} \end{bmatrix} \varepsilon_{sh,i} = D_c \varepsilon_i + f_{cr,i} - f_{sh,i}$$

(3.83)

with

$$D_{c,i} = \begin{bmatrix} A_c & B_c \\ B_c & I_c \end{bmatrix} E_{c,i}$$

(3.84)

The strain vector ε_j is obtained by solving equation (3.81), as in the analysis presented earlier:

$$\varepsilon_{jk} = D_j^{-1}\left(r_{e,j} - f_{cr,j} + f_{sh,j} - f_{p,init} + f_{p,rel,j}\right) =$$
$$= F_j\left(r_{e,j} - f_{cr,j} + f_{sh,j} - f_{p,init} + f_{p,rel,j}\right) \tag{3.85}$$

in which

$$F_j = \frac{1}{R_{A,j}R_{I,j} - R_{B,j}^2}\begin{bmatrix} R_{I,j} & -R_{B,j} \\ -R_{B,j} & R_{A,j} \end{bmatrix} \tag{3.86}$$

Finally, the stress distributions at time τ_j can be determined from the constitutive relationship:

$$\sigma_{c,j} = E_{c,j}\left(\varepsilon_j - \varepsilon_{sh,j}\right) + \sum_{i=0}^{j-1} F_{e,j,i}\sigma_{c,i} = E_{c,j}\left\{\begin{bmatrix} 1 & y \end{bmatrix}\varepsilon_j - \varepsilon_{sh,j}\right\} + \sum_{i=0}^{j-1} F_{e,j,i}\sigma_{c,i}$$

(3.87)

$$\sigma_{s,j} = E_s\varepsilon_j = E_s\begin{bmatrix} 1 & y_s \end{bmatrix}\varepsilon_j \tag{3.88}$$

$$\sigma_{p,j} = E_p\left(\varepsilon_j + \varepsilon_{p,init} - \varepsilon_{p,rel,j}\right) = E_p\begin{bmatrix} 1 & y_p \end{bmatrix}\varepsilon_j + E_p\varepsilon_{p,init} - E_p\varepsilon_{p,rel,j} \tag{3.89}$$

Similarly to the short-term analysis, also in the long-term analysis an iterative procedure should be run for each time step in order to null the effects of all those layers with a tensile stress higher than the threshold fixed by the tensile strength. Usually the iterative procedure continue until the changes in terms of strain (i.e. $\varepsilon_{r,j}$ or k_j) between two following iterations are smaller than the threshold chosen at the beginning of the analysis from the operator. In my MATLAB model, the change in terms of strain is calculated as:

$$error\_\varepsilon_{r,j} = \frac{\varepsilon_{r,iteration,j} - \varepsilon_{r,iteration-1,j}}{\varepsilon_{r,iteration-1,j}} \tag{3.90}$$

and it must be smaller than a certain value $error\_OK$.

3.4 Derivation of the deflection of a supported beam for which the curvatures at the supports and at the mid span are known

In this paragraph, it is explained how to calculate the deflection shape of a member of a continuous span once the curvature is known at three different cross sections. Let's consider the following supported beam represented in Figure 3.5.
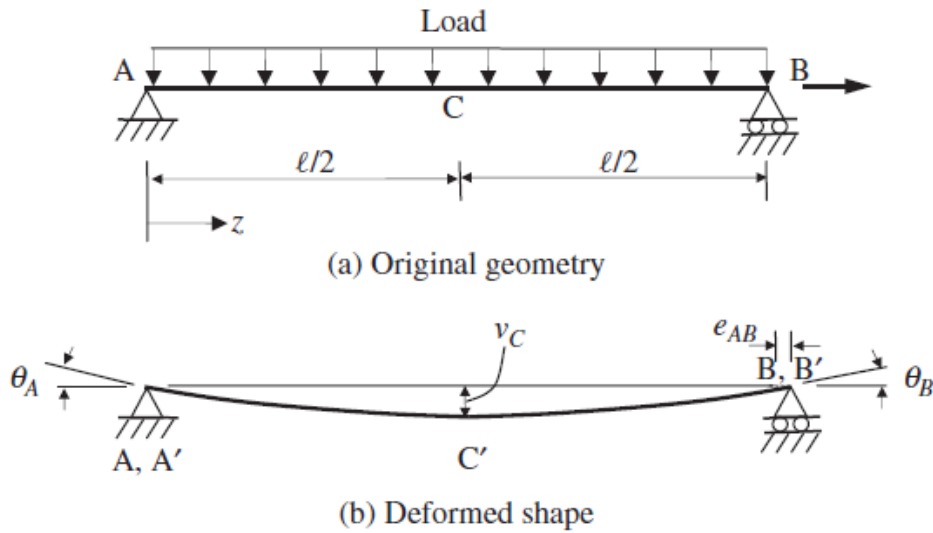
(a) Original geometry

(b) Deformed shape

Figure 3.5 – General deflected shape of a continuous beam

The solid line represents the initial configuration of the simply supported beam, while the dotted line represents its deflected shape under a certain load condition. The shape can be analytically defined through the function $v(z)$ taken as positive for downwards deflections. First of all, let's assume that through a cross sectional analysis the curvatures at the two supports (κ_A and κ_B) and at the mid span (κ_C) are determined; then exploiting that the curvature is proportional to the second derivative of the deflection function and that the deflection at the two supports A and C is null, the following five relations can be written:

$$v(0) = 0 \tag{3.91}$$

$$v(l) = 0 \tag{3.92}$$

$$v''(0) = -\kappa_A \tag{3.93}$$

$$v''(l/2) = -\kappa_C \tag{3.94}$$

$$v''(l) = -\kappa_B \tag{3.95}$$

Each one of these five equations (from equation (3.91) to (3.95)) is independent and thus they are sufficient to interpolate the exact deflection with a 4th order polynomial equation such that:

$$v(z) = az^4 + bz^3 + cz^2 + dz + e \tag{3.96}$$

The second derivative of that polynomial equation, and thus the curvature, is:

$$v''(z) = 12az^2 + 6bz + 2c \tag{3.97}$$

Substituting conditions (3.91), (3.92), (3.93) and (3.95) into equations (3.96) and (3.97), they become

$$v(0) = e = 0 \tag{3.98}$$

$$v(l) = al^4 + bl^3 + cl^2 + dl = 0 \tag{3.99}$$

$$v''(0) = 2c = -\kappa_A \tag{3.100}$$

$$v''(l/2) = 3al^2 + 3bl + 2c = -\kappa_C \tag{3.101}$$

$$v''(l) = 12al^2 + 6bl + 2c = -\kappa_B \tag{3.102}$$

and solving this system of five equations in 5 unknowns, the coefficients of the starting polynomial can be found:

$$
\begin{aligned}
e &= 0 \\
c &= -\frac{\kappa_A}{2} \\
a &= \frac{1}{3l^2}\left(\kappa_C - \frac{\kappa_B}{2} - \frac{\kappa_A}{2}\right) \\
b &= \frac{1}{l}\left(\frac{\kappa_B}{6} + \frac{\kappa_A}{2} - \frac{2\kappa_C}{3}\right) \\
d &= l\left(\frac{\kappa_C}{3} + \frac{\kappa_A}{6}\right)
\end{aligned}
\tag{3.103}
$$

Therefore, with a final substitution, the analytical expression of the deflection function becomes:

$$v(z) = \frac{1}{3l^2}\left(\kappa_C - \frac{\kappa_B}{2} - \frac{\kappa_A}{2}\right)z^4 + \frac{1}{l}\left(\frac{\kappa_B}{6} + \frac{\kappa_A}{2} - \frac{2\kappa_C}{3}\right)z^3 - \frac{\kappa_A}{2}z^2 + l\left(\frac{\kappa_C}{3} + \frac{\kappa_A}{6}\right)z$$
$$\tag{3.104}$$

Now substituting z with $l/2$, it is very easy to evaluate the deflection at the mid span in function of the curvature:

$$v_{midspan} = v\left(\frac{l}{2}\right) = \frac{l^2}{96}\left(10\kappa_C - \kappa_A - \kappa_B\right) \tag{3.105}$$

Chapter 4

Validation of the numerical models: comparison with previous experimental measurements

> *"Scientists investigate that which already is; engineers create that which has never been."*
> *[Albert Einstein]*

4.1   Description of the previous experimental test

This paragraph intends to evaluate the ability of the proposed method of analysis to predict the long-term behaviour of composite post-tensioned slabs based on long-term experimental measurements recently collected at the University of Sydney (20). As part of this study 3 post-tensioned slabs were monitored over a period of time. These included one solid slab and two composite samples. The non-uniform free shrinkage distribution was obtained monitoring the total deformation exhibited by four concrete slabs through their thickness. The shrinkage values taken from this experiment are reported in the following Table 4.1.

Figure 4.1 – Shrinkage slabs used in the previous test

Day from the pour	SOLID or SUPPORT slab			CONDECK slab		PRIMEFORM slab	
	Top	Bottom	Mean	Top	Bottom	Top	Bottom
8	0	0	0	0	0	0	0
9	4	8	6	56	16	-28	48
12	-52	-28	-40	-12	-28	-84	32
13	-40	-32	-36	-4	24	-100	40
14	-48	-20	-34	-16	12	-80	20
15	-68	-56	-62	-24	4	-96	32
16	-72	-56	-64	-36	4	-112	48
19	-80	-56	-68	-72	8	-112	24
21	-112	-84	-98	-100	-20	-156	12
22							
23	-132	-112	-122	-140	-16	-188	16
26	-112	-96	-104	-100	4	-168	36
40	-200	-196	-198	-232	4	-268	32
54	-232	-196	-214	-268	-8	-288	24
65	-300	-252	-276	-340	-20	-360	16
116	-332	-244	-288	-388	16	-412	48
159							
171							
197	-524	-396	-460	-560	-100	-560	152
214	-516	-400	-458	-598	-42	604	62
239	-556	-436	-496	-620	-56	-624	0

Table 4.1 – Shrinkage values used for the numerical model validation

The shrinkage results obtained from the four concrete slabs, were used after to perform a numerical analysis on the three post-tensioned composite slabs and these results were later compared with the experimental ones obtained through the test shown in Figure 4.2. In this comparison, the non-uniform shrinkage distribution is adopted and, for the analytical formulation, the equations (3.7) and (3.8) are used to take in consideration this effect. The three cross sections under examination both in the experimental test and in the numerical analysis are shown in the next Figure 4.3. More in detail, there are three main kinds of cross section (solid, Condeck HP and Primeform) and a general one (support) which is similar for all the three different kinds of slabs.

Figure 4.2 – Simply supported post-tensioned slabs used in the previous test
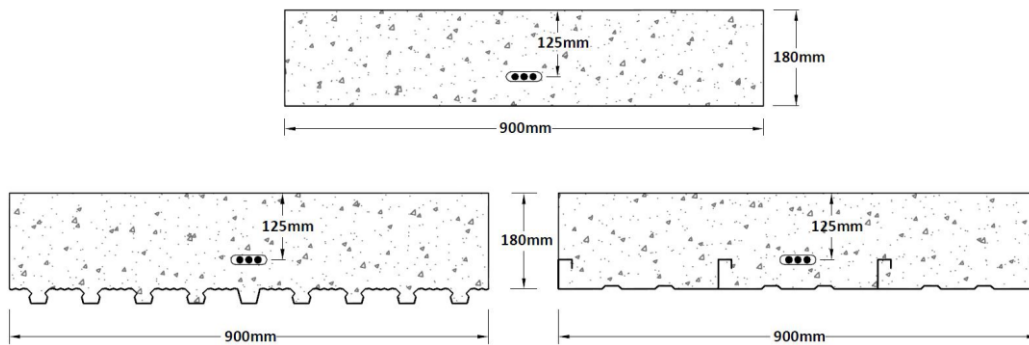
Figure 4.3 – Solid slab, PrimeForm Slab and Condeck slab cross sections

In Figure 4.4 and Figure 4.5 are shown the two kinds of deck used in this composite slab.

Figure 4.4 – Condeck HP® composite decking

Figure 4.5 - PrimeForm® composite decking

The creep properties of the concrete, expressed in terms of the creep coefficient $\varphi(t,t_0)$, were measured by means of standard creep tests. These information are sufficient for the AEMM, because this method requires a simple vector of creep coefficients, but it is not for the SMM, because in this second case a complete matrix of creep coefficients is required. To solve this problem, it has been considered the analytical formulation provided in the Appendix B of

the Eurocode 2 (3).

To summarize all the necessary information required to perform the numerical analysis, look at the following Table 4.2.

		SOLID cross section At mid span	CONDECK cross section At mid span	PRIMEFORM cross section At mid span	SUPPORT cross section At support
Applied actions	$N_e \; [kN]$	0	0	0	0
	$M_e \; [kNm]$	17.5	17.5	18.37	-0.73
	$P_{init} \; [kN]$	469	469	469	469
Concrete parameters	$b \; [mm]$	900	900	900	900
	$D \; [mm]$	180	180	180	180
	$E_{c0} \; [MPa]$	31500	31500	31500	31500
Steel parameters	$E_s \; [GPa]$	-	-	-	-
	$A_s \; [mm^2]$	-	-	-	-
	$y_s \; [mm]$	-	-	-	-
Deck parameters	$E_d \; [GPa]$	-	200	200	-
	$A_d \; [mm^2]$	-	1090	846	-
	$y_d \; [mm]$	-	64.71	90	-
Post-tensioned parameters	$E_p \; [GPa]$	200	200	200	200
	$A_p \; [mm^2]$	334	334	334	334
	$y_p \; [mm]$	27	22	36	-10

<div align="center">Table 4.2 – Input data for the cross sectional analysis</div>

4.2   Validation of the models: comparison of the results

Now that all the input information are provided, the analysis can be run. Based on the equation reported in **(3.105)** and on the cross section analysis, the deflection at the mid span can be calculated. The results obtained are shown in the following Figure 4.6, Figure 4.7, Figure 4.8, and Figure 4.9.

Proceeding in order, Figure 4.6 shows the experimental deflections obtained for the three different slabs. It is important to underline how the deflection of the two slabs with deck are bigger respect to the deflection of the solid slab. This is

due to the fact that the steel decks cover one concrete surface and they do not allow the development of uniform shrinkage effects.
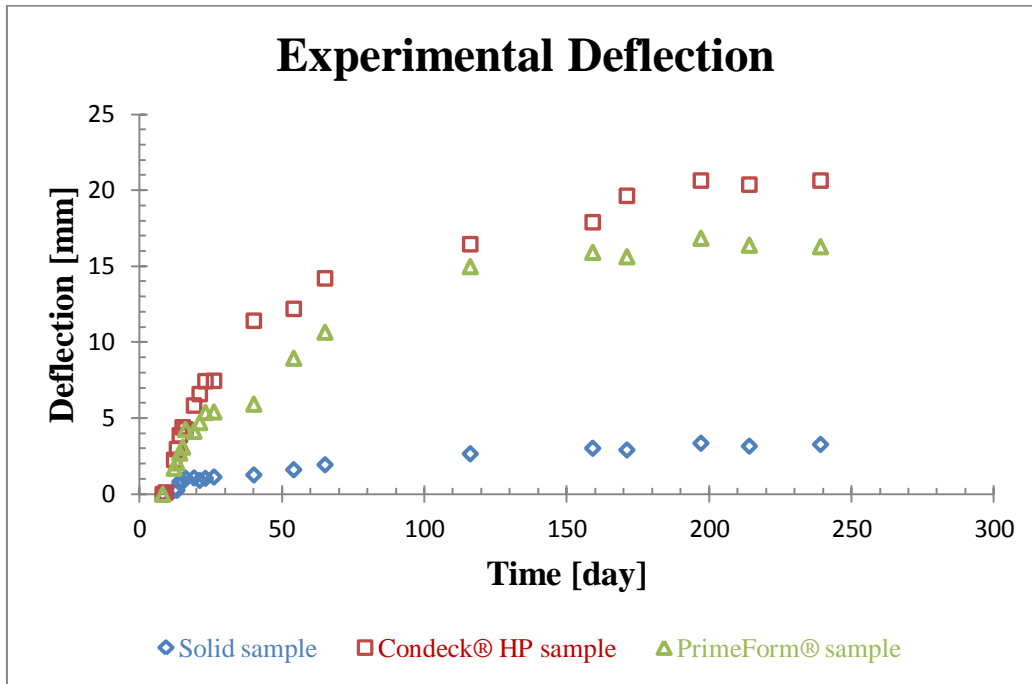
Figure 4.6– Experimental deflection for the three different slabs

The proposed method of analysis is able to predict the experimental measurements well as highlighted in Figure 4.7.
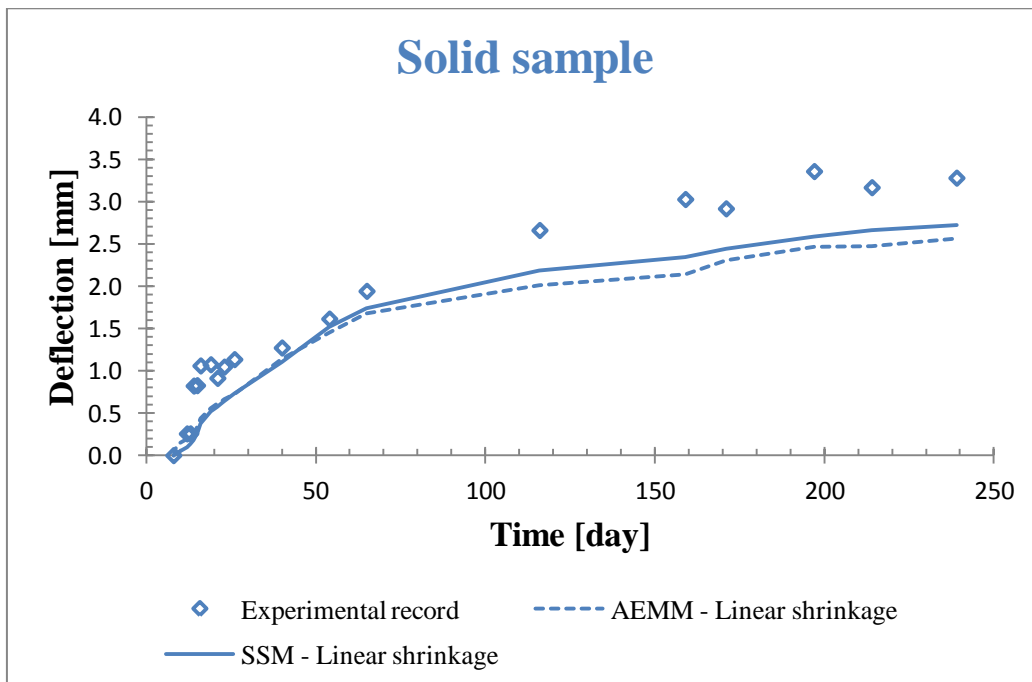
Figure 4.7 – Comparison of the deflections obtained through the numerical models and the experimental test for the "Solid sample"
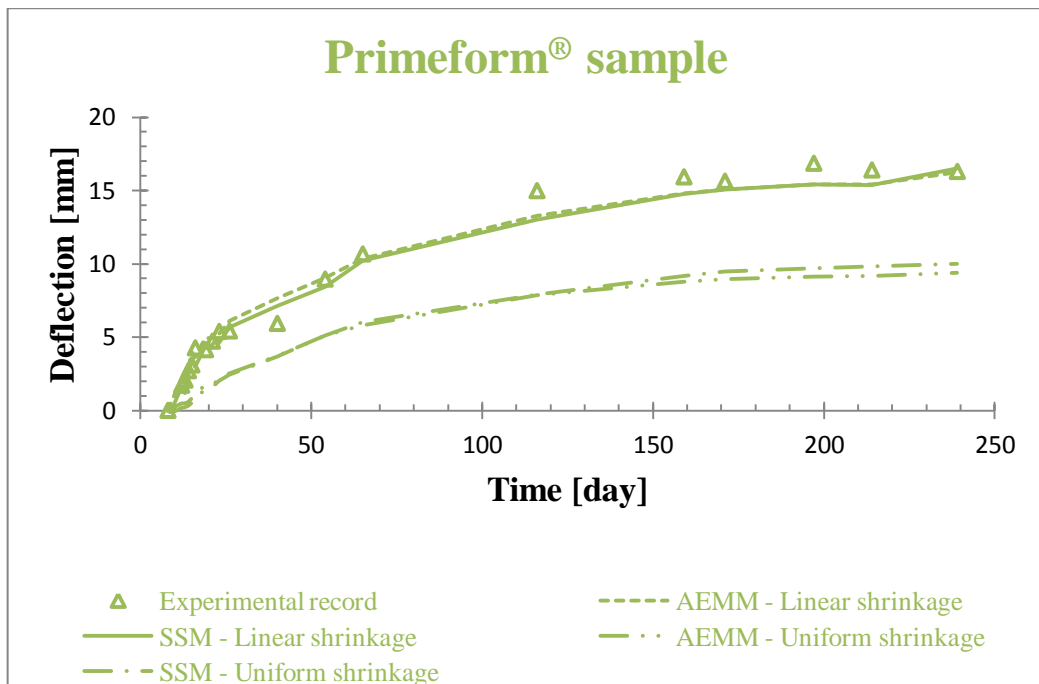
The same kind of comparison can be done for the Condeck HP and the PrimeForm slabs in Figure 4.8, and Figure 4.9. In these cases, the two analytical

models with linear shrinkage profile match the experimental readings well.
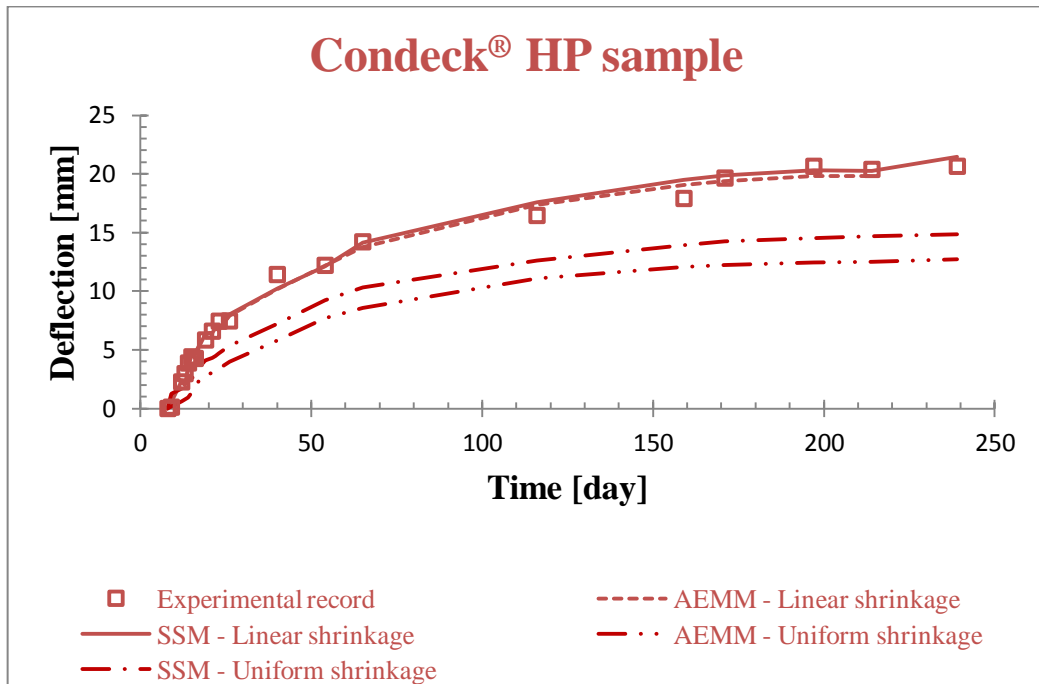
Figure 4.8 – Comparison of the deflections obtained through the numerical models and the experimental test for the "Condeck sample"

Figure 4.9 – Comparison of the deflections obtained through the numerical models and the experimental test for the "PrimeForm sample"

In the previous Figure 4.7, Figure 4.8, and Figure 4.9, for each of them, there are also plotted the curves in the case of constant shrinkage profile along the section. This casuistry underestimates evidently the real behaviour of the slabs in terms of deflections. And thus the designer should pay particular attention to the

shrinkage profile used because it is responsible for the final deflection.

This paragraph, in conclusion, has demonstrated how both the AEMM and the SSM are able to well predict the deflection and thus they can be considered reliable also in the following calculation of the deflection for the reinforced concrete slabs.

Chapter 5

Experimental program

"Engineers like to solve problems. If there are no problems handily available, they will create their own problems."
[Scott Adams]

5.1 Overview

The aim of this project is to investigate the behaviour of reinforced composite slabs under service loadings when part of the cross section results cracked and how the shrinkage can interfere with this behaviour. The experimental study involved the fabrication of 10 slabs with different configurations and several samples for the shrinkage measurements. The main difference among the slabs was that 4 of them were stored in the fog room, a room with a 100% constant humidity, and the other 6 were taken in the laboratory at open air. There are also differences in terms of number of reinforcement and instrumentation used. After more than a month after the cast, the cross section of the slabs were partially cracked with a hydraulic jack and then the slabs were subjected to three different constant loads applied through some weight. The test enabled to have a better idea on how shrinkage and creep develop in the case of cracked cross section and how they influence the general behaviour in terms of deflections.

All the samples were monitored through a data logger and record of deformations and redistribution of stresses between concrete and steel were taken every hour, 24 hours per day.

Shrinkage samples were used to measure shrinkage and to obtain a profile through the cross section. In addition, the shrinkage sample stored in the fog room together with the main slabs gave an indication on how shrinkage is avoided in case of 100% humidity environment.

The relevant dates of the experiment were:

6 October 2011: concrete pour of the 10 slabs and all the samples used for shrinkage measurements

7, 8 and 9 December 2011: partial cracking of the cross section of all the slabs and following application of the sustained load

5.2 Specimens description

There are two main categories of specimen: shrinkage samples and simply supported slabs. The first category is used to get data of shrinkage in order to use them as input in the following numerical analysis to obtain theoretical deflections, while the second category is the heart of this laboratory project and will provide the experimental deflections. In particular, these two categories and their preparation are explained in the next section

5.2.1 Shrinkage and creep samples

There are three different kinds of shrinkage samples:

 2 cylinders (Φ 150mm diameter and 300 mm high);

 1 non standard prism (500 mm x 100 mm x 100 mm);

 3 standard prisms (280 mm x 75 mm x 75 mm).

They are shown all together in the following Figure 5.1.

Figure 5.1 – Shrinkage samples

The standard prisms present a couple of Demec targets glued on the surface of the concrete on two opposite sides, while the non standard prism has a couple of targets on three over four edges. The shrinkage readings taken from the prism are used directly in the numerical model as shrinkage coefficient and the two opposite sides represent the top and the bottom surface of the simply supported slabs, and thus they allow a linear shrinkage distribution through the cross section.

The prisms are collocated on two little pieces of wood in order to permit the air to surround all the faces of the samples and to avoid the limitation of the shrinking effects on certain sides. There is also an additional reason because of the prisms are seated on these timber joists. When the operator takes the reading, the targets under examination are on the top surface of the prism, and consequently the other couple, at the opposite side of the sample, is on the bottom surface. If the bottom surface, and thus also the target couple, touches directly the support surface, the target can be altered or exposed to some force and the reading can be damaged. Thus using a couple of timber joist, this problem is avoided and the target will never touch any surface. The arrangement procedure adopted can be seen in the following Figure 5.2 and Figure 5.3.

Figure 5.2 – Standard prism (280 mm x 75 mm x 75 mm)
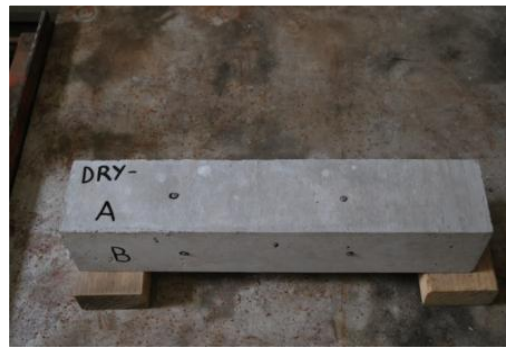
Figure 5.3 - Non standard prism (500 mm x 100 mm x 100 mm)

The three cylinders shrinkage readings do not deal directly with shrinkage. In fact, since in the test there is also a deformation component due to creep, and since it is not possible to calculate it independently from shrinkage, the idea is to calculate first the shrinkage in a dependent way and then obtain the creep subtracting the shrinkage component from the total one. More in detail, the same day of the cracking and the loading of the slabs, creep will start in the slabs. To measure it a machine called creep rig is set up. This device will provide a global deformation consisting of the sum of the shrinkage and the creep components; but since the analytical model requires two different components, the only chance is to obtain creep subtracting the shrinkage to the total deformation. And to do so, it is necessary to calculate shrinkage first.

Since the creep rig machine works with cylindrical samples, shrinkage should be measured directly on cylindrical samples. The disposal of the Demec target on the sample is equal to the one used on the prism, and thus on two opposite side.

54

The unique difference is that for cylinders the distance to be used between the two targets must be 100 mm, in order to avoid border effects. Actually, on that sample, as you can appreciate with attention from Figure 5.4, there are four Demec targets and they all allow for both the 100 mm and 200 mm readings. This was done because the laboratory supervisor wanted to collect border effects data, but this evaluation does not concern the present thesis work.

Figure 5.4 - Cylinder (Φ 150mm diameter and 300 mm high)

Usually, cylinders are stored in a vertical position, to reduce as much as possible deformations not due to shrinkage, but for the reading it is easier to seat the sample horizontally. Because of the same reason explained before, it is highly recommended to seat the sample horizontally on two timber joists during the reading process, as shown in Figure 5.4.

An exact copy of the samples described up to here are stored also in the fog room because the test requires also some samples in which the shrinkage is avoided, at least until the day in which the slabs are taken off the fog room, cracked and loaded. Some pictures of the shrinkage samples stored in the fog room are shown in Figure 5.5, Figure 5.6 and Figure 5.7.

Figure 5.5 – Shrinkage samples and slabs stored in the fog room

Figure 5.6 – Shrinkage prisms stored in the fog room

Figure 5.7 – Shrinkage cylinder stored in the fog room

5.2.2   Simply supported slabs

5.2.2.1 General description

The ten reinforced slabs prepared for the test are shown in the following Table 5.1. They differentiate in terms of number of bars, type of curing of the specimen after the pouring, load level to apply after the cracking and presence or not of strain gauges on the steel bars.

56

SLAB NAME	NUMBER OF REINFORCEMENT	TYPE OF CURING	LOAD LEVEL	STRAIN GAUGE
DRY3-1A	3	8 days wet	1 (large)	Yes
DRY3-1B	3	8 days wet	1 (large)	No
FOG3-1A	3	Fog room	1 (large)	Yes
FOG3-1B	3	Fog room	1 (large)	No
DRY3-2A	3	8 days wet	2 (medium)	Yes
DRY3-2B	3	8 days wet	2 (medium)	No
FOG3-2A	3	Fog room	2 (medium)	Yes
FOG3-2B	3	Fog room	2 (medium)	No
DRY2-3A	2	8 days wet	3 (small)	Yes
DRY2-3B	2	8 days wet	3 (small)	No

Table 5.1 - Characteristics of the ten simply supported slabs

The layout and the relevant dimensions of a slab with three reinforcing bars is reported in the following Figure 5.8.
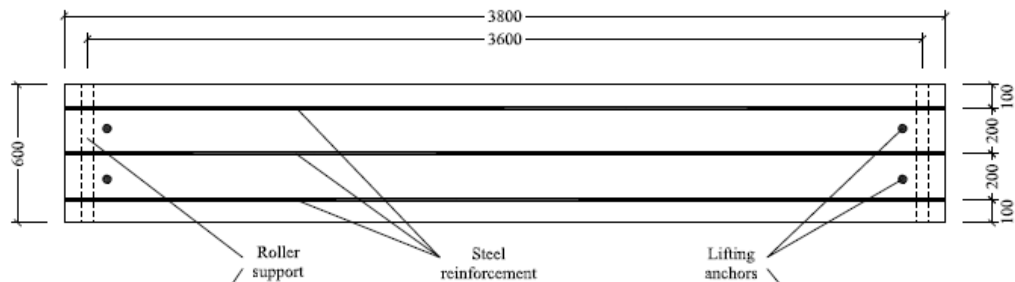
Figure 5.8 – Plane view of the slab with three reinforcing bars

In the following Figure 5.9 and Figure 5.10 are shown the slabs soon after the pouring phase, respectively stored in the structural laboratory at environmental conditions and in the "fog room" at a 100% relative humidity condition.

Figure 5.9 – Poured slabs stored in the structural laboratory at environmental conditions

Figure 5.10 – Poured slabs stored in the "fog room" at 100% humidity condition

5.2.2.2 Lifting anchors

Since the test comprises the movement of the concrete slabs more than once

after their pouring, the slabs have a couple of lifting anchors on the two borders. The problem is particularly relevant once the slabs are cracked and should be moved from the testing rig to their final position on the supports for the long term analysis. For this reason, and since after the cracking the middle part of the slab is the weak point, the idea was to lift each slab with a steel beam from the borders. The steel beam is designed to be of the same length of the slabs and it is connected to them through small chains strained in a vertical direction. The steel beam is, in turn, lifted by a forklift. In this way, the movement of the slab is easier, faster and safer.

Figure 5.11 – Lifting anchors before the pour

Figure 5.12 – Detail of the lifting anchors before the pour

Figure 5.13 – Anchors and steel beam before the lifting of slab

Figure 5.14 – Handling of the slab from the concrete laboratory to the structural laboratory

5.2.3 Loads

Three main categories of concrete blocks have been built to be use as loads when the slabs are cracked; their dimensions are:

4 large concrete blocks (1800 mm x 500 mm x 470);

4 medium concrete blocks (1800 mm x 500 mm x 270);

2 small concrete blocks (1800 mm x 500 mm x 200).

Figure 5.15 - 4 medium concrete blocks   **Figure 5.16 - 2 small concrete blocks**

5.2.3.1   Design procedure of the load used in the test

This small sub paragraph shows the procedure adopted to design the dimension of the load used in the test. The length and the width of the loads are fixed from the beginning for all the load levels, while the height is the dimension which varies according to the stress level imposed in the steel. The comparison is done between two moments, one calculated through the structural scheme adopted in the load phase and the other through the modular ratio theory.

The bending moment at a certain cross section, according to the modular ratio theory, is calculated through a linear elastic analysis and it is based on the following assumptions:

- plane section remains plane;

- perfect bond between concrete and reinforcing bars;

- stress-strain relationships for both concrete and steel are linear and elastic.

The steel reinforcing bars are treated as an equivalent concrete area by multiplying their area with the modular ratio n (where $n = E_s / E_c$), while the other cross-section properties are calculated based on structural analysis concepts. In this analysis, concrete cannot carry any tension stress once it is cracked. This procedure, known as *modular ratio theory*, does not account for time-dependent deformation due to shrinkage and creep, and it does not include tension stiffening effects.

Assuming a rectangular concrete cross section, as the one represented in Figure 5.17 with a bottom reinforcing steel layer and subjected to an applied

moment M, two main unknowns should be taken into consideration regarding the stresses and the deformations: the depth of the neutral axis $d_n = kd$ and the top fibre compressive strain ε_{top}.

(a) Cross-section   (b) Strains   (c) Stresses   (d) Forces
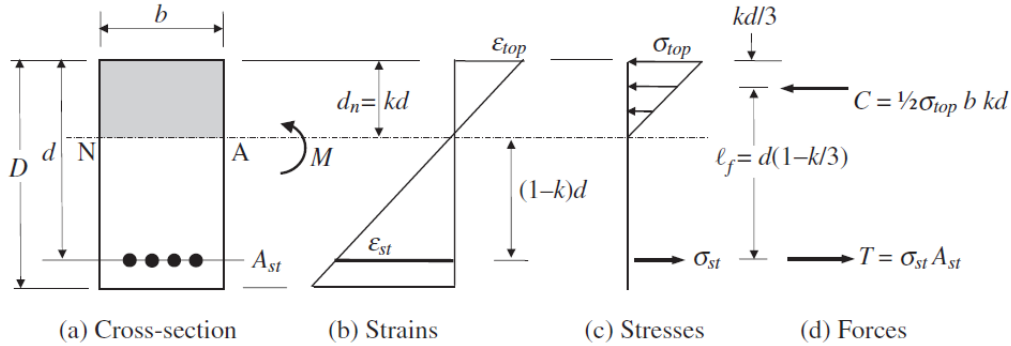
Figure 5.17 – Strains, stresses and forces on a cracked section in bending (15)

The neutral axis depth can be calculated enforcing the equilibrium of longitudinal forces between the resultant compressive and tensile forces:

$$C = T$$
$$0.5\sigma_{top}bkd = \sigma_{st}A_{st} \tag{5.1}$$

Assuming linear–elastic stress-strain laws for the compressive concrete and the reinforcement, equation (5.1) becomes:

$$0.5k = \frac{\sigma_{st}}{\sigma_{top}}\frac{A_{st}}{bd} = \frac{\varepsilon_{st}E_s}{\varepsilon_{top}E_c}\frac{A_{st}}{bd} = \frac{\varepsilon_{st}}{\varepsilon_{top}}n\rho \tag{5.2}$$

where ρ is the tensile reinforcement ratio A_{st}/bd. According to compatibility, the strain diagram should be linear and thus:

$$\frac{\varepsilon_{st}}{\varepsilon_{top}} = \frac{(1-k)d}{kd} = \frac{1-k}{k} \tag{5.3}$$

Substituting equation (5.3) into equation (5.2) gives:

$$0.5k = \frac{1-k}{k}n\rho \tag{5.4}$$

and solving this quadratic equation for k gives:

$$k = \sqrt{(n\rho)^2 + 2n\rho} - n\rho \tag{5.5}$$

As it can be seen from the previous equation, the quantity k, and thus also the depth of the neutral axis, depends only on the reinforcement ratio ρ and the

modular ratio n, while it is independent from the applied moment M. The depth of the neutral axis remains constant after cracking as the moment increases, until either the reinforcing steel yields or the concrete compressive stress distribution becomes curvilinear.

Once the quantity k is determined, the top fibre concrete stress σ_{top} and the steel stress σ_{st} can be found from the moment equilibrium equation:

$$M = Cl_f = Tl_f = \frac{1}{2}\sigma_{top}bdk^2\left(1-\frac{k}{3}\right) = \sigma_{st}A_{st}\left(1-\frac{k}{3}\right) \tag{5.6}$$

and thus

$$\sigma_{top} = \frac{2M}{bd^2k\left(1-\dfrac{k}{3}\right)} \tag{5.7}$$

$$\sigma_{st} = \frac{M}{A_{st}d\left(1-\dfrac{k}{3}\right)} \tag{5.8}$$

As demonstrated in equations (5.7) and (5.8) the stresses in both the concrete and the steel depends linearly on the applied moment M. Starting from the assumed stress and strain distribution, the flexural rigidity of the cracked section $\left(E_cI_{cr}\right)$ may be calculated from the curvature as follows:

$$\frac{M}{E_cI_{cr}} = \frac{\varepsilon_{top}}{kd} = \frac{\sigma_{top}}{E_ckd} = \frac{2M}{E_cbd^3k^2\left(1-\dfrac{k}{3}\right)} \tag{5.9}$$

From equation (5.9), the second moment of area of the cracked section is:

$$I_{cr} = \frac{1}{2}bd^3k^2\left(1-\frac{k}{3}\right) \tag{5.10}$$

In our case, the unknown is not the stress in the steel reinforcement but the moment applied and thus expression (5.6) should be used. Actually, the moment applied can be obtained from the static scheme used in function of the height of the weight used as load. Using the isostatic scheme represented in the following Figure 5.18, the moment at the mid span can be calculated as follows:

$$M\left(x=l\right) = \frac{F+P}{2}l = \frac{1}{2}Fl + \frac{1}{2}Pl \tag{5.11}$$

where F and P represent, respectively, the weight of the concrete block used as load and the self weight of the slab. P is completely known, because the three dimensions are already known, while F is in function of the height of the block, the unknown quantity of the whole problem. They are:

$$\begin{aligned} F &= L_{load} b_{load} D_{load} \rho_{concrete} = \\ &= 1800 \cdot 500 \cdot D_{load} \cdot 24 \cdot 10^{-6} = \\ &= 21.6 \cdot D_{load} \left[N \right] \end{aligned} \tag{5.12}$$

$$\begin{aligned} P &= L_{slab} b_{slab} D_{slab} \rho_{concrete} = \\ &= 3600 \cdot 600 \cdot 180 \cdot 24 \cdot 10^{-6} = \\ &= 9331.2 \left[N \right] \end{aligned} \tag{5.13}$$
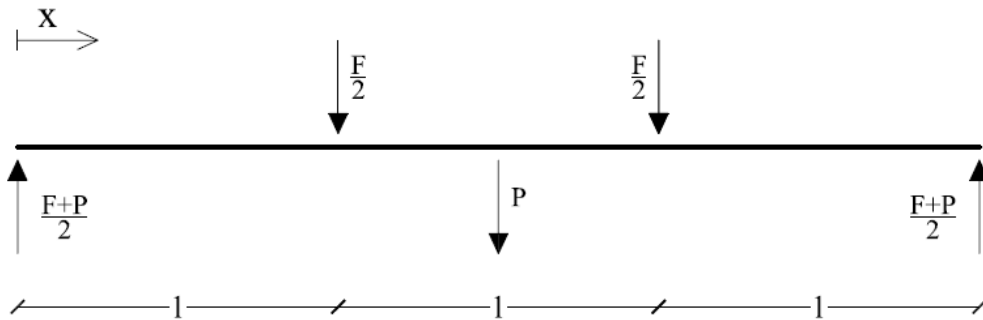
Figure 5.18 – Static scheme used for the calculation of the load to use in the test

Imposing the equality between equations (5.6) and (5.11), and solving respect D_{load}, after some analytical passages the expression becomes:

$$D_{load} = \frac{\dfrac{2}{l}\left(M - \dfrac{1}{2} Pl \right)}{L_{load} b_{load} \rho_{concrete}} \tag{5.14}$$

Using this last expression, it is now possible to calculate what required. In the following Table 5.2 are reported the values of the final load heights according to the steel stress level and the properties of the reinforcement bar chosen.

Steel stress	*Reinforcement*	*L_{load}*	*b_{load}*	*D_{load}*
269 MPa	3Φ12	1800	500	470
204 MPa	3Φ12	1800	500	270
269 MPa	2Φ12	1800	500	200

Table 5.2 – Load block height according to the steel stress level and the reinforcement bars chosen

5.3 Experimental procedure

5.3.1 Shrinkage samples and creep rig

A couple of cylindrical shrinkage samples, both the "environmental condition" ones and the "fog room" ones, are monitored with a couple of concrete strain gauges to record how the shrinkage developed in time. In addition other three "environmental condition" and three "fog room" cylindrical samples, always with a couple of strain gauges attached for each of them, are used in the creep rig to obtain the measure of creep. The creep rig machine is reported in the following Figure 5.19.

Figure 5.19 – Creep rig device

Since the creep rig gives both the shrinkage and the creep deformations together, the pure creep strain can be measured subtracting from the total deformation the shrinkage one, which is known from the samples monitored with strain gauges, but without any applied load.

5.3.2 Simply –supported slabs

The aim of the project is to monitor the behaviour of the slabs for a long period under a certain load comparable to a serviceability load condition in the case of a cross section partially cracked.

The same experimental procedure is followed for all the ten slabs. The test provides that the slabs rest on a couple of rolling supports under their self weight and a certain load. For more details refer to the scheme reported in APPENDIX A to appreciate the typical exact final setup of the slabs. Below are summarized

the main operations from the day of the pour, defined as day 0, to the final configuration of the test when the measurement started to be recorded.

Day 0:

Concrete is poured in the formwork

At this stage, the "8 days wet" slabs are sustained by a system of small timber props on the entire length, while the "fog room" slabs are sustained on wheeled trolley to permit their movement in the fog room after the pouring

Curing operations start for both the "8 days wet" and the "fog room" slabs

Day 4:

Removal of the formwork

Day 8:

Last day of curing operations for the "8 days wet" slabs

Days 62,63 and 64:

Test phase 1 - Cracking of the cross section for all the slabs

Test phase 2 - The slab is simply supported and the sustained load is applied

Test phase 3 - Start to record the deformations and the deflection in the specimen

5.4 Instrumentation

Although results are fundamental in any kind of test, before obtaining them, it is necessary to organize a reliable system of instrumentation. Independently from the accuracy taken in the specimen preparation, if the instrumentation is not set correctly, all the results can be affected by errors and consequently also their reliability decreases. A good instrumentation preparation provides:

identifying all the relevant variables which must be monitored;

identifying the location on the specimen where the measurement device should be installed and check any possible problem;

planning the final position of the specimens taking into account that space among them should be enough to allow the following readings, but also that space in the laboratory is limited and it is shared with other people; especially in long-term test, space becomes fundamental because, once you start to take the reading, cannot be displaced and thus you must be sure that the planning chosen

at the beginning fits the needs of all the people in the laboratory and the one of the test itself;

be sure that the installed devices do not interfere with the general behaviour of the specimen;

keeping tracking of the instrumentation setting through detailed drawing in order to allow possible future changes;

organizing and storing the results in spreadsheets in order to facilitate the following treatment of the data.

All these factors grow in importance with the increase of the number of specimens and of the number of devices used for measurements. In this test, there are at least four different kind of measurement devices, as it can be seen in the next paragraph, and three main categories of parameters observed: deformation, displacements and temperature. Deformations were taken both inside and outside on the surface of the slabs, while displacements regard essentially the deflection at the mid span of the slab. Temperature is also fundamental because it gives an idea on how the test is influenced by its changes. Thus, as it can be seen, in this test the planning of the instrumentation of the ten slabs is fundamental and it requires a lot of time to be satisfactory.

5.4.1 Measurement devices

5.4.1.1 Demec targets

This measurement technique allows to measure the deformation at a certain point located on the specimen surface. The system works with two targets and an electronic device capable of taking readings from the two targets. The targets should be glued on the specimen surface aligned in the same direction of the one in which deformation will be calculated, while the electronic device has a precision of 1/1000 of a millimetre. There are two electronic devices and they differ because one is 200 mm long while the other is 100 mm long. The first one is used for measurements on prismatic samples while the 100 mm long is used for cylindrical sample, in order to avoid border effects.

Figure 5.20 - Target　　**Figure 5.21 – Two electronic devices (200 mm and 100 mm long)**　　**Figure 5.22 – Measurement with a Demec target**

Figure 5.23 – Reading on the display of the device

Assuming certain lengths l_0 , l_1 , ... , l_j respectively at time τ_0 , τ_1 , ... , τ_j , the deformations can be calculated as $\dfrac{l_1 - l_0}{l_0}$ at time τ_1 or $\dfrac{l_j - l_0}{l_0}$ at time τ_j .

The real advantages of this device is that it can be installed everywhere, on any kind of material and the reading can be taken also from a not expert person. The disadvantages are that the reading is manually, maybe not in a comfortable position, and it requires a certain amount of time, especially if the number of targets to check is high.

5.4.1.2 Strain Gauges Transducers

The strain gauge transducer is a device used to measure the deflection of the slab. It can be compared to an LVDT. This device is used both during the first phase of the test when the slabs are cracked and in the second one, during and after the application of the sustained load, for the long term deflection measurement. In the following Figure 5.24 and Figure 5.25 is reported this

device.

Figure 5.24 – Strain gauge transducer

Figure 5.25 - Strain gauge transducer

5.4.1.3 Strain gauges

As defined in (22), a strain gauge is a device used to measure the strain of an object. Invented in 1938, the most common type of strain gauge consists of an insulating flexible backing which supports a metallic foil pattern. The gauge is attached to the object by a suitable adhesive, such as cyanoacrylate. As the object is deformed, the foil is deformed too, inducing its electrical resistance to change. This resistance changement is related to the strain by the quantity known as the gauge factor, which can be read on the product box of the strain gauge.

There are several kinds of strain gauge according to the material under investigation, but in all the cases, their measurement can be read by a computer software and can be therefore recorded at a given frequency through the data logger.

In this test, strain gauges were installed only on the steel bar, more in detail there are 6 strain gauges for each bar instrumented (not all the steel bars in the specimen are instrumented); they are located in couples on opposite sides of the bar and their flexible backings go out from the formwork all on the same side, in order to reduce as much as possible their influence on the general behaviour.
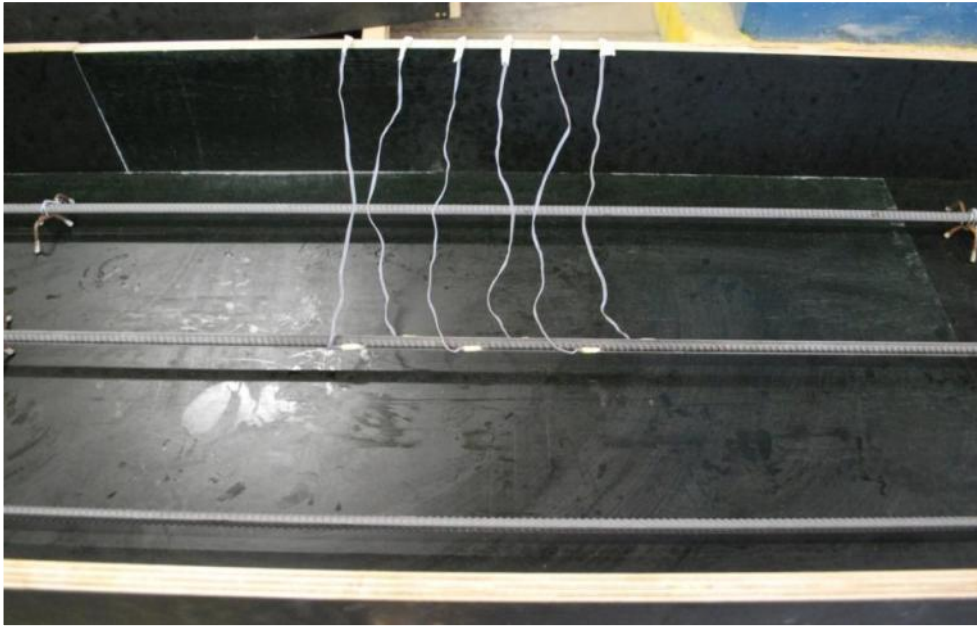
Figure 5.26 – Strain gauges installed on the steel bar

For more information regarding the installation of a strain gauge on the steel bar refer to APPENDIX B.

5.4.1.4 PI transducers

The PI displacement transducer has a simple structure: a combination of strain gauges and an arch-shaped spring plate, the former attached to the ends of the latter. There are several models depending from the gauge lengths. This transducer is used to measure the crack opening displacement occurring within each gauge length on the surface of concrete or to measure the displacement of various structures.

The features of this product are the stability of the measurement with a simple shape, the versatility of the gauge length and the easiness of handling it.

On this test, two PI transducers are used for each slab, both during the first phase and the second phase of the test. The two PI are located, respectively, on the top and bottom surface of the slabs, at the mid span, as it can be seen from Figure 5.27 and Figure 5.28.
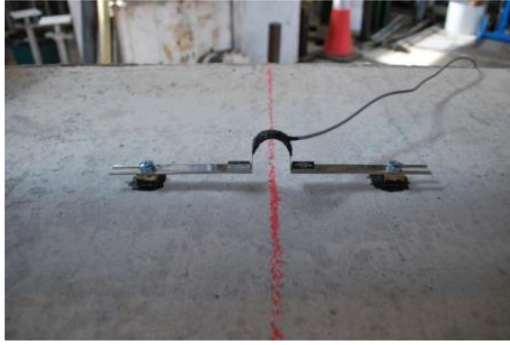
Figure 5.27 – PI transducer applied on the top surface of the slab

Figure 5.28 - PI transducer applied on the bottom surface of the slab

5.4.1.5 Data logger

A data logger is an electronic device that records data over time or in relation to location either with a built in instrument or sensor or via external instruments and sensors. In our case, the data logger collects the measurements taken by strain gauge transducers, steel strain gauge and PI transducer. Some data loggers interface with a personal computer and utilize software to activate the data logger and view and analyse the collected data, while others have a local interface device (keypad, LCD) and can be used as a stand-alone device. In this test a data logger interfaced with a personal computer has been used. Data loggers vary between general purpose types for a range of measurement applications to very specific devices for measuring in one environment or application type only.

One of the primary benefits of using data loggers is the ability to automatically collect data on a 24-hour basis. Upon activation, data loggers are typically deployed and left unattended to measure and record information for the duration of the monitoring period. This allows a comprehensive monitoring and an accurate picture of the environmental conditions, such as air temperature and relative humidity, and, most important for the scope of this project, deformations.

Figure 5.29 – Data logger front view

Figure 5.30 – Data logger back view

This test and the instrumentation used required a total of 80 channels.

5.4.2 Instrumentation layout

For more detail regarding the arrangement of the instrumentation on the slabs refer to the Autocad drawings reported in APPENDIX A.

Chapter 6

Shrinkage and creep results, experimental test and instantaneous and long-term results

"Theory is when we know everything but nothing works. Praxis is when everything works but we do not know why. We always end up by combining theory with praxis: nothing works and we do not know why."
 [Albert Einstein]

6.1 Shrinkage result

6.1.1 Before the experimental test

In this first paragraph of the chapter, there are reported the shrinkage graphs development, both for the "dry" and the "fog" samples, before the experimental test took place. More in detail, there is a graph for each kind of specimen monitored with the manual reading operations described before.

The first four graphs, relative to the "dry" samples, show a huge development of the shrinkage in time before the test take place: a value of around 500 microstrain is reached by all the samples. It is important to notice how the shrinkage starts to develop around the 10th day, because in the first week after the pour the specimens where subjected to some curing operation, as described in the previous chapter.
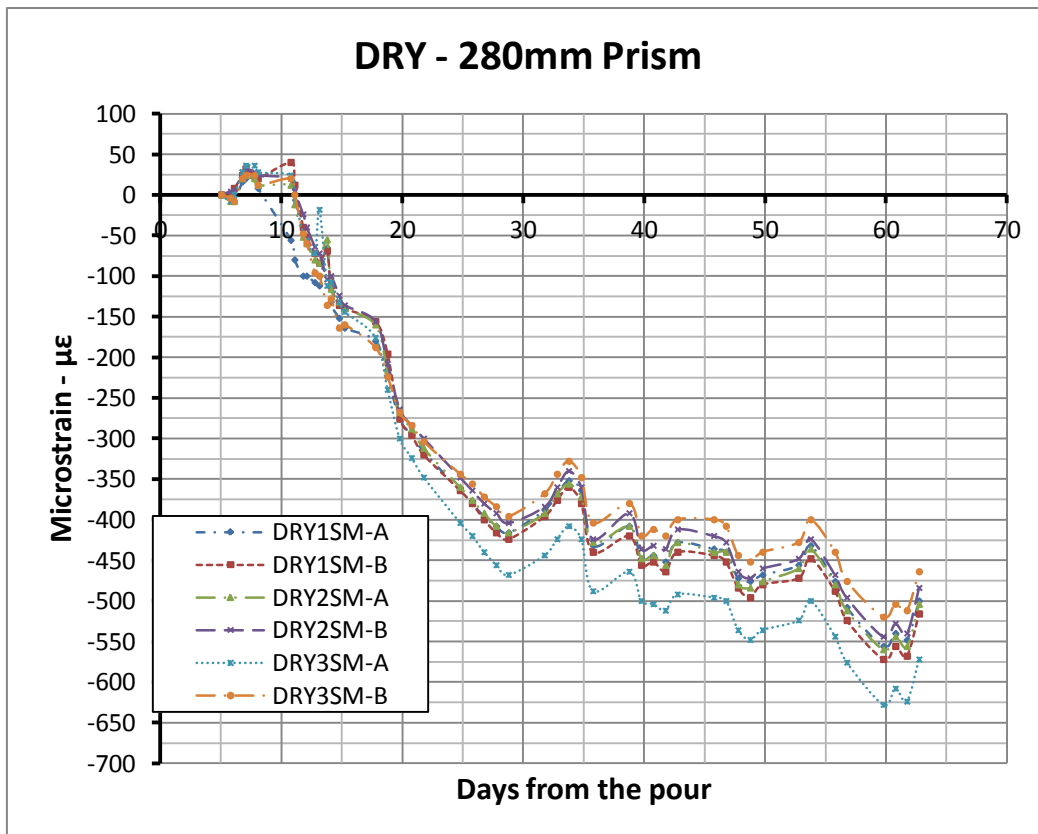
Graph 6.1 – Shrinkage values for the specimens "DRY – 280mm Prism"
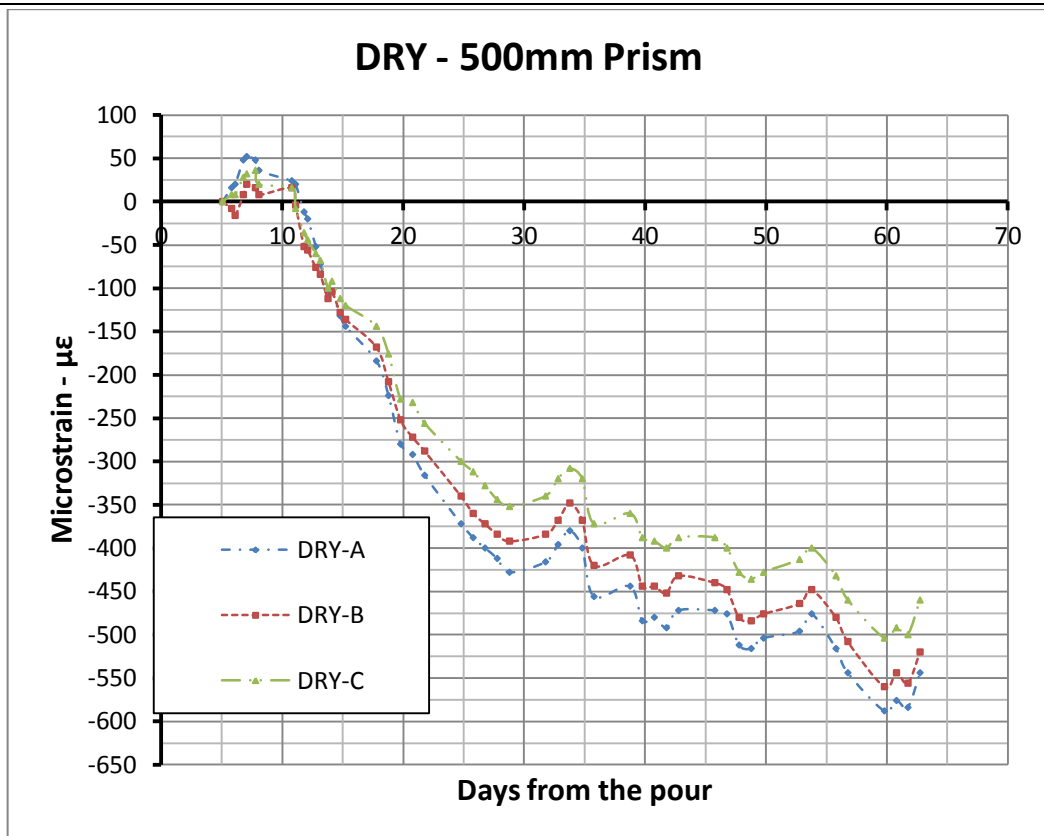
Graph 6.2 – Shrinkage values for the specimens "DRY – 500mm Prism"
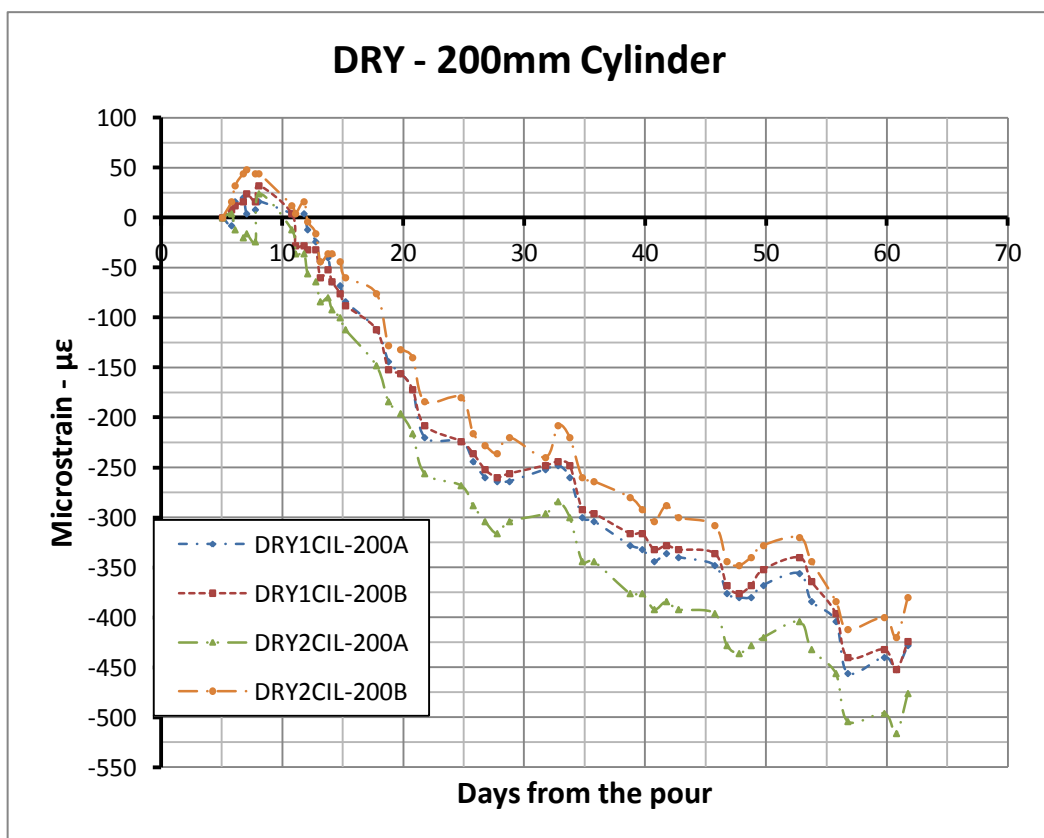
Graph 6.3 – Shrinkage values for the specimens "DRY – 200mm Cylinder"
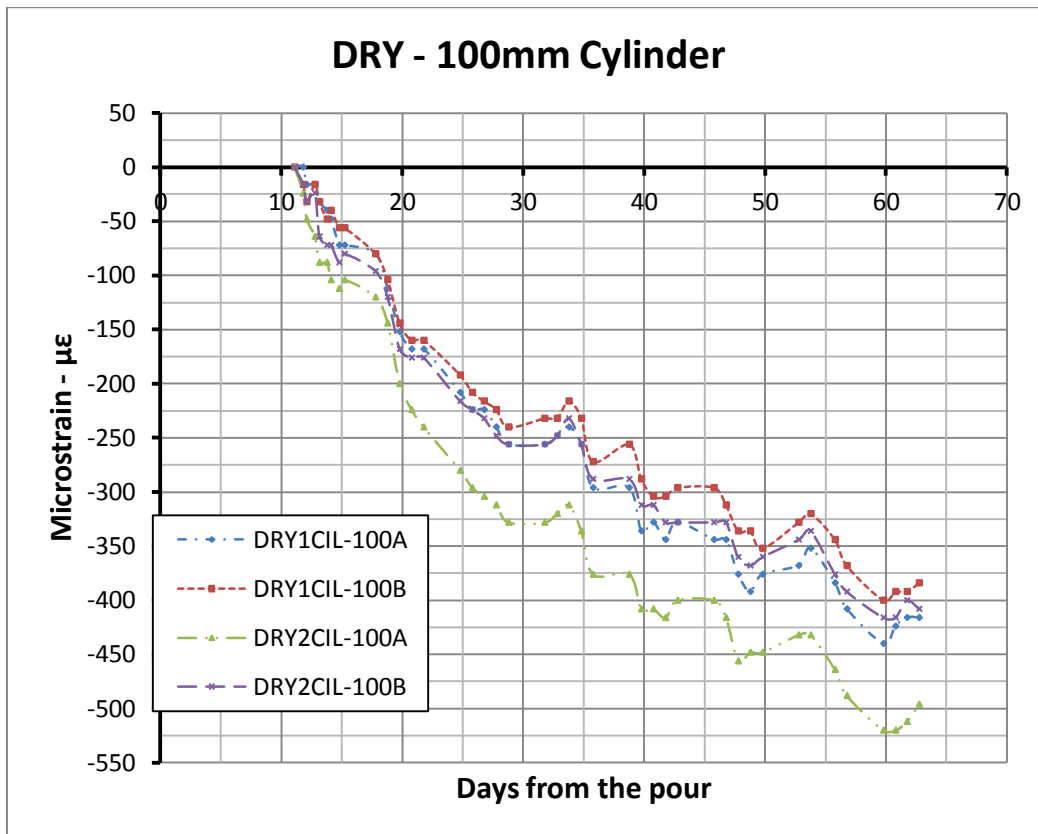
Graph 6.4 – Shrinkage values for the specimens "DRY – 100mm Cylinder"

From Graph 6.5 to Graph 6.8, the values of the shrinkage reported are relative to the "fog" samples. It is nice to see how also in those cases, the results are extremely consistent among all the kind of specimen. In fact, the value of the shrinkage bounces between -50 and +50 microstrain. This mean that the use of a room with 100% humidity as curing operation, avoid the development of the shrinkage effects on the samples. Obviously it is only a matter of delaying the development of the shrinkage and not to cancel it. For this reason it might be very useful for future studies regarding shrinkage and time-dependent effects.
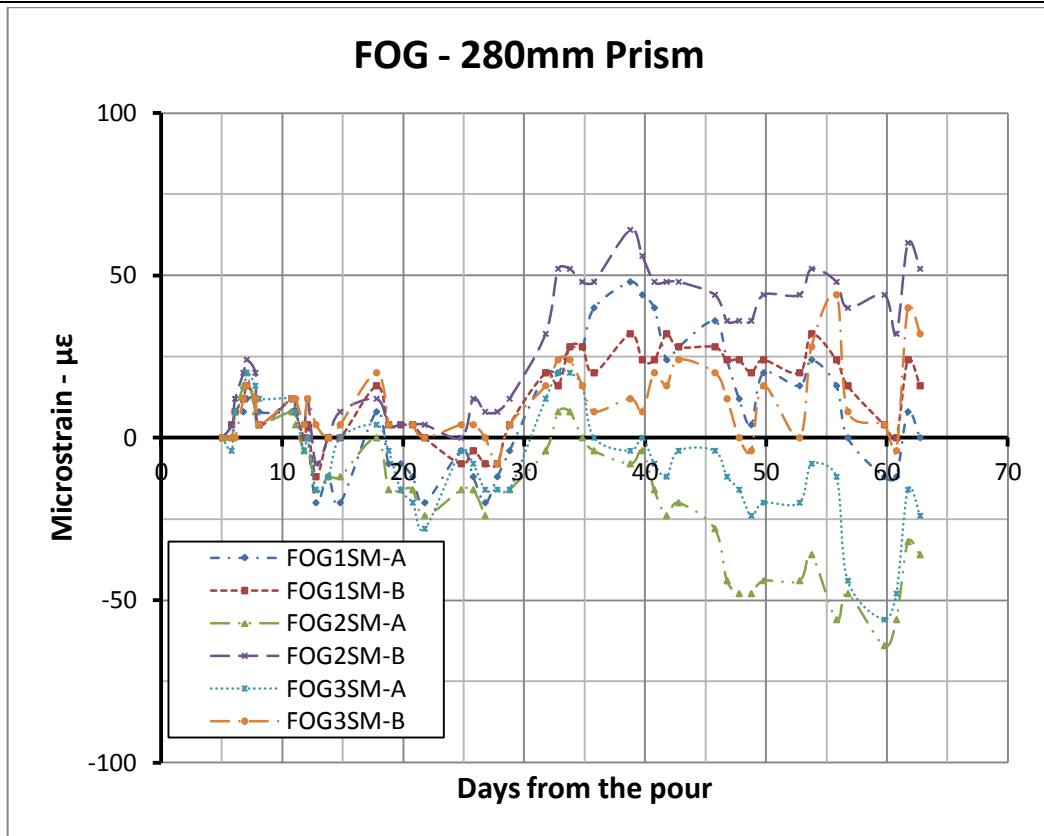
Graph 6.5 – Shrinkage values for the specimens "FOG – 280mm Prism"
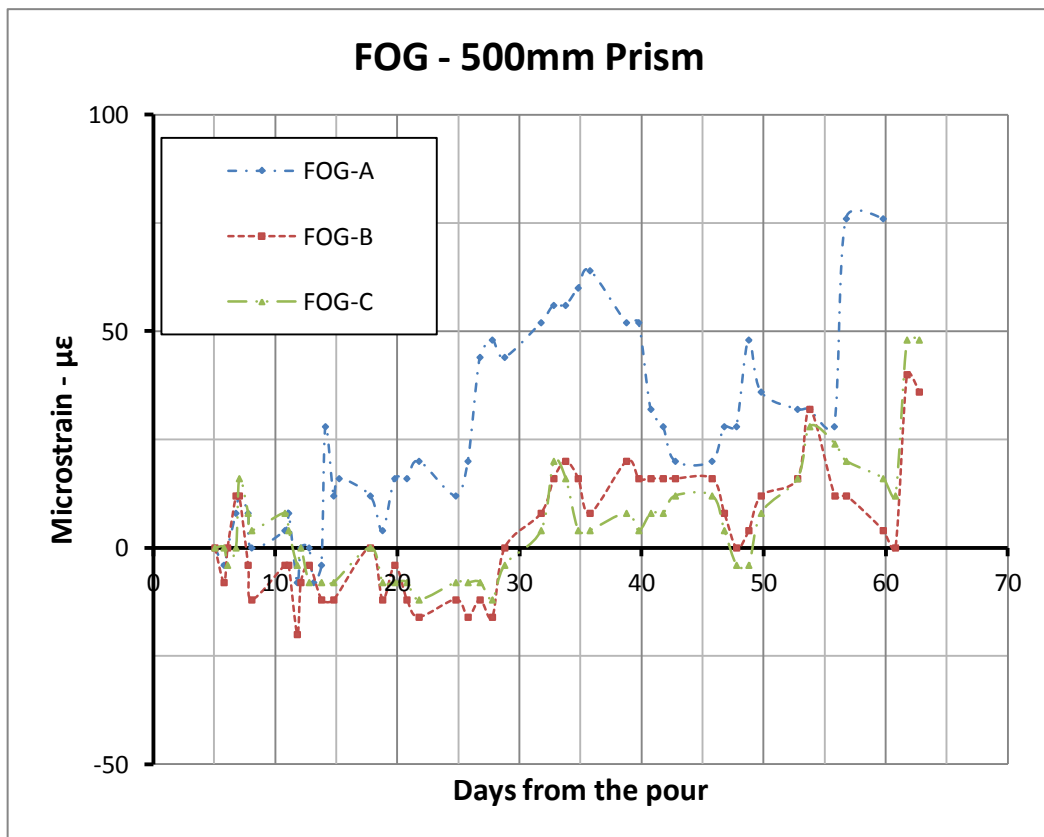
Graph 6.6 – Shrinkage values for the specimens "FOG – 500mm Prism"

75
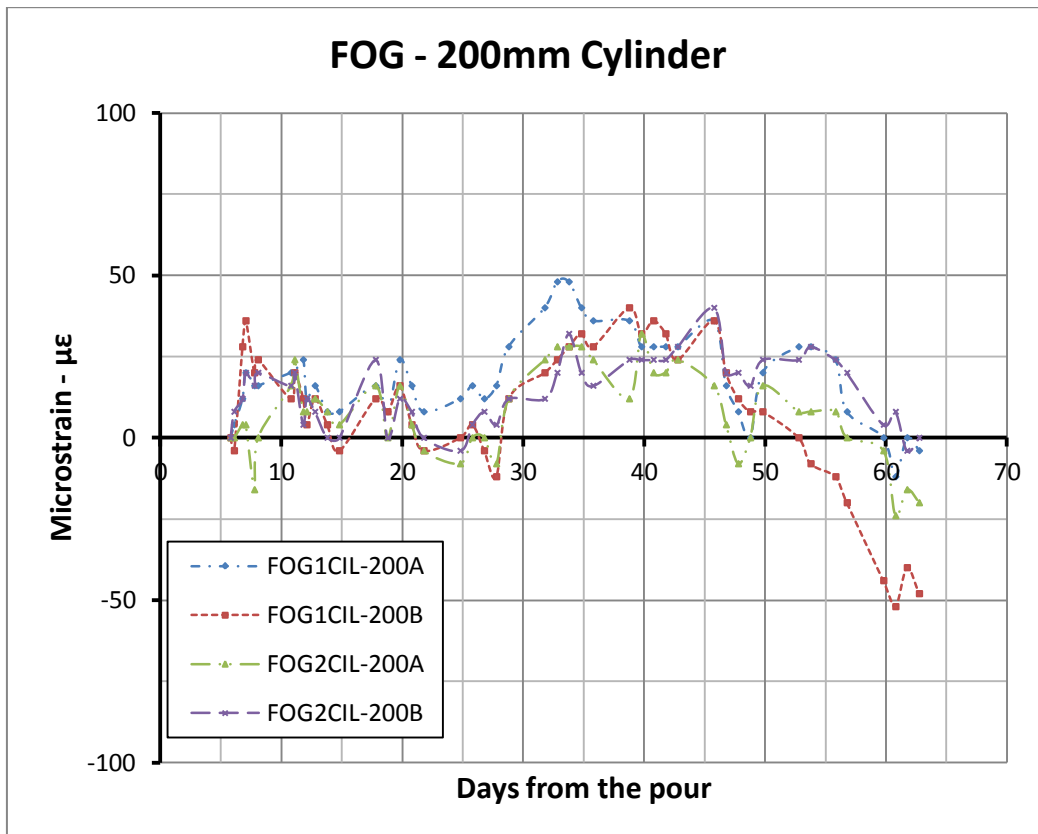
Graph 6.7 – Shrinkage values for the specimens "FOG – 200mm Cylinder"
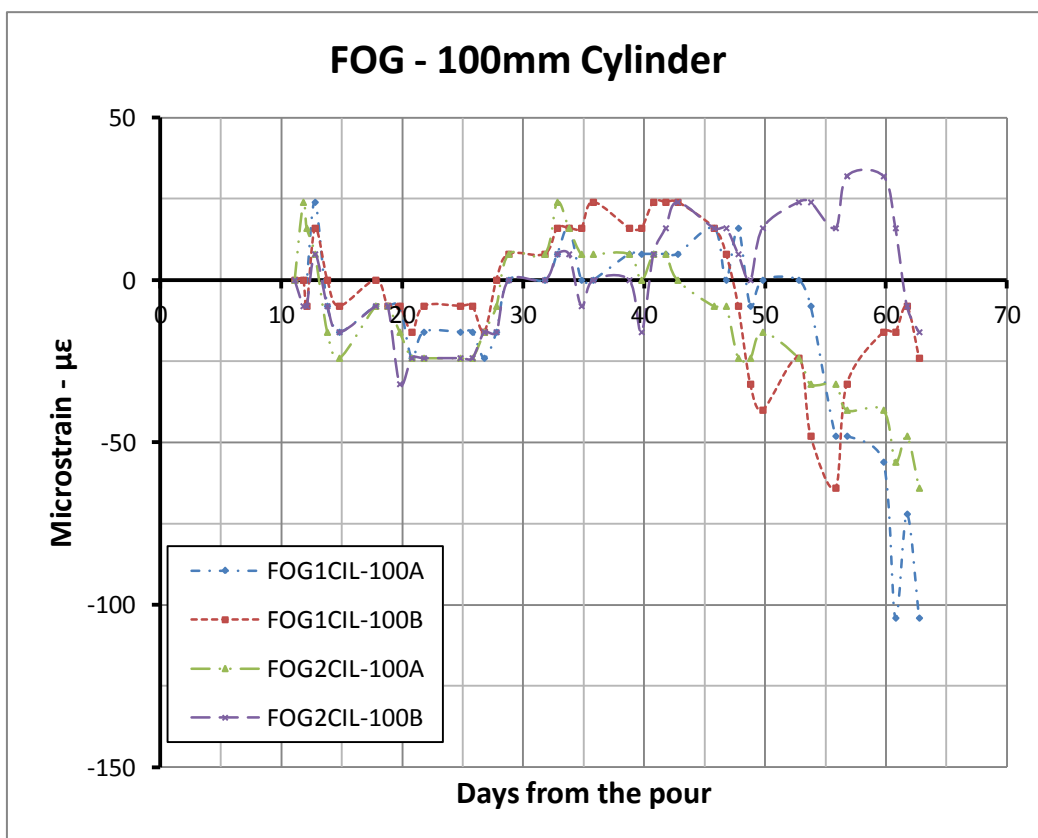
Graph 6.8 – Shrinkage values for the specimens "FOG – 100mm Cylinder"

6.1.2   After the experimental test

In this second part of the paragraph, there are the long-term shrinkage results. A couple of cylindrical samples, for both "dry" and "fog" conditions, are monitored with two concrete strain gauges each and the readings are recorded through the data logger. In this way the readings are continuous and do not present the uncertainty related to human errors that are present in the Demec manual readings used before the test.

After the experimental test, only the shrinkage measures on cylindrical samples are used, because they are the most reliable and useful for this kind of test. In the following Graph 6.9, the long-term shrinkage development for the "dry" specimens is reported. The analogous for the "fog" specimens is reported in Graph 6.10
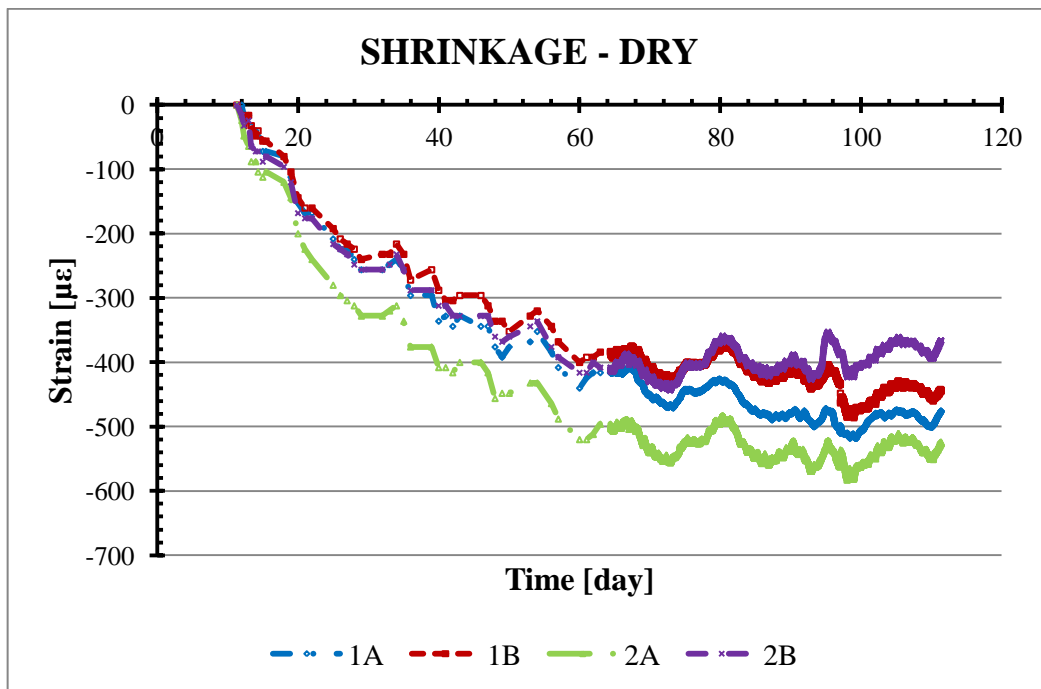

Graph 6.9 – Long-term pure shrinkage effects for the specimens "DRY – Cylinder". For an enlarged graph refer to APPENDIX D

Some important considerations must be done regarding these two graphs. First of all, for both the graphs, there are also the measures taken in the first 64 days between the pour and the experimental test, with the Demec readings. These are useful to understand how the shrinkage starts to develop as soon as the concrete dry after the pour and it does not depend from the load applied. The manual reading can be easily distinguished by the electronically ones because they are more sparse. In fact, there is only 1 manual reading for each day, while there are 144 electronic readings per day (one each 10 minutes). Regarding the "dry" samples, it is possible to see how the shrinkage effects tend to become less relevant in time, after the experimental test, respect to the initial period when they are really effective. On the contrary, this is not true for the "fog" specimens. In fact, these ones, as it was shown also in the previous Graph 6.8, since were stored in the fog room for the first 64 days, did not developed any relevant shrinkage before the experimental test; later on, 64 days after the pour, and thus after they are taken out from the fog room and exposed to normal environmental conditions, they start to develop shrinkage effects quite rapidly. On average before day 100, the specimens have developed 200 microstrains.

An important notice should be done regarding sample 1B of the SHRINKAGE – FOG series. As it can be noticed, there are some missing readings, approximately between day 64 and day 100. This is due to the fact that

the strain gauge installed on the specimen does not work properly and the readings taken in that period are not reliable. After the substitution of that strain gauge, the measures start to be reliable and thus reported in the graph.

6.2   Creep result

As discussed in Chapter 2, creep effect is stress dependent. Since creep and shrinkage effects develop simultaneously and since shrinkage cannot be stopped or avoided at environmental conditions, in order to calculate the pure creep, it is necessary to subtract the pure shrinkage effects from the total one. To do so in this test, the pure shrinkage is know from the results exposed in the previous paragraph 6.1; and thus what is missing is the total effect of both creep and shrinkage. This total effect is reported below in the following Graph 6.11 and Graph 6.12, respectively for "dry" and "fog" specimens.
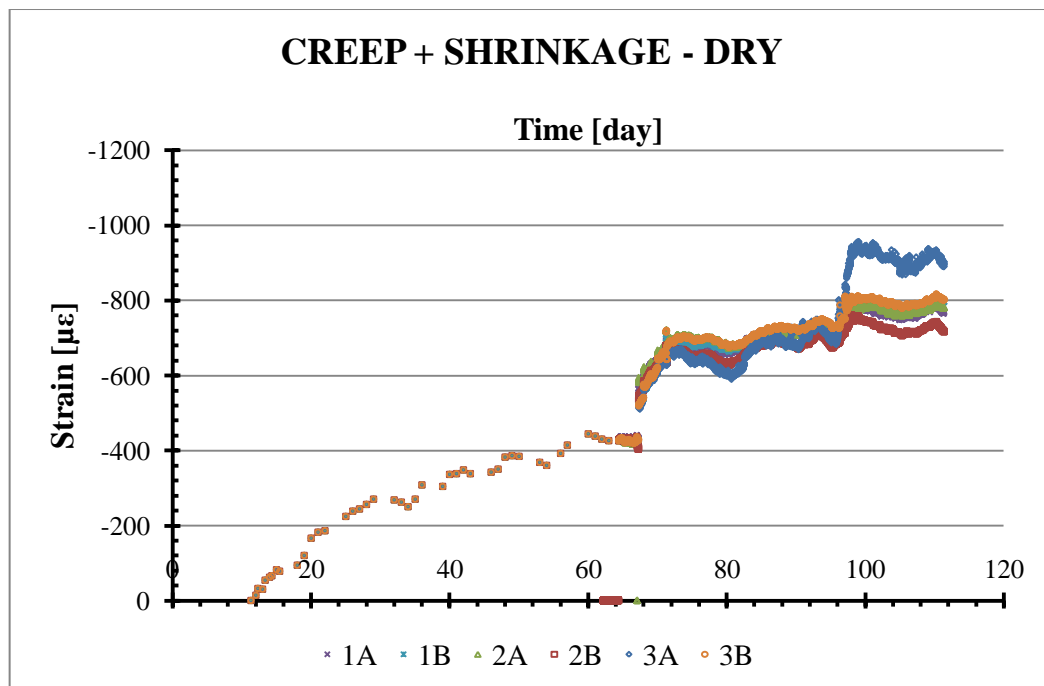
Graph 6.11 – Long-term creep + shrinkage effects for the specimens "DRY – Cylinder". For an enlarged graph refer to APPENDIX D
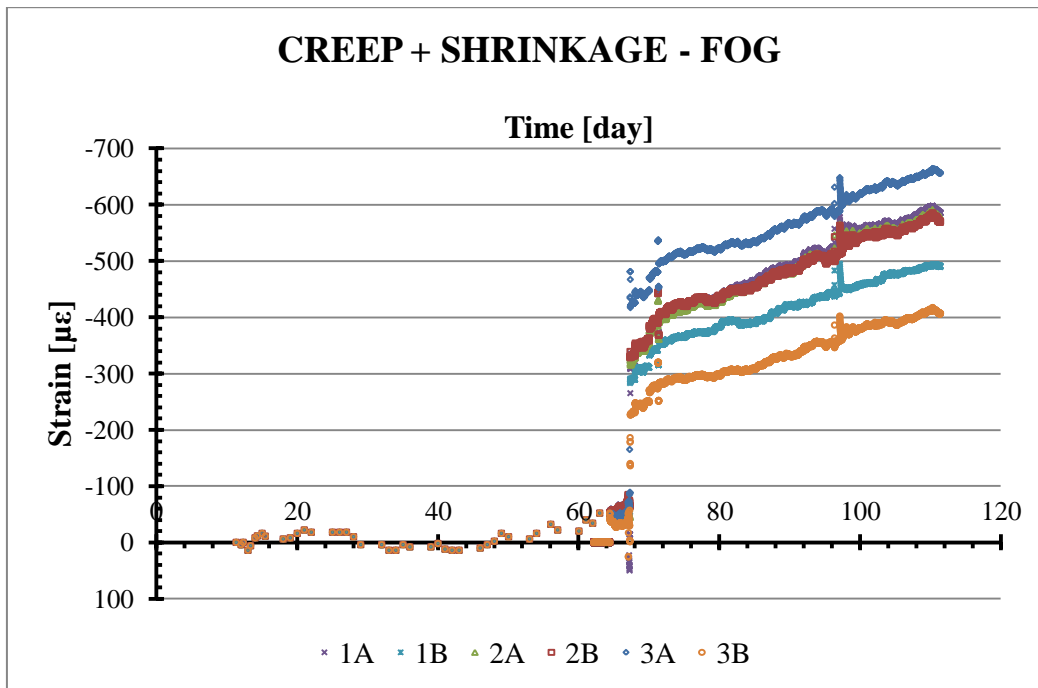
Graph 6.12 – Long-term creep + shrinkage effects for the specimens "FOG – Cylinder". For an enlarged graph refer to APPENDIX D

With reference to the most consistent part of these two graphs, it appears clear how the total effect (creep plus shrinkage) of the "dry" samples develop slower than in the "fog" samples. This is true because, as previously mentioned, the shrinkage effect in the "dry" samples at day 64 develops slower than in the "fog" sample.

As previously said, the pure creep effect can be obtained subtracting the shrinkage effect to the total one; the two graphs of the pure creep are reported below in Graph 6.13 and Graph 6.14.
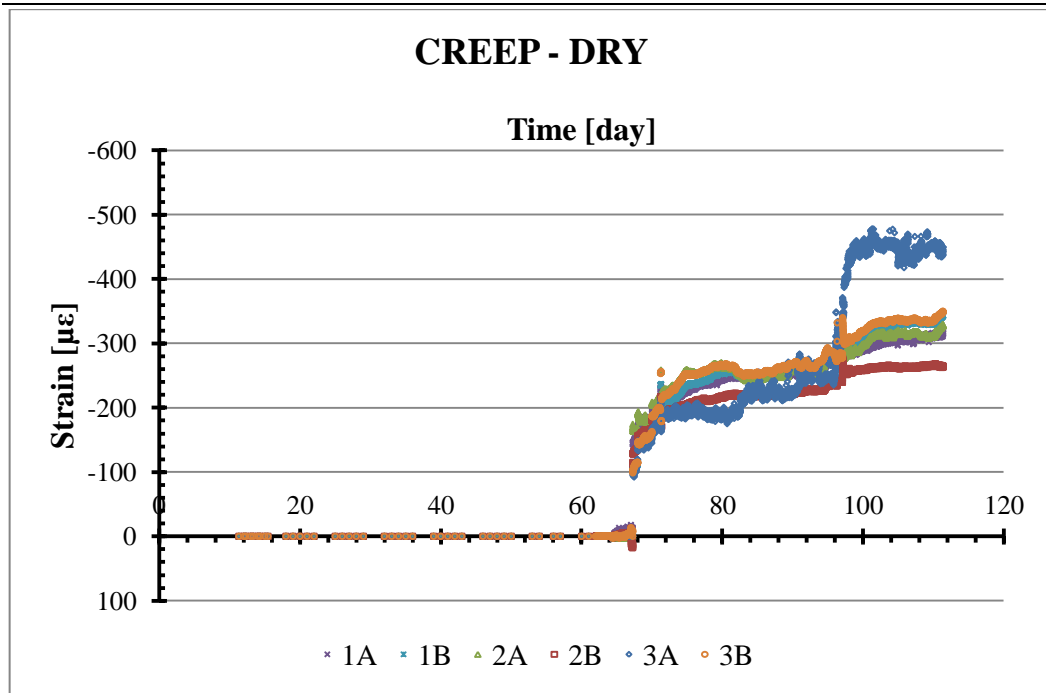
Graph 6.13 – Long-term pure creep effects for the specimens "DRY – Cylinder". For an enlarged graph refer to APPENDIX D
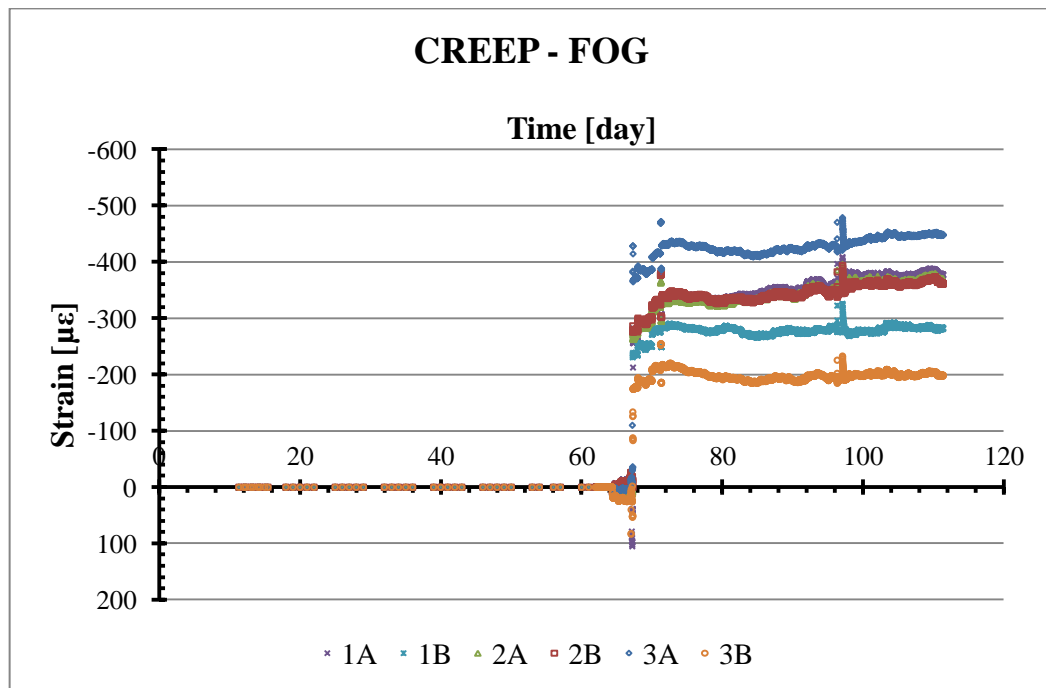
Graph 6.14 – Long-term pure creep effects for the specimens "FOG – Cylinder". For an enlarged graph refer to APPENDIX D

Since there are four shrinkage measurements, in the calculation of the pure creep, an average measure of them is used. In this way the presence of possible mistakes and local effects is smoothed. The creep propagation, as it can be seen from the two previous Graph 6.13 and Graph 6.14, is really similar, for both the "dry" and the "fog" samples, because the load and the external conditions are exact the same for both of them. It is really nice to see, around day 97, the little

81

jump presents in the graphs. This is due to the additional charging applied to the creep rig machine.

6.3   Experimental test

The experimental test can be divided in two phases. First, the slab is subjected to a load in order to create a series of cracks, and then the slab is positioned on two roller supports and it is subjected to a long-term sustained load. These two phases are shown, respectively, in Figure 6.1 and Figure 6.2.

Figure 6.1 – H-frame scheme used to crack the slabs during the first phase of the experimental test

Figure 6.2 – View of the slab subjected to the large sustained load during the second phase of the experimental test

Regarding the first phase, the load is applied at third points of the span through the use of a spreader beam in order to create several cracks along the middle part of the slab; the final cracking pattern, once the load has reached the desired value, is similar to the one represented in Figure 6.3. This pattern is similar to the one reached from common slabs after several years of activity and it is required because the final aim of the test is to analyse the behaviour of the reinforced concrete slabs in the case of several cracked cross sections.

Figure 6.3 – Cracking pattern reached in the slabs at the end of the first phase of the experimental test

6.4 Instantaneous results

In this first phase of the test, the results obtained in terms of cracking moments are significantly different between the "environmental condition" and the "fog room" slabs. This difference derives from the different hydration, and thus shrinkage, conditions. In fact, the "fog room" samples have developed a higher resistance respect to the correspondent "environmental condition" ones. However, in both "environmental condition" and "fog room" slabs, the maximum load applied in this first phase of the test is around 30% more than the one correspondent to the cracking moment. The comparison between the two cracking moment can be done looking at the following Graph 6.15 and Graph 6.16.

DRY: Load - Deflection
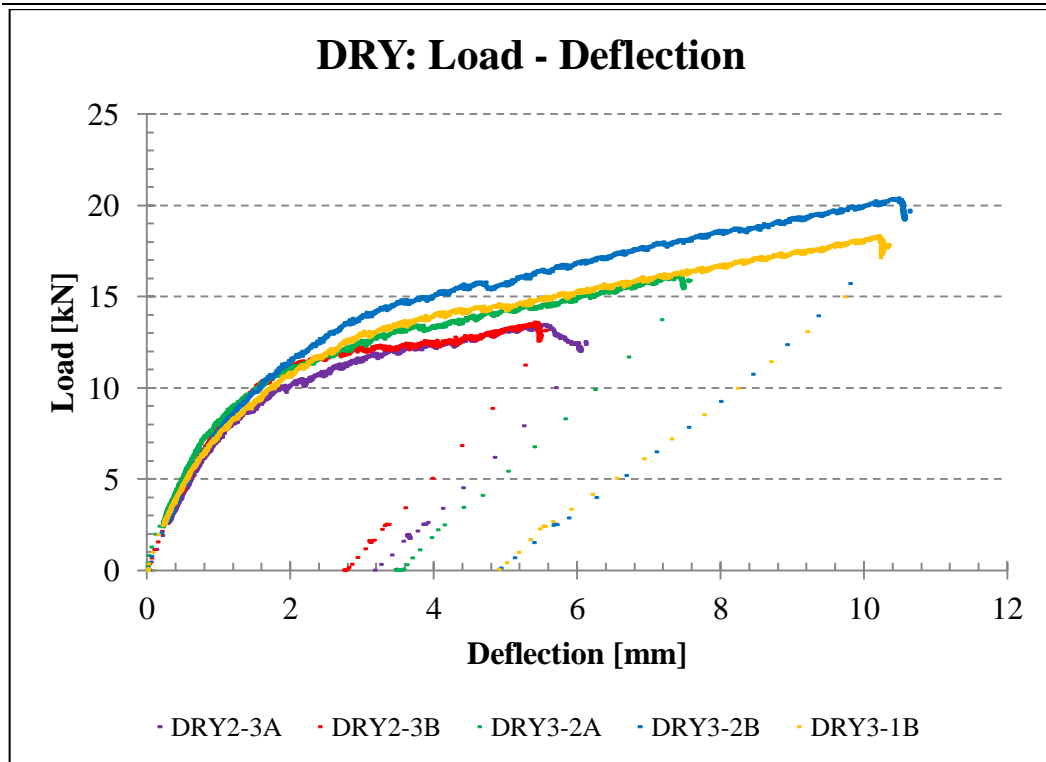
Graph 6.15 – Load – Deflection curve of the dry samples

FOG: Load - Deflection
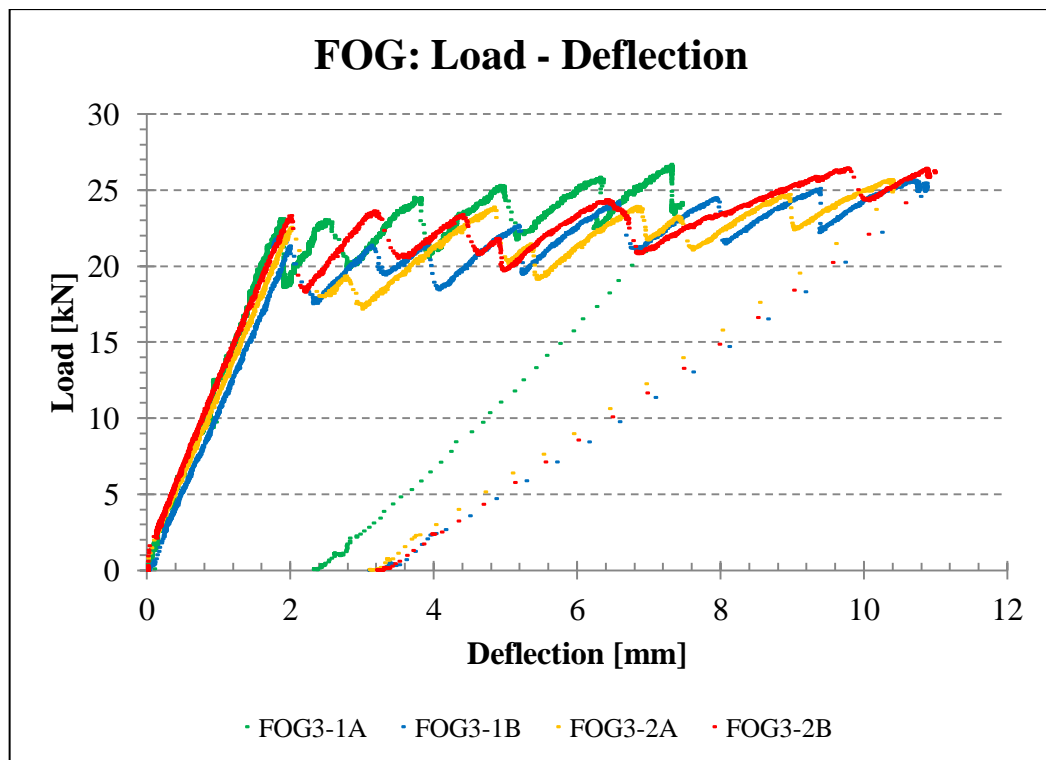
Graph 6.16 – Load – Deflection curve of the fog samples

Another important consideration regards the crack formation should be done. As it can be noticed from Graph 6.16, every time that a crack appear in the "fog room" slabs, there is a huge drop in the load. On the other hand, for the "environmental condition" slabs, this is not valid. Graph 6.15 shows how the

85

load-deflection plot for the dry samples does not have this huge drop, but a bigger number of smaller drops, closer each one to the other in terms of absolute load. This can be explained by the fact that the cracks are smaller but more numerous. In fact for the dry samples, during the experiment, was more difficult to find the crack openings and only after a while after the appearance of them in the data logger monitor, it was possible to distinguish them by naked eye. In addition, in several cases of dry sample, the crack appears only on one side of the slabs and it propagates until the other side only with the increase of the load. For the fog samples, instead, this does not happen because the cracks were sharp and they cross the entire width of the cross section as soon as they appear.

The second kind of graph reported in Graph 6.17 and Graph 6.18 regards the plot between Load and PI displacement on the bottom surface in the mid span of the slabs. As previously, it is possible to notice a substantial difference between dry and fog samples. Dry slabs are more homogeneous and the displacement increases uniformly for increasing load. This confirms that, as previously said, the cracks appeared on the bottom surface are numerous, but relatively small. The fog samples, however, show a huge increase of the displacement also in the case of decreasing load. Since the decreasing load corresponds to a crack formation, it is possible from this graph to estimate the dimension of that crack.
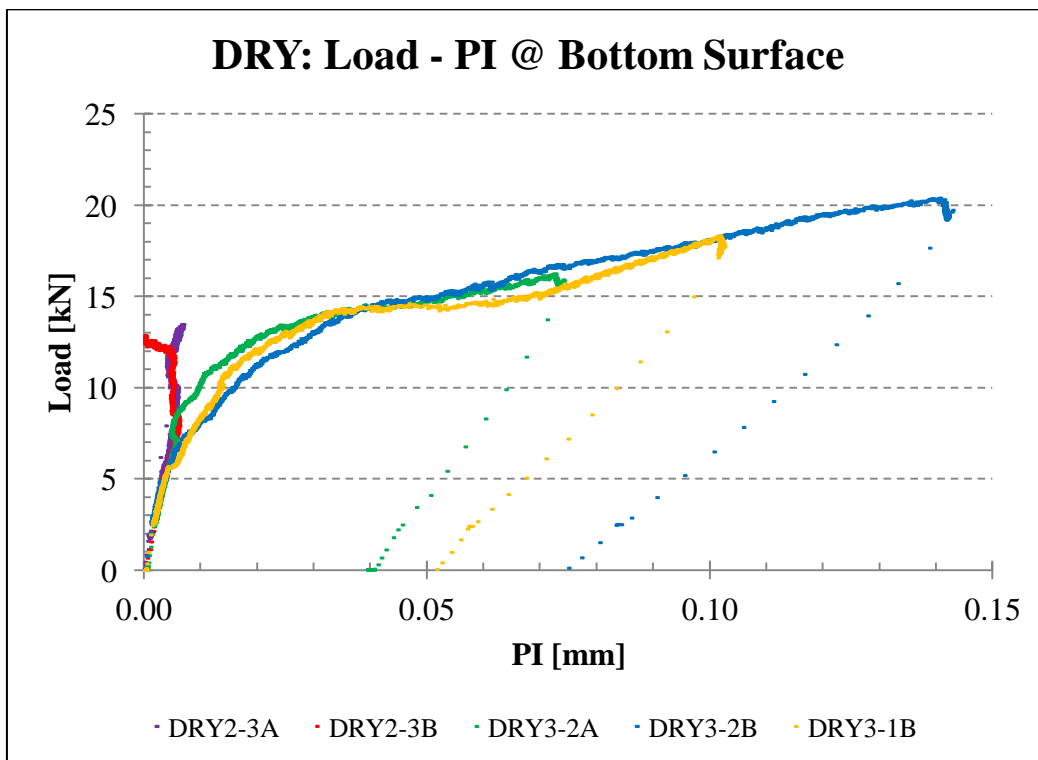
Graph 6.17 – Load – PI displacement curve at the bottom surface of the dry samples

FOG: Load - PI @ Bottom Surface
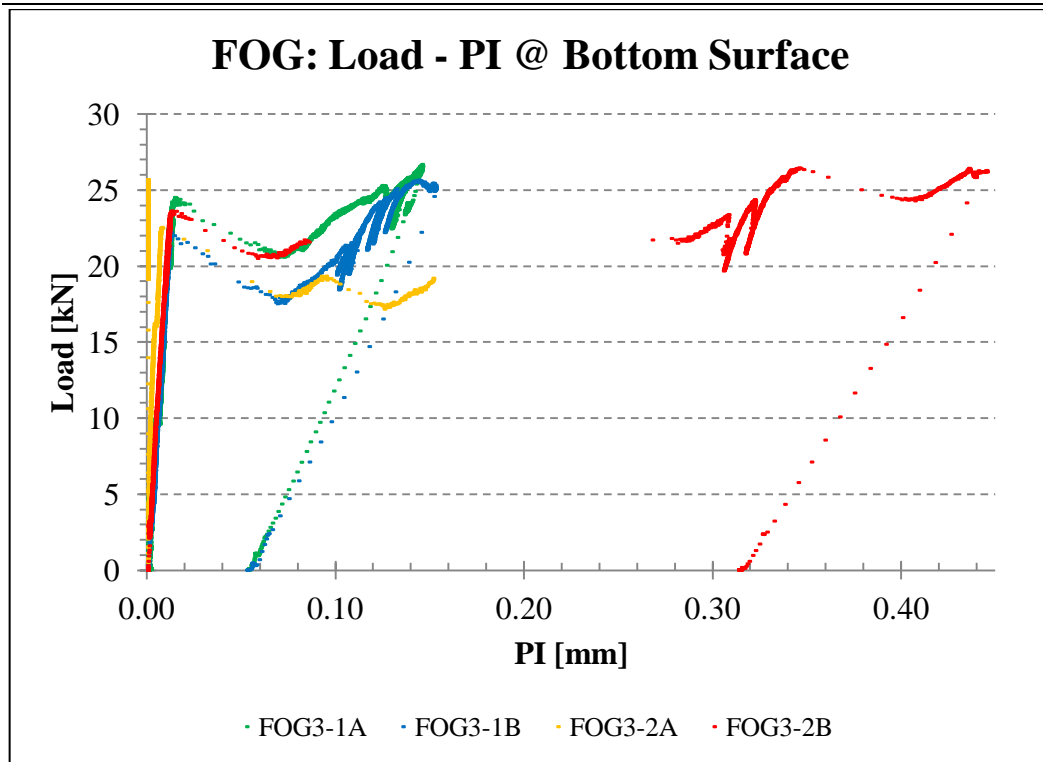
Graph 6.18 – Load – PI displacement curve at the bottom surface of the fog samples

A special consideration should be done for the FOG3-2B and the FOG3-2A samples shown in Graph 6.18. A non expert person might think that there is an error in the PI transducer record. This is not true. The reality is that, for the FOG3-2B sample, a crack appears between the two targets at which the PI is attached and thus the displacement is really big compared to the other because the entire crack opening does not redistribute on the entire length of the slab but, instead, it is carried out entirely by the PI. For the FOG3-2A sample, the record is so short because, at that point where it stops, a crack hits the target of the PI and thus, from that point on, the record is no more reliable.

Finally the graphs reported in Graph 6.19 and Graph 6.20 represent the plot between Load and PI displacement on the top surface in the mid span of the slabs. First of all, it should be noticed how the displacement is negative. This means that the top surface is subjected to a shortening and no more an elongation as for the bottom surface and thus that the stress is a compression. Speaking in terms of absolute values, the displacements regarding the top surface are about one third of the displacements taking place on the bottom surface.
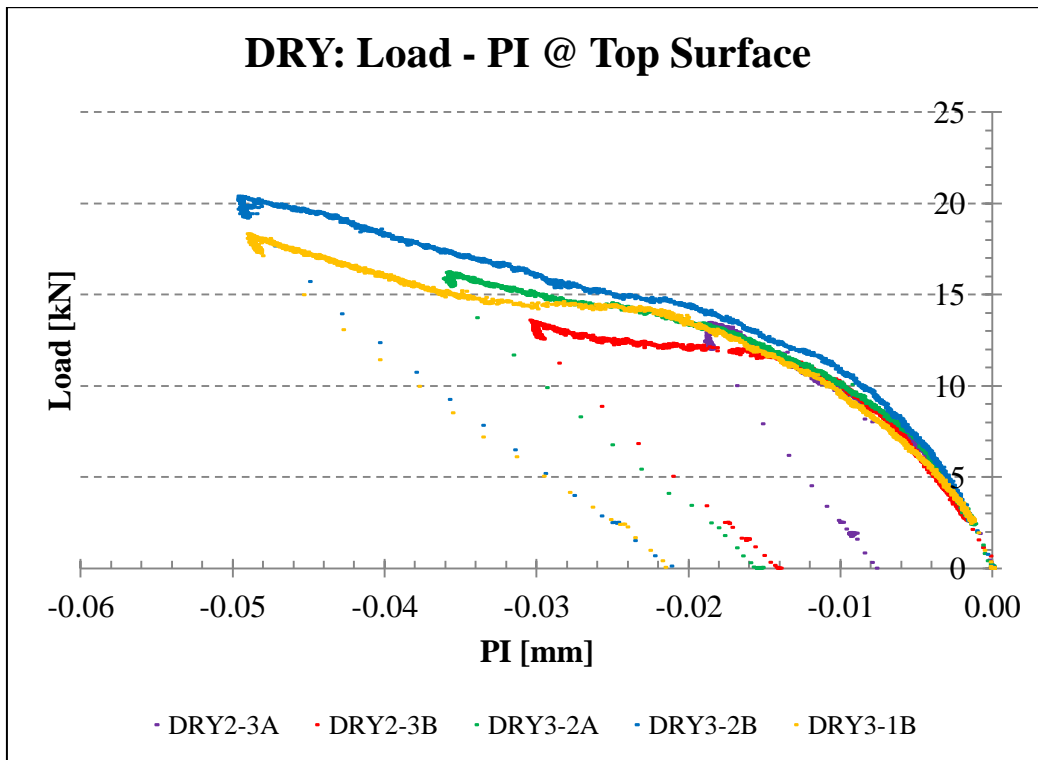
Graph 6.19 – Load – PI displacement curve at the bottom surface of the dry samples
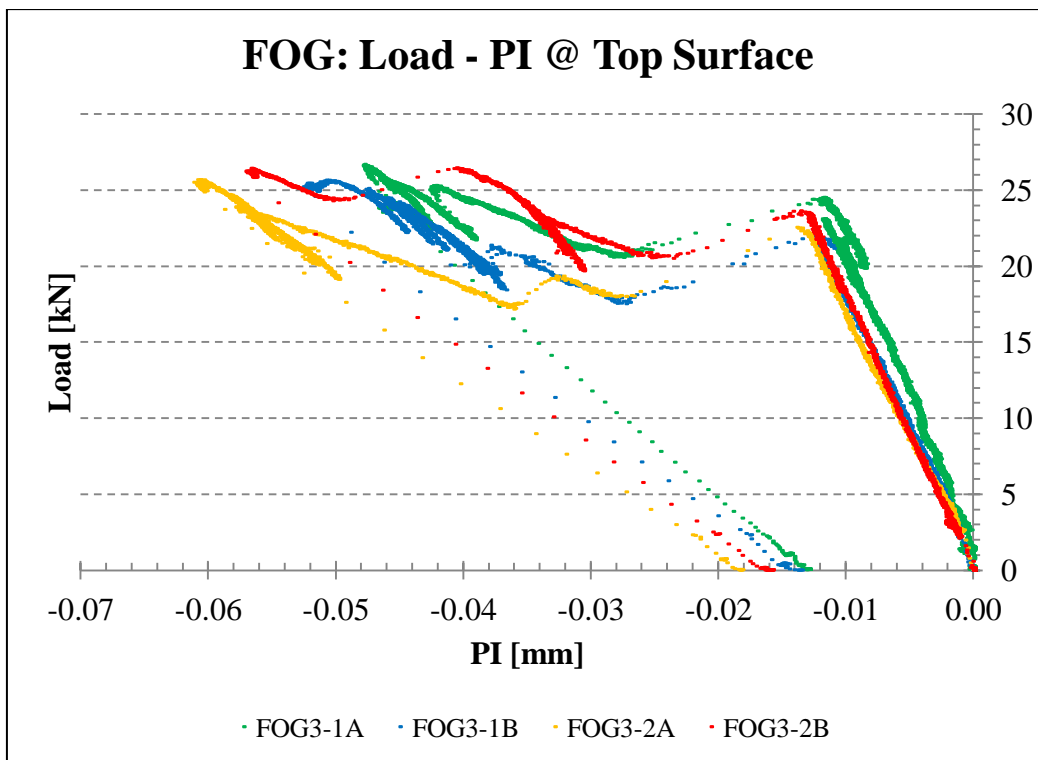
Graph 6.20 - Load – PI displacement curve at the top surface of the fog samples

6.5   Long-term results

In this paragraph, all the graphs reported are plotted against the time. A first series of three graphs shows the deflections according to the load applied on the

slab. Then a second series shows the strain distribution in the steel bar and a third series is plotted with the displacements at the top and bottom surface of the slab through the record obtained by the PI transducers. But let's consider these series of results more deeply.

6.5.1 Mid span deflection

This first series of graphs shows the trend of the deflection against the time. There are three different graphs according to the load applied on the slab, from the heaviest to the lightest. Since the entire test took three days to be completed, some samples has one or a couple of days of measurement less the initial one, but considering that the entire test will last for several months, a couple of days is irrelevant for the purpose of the test. The three graphs under discussion are reported in Graph 6.21, Graph 6.22 and Graph 6.23.
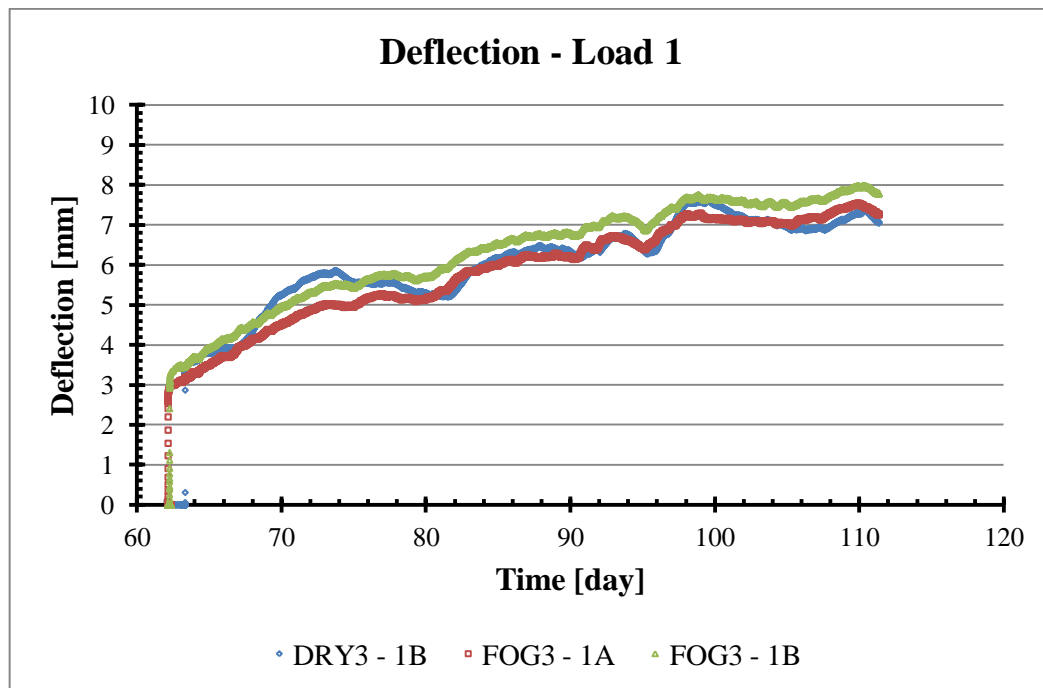
Graph 6.21 - Deflection curves for the samples subjected to Load 1. For an enlarged graph refer to APPENDIX D
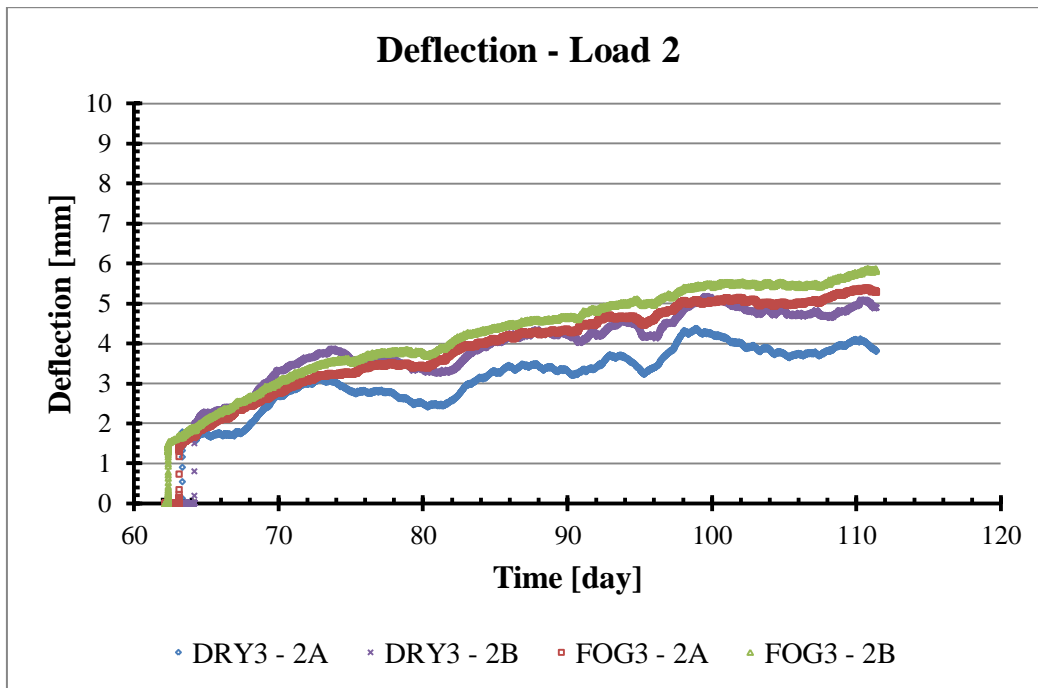
Graph 6.22 - Deflection curves for the samples subjected to Load 2. For an enlarged graph refer to APPENDIX D
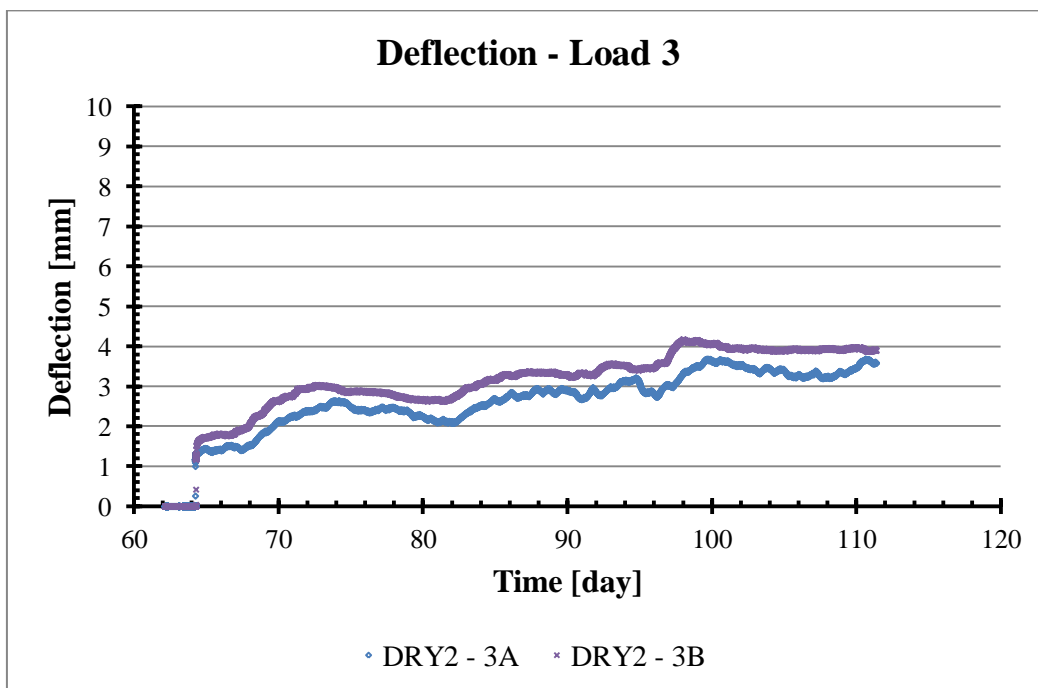
Graph 6.23 - Deflection curves for the samples subjected to Load 3. For an enlarged graph refer to APPENDIX D

First of all, comparing the three curves, it can be noticed how the slope of the curve is higher for the highest load, while it is less steep for the lower load. This is reasonable, because it means that the deflection is directly dependent from the load applied. The higher is the load, the higher is the deflection.

Secondly, the instantaneous deflection, the one recorded at the initial time (day 62), is higher for higher load. It goes from around 3.5 mm for the highest

90

load, to 1.5 mm for the smallest load, passing through the 2 mm deflection of the medium load.

In addition, it can be noticed how the deflection trend for the samples with the same geometric properties is similar. The curves have exactly the same shape and the same variation in time. The unique difference is related to the initial instantaneous deflection, which, on the other hand, strictly depends on how the cracks appear and how much they propagate along the cross section. This condition cannot be controlled in any way, because the cracks appearance and their extension cannot be forecasted or limited. The only parameter that can be checked to guarantee the same crack development is the applied load during the cracking operations, and, as it can be seen from the graph presented in the section 6.4, it is approximately the same for the two categories of slabs ("dry" and "fog").

Furthermore, another important difference can be noticed from the proposed Graph 6.21, Graph 6.22 and Graph 6.23. In all the load cases, the "dry" samples are sufficiently different from the "fog" ones. In fact the first ones have a wavy behaviour, while the "fog" samples are more linear in time. Probably this effect is due to the fact that the dry samples are more susceptible to the environmental changes since the major shrinkage already took place before the test; on the other hand, the shrinkage effect is sufficiently effective on the fog samples and thus the slabs do not suffer too much for environmental changes. However, independently from the shape of the curve, the pure deflection value is quite similar for both "dry" and "fog" samples, at least for the time period up to 40 days after the beginning of the test.
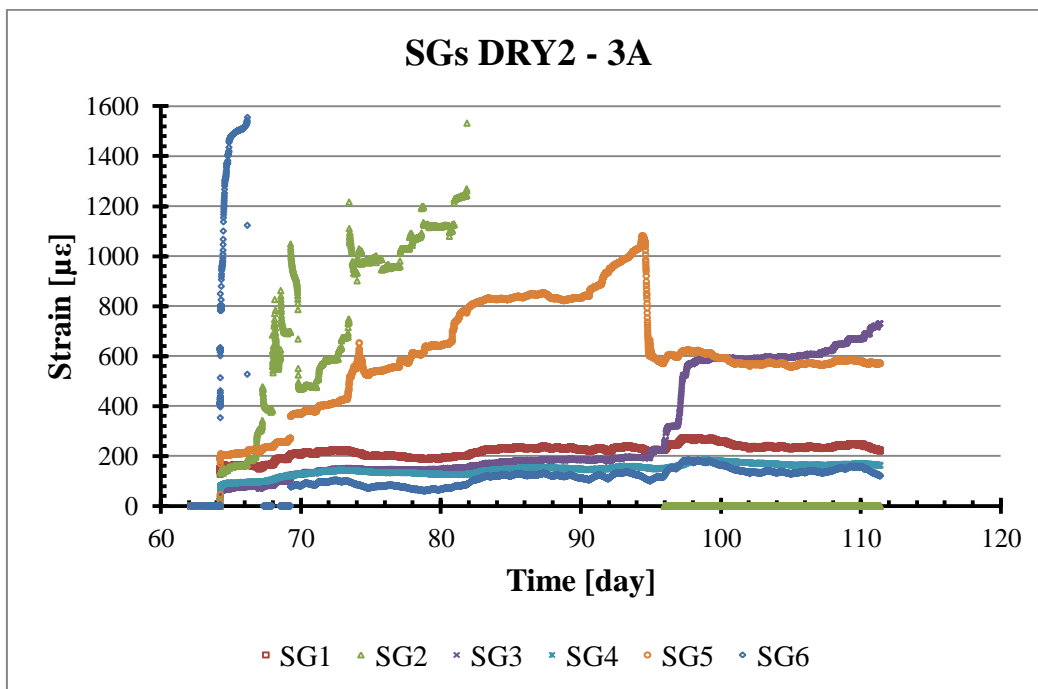
6.5.2 Strain in the steel bar

This paragraph wants to show the strain presents in the steel bar. The results are provided by the six strain gauges installed on one bar for each of the four samples. As it can be seen from the following Graph 6.24, Graph 6.25, Graph 6.26 and Graph 6.27 the results are not so reliable, because there are big jumps in the steel strain without any reasonable or understandable motivation; only in the sample FOG3 − 1A, apparently, the results seem to be consistent, because all the curves have the same trend and development in time. In any case, for the purpose of this thesis, it is important to show all the results, also the worst ones, because, in that way, the reader can understand which of these are reliable and which are
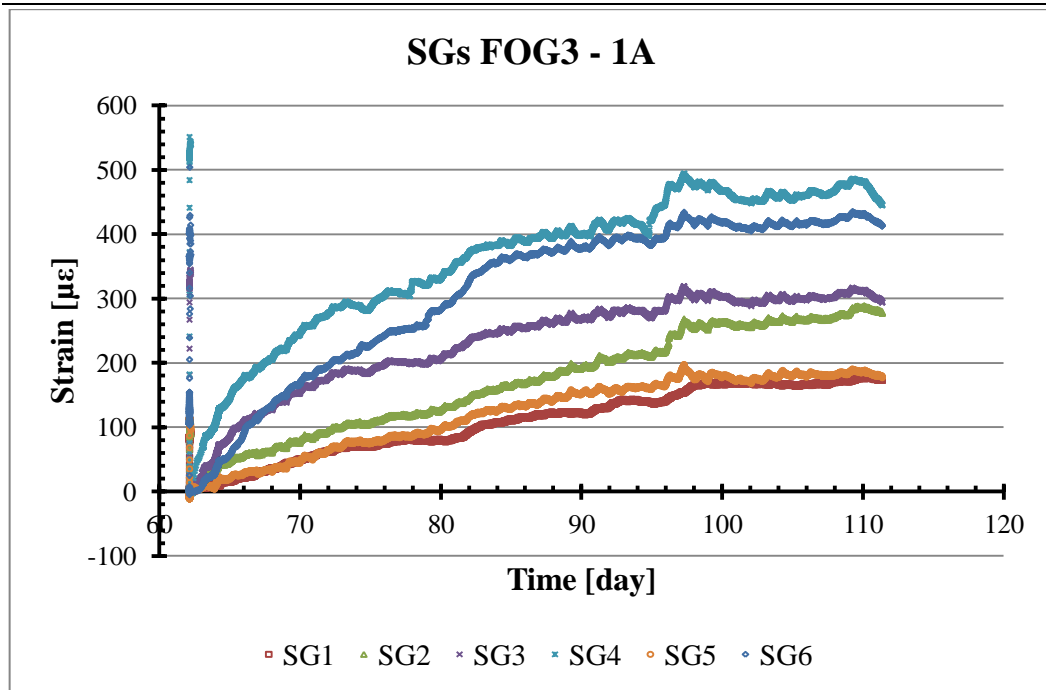
not. It can be also a good suggestion for future studies on the same topics in terms of instrumentations to be used.
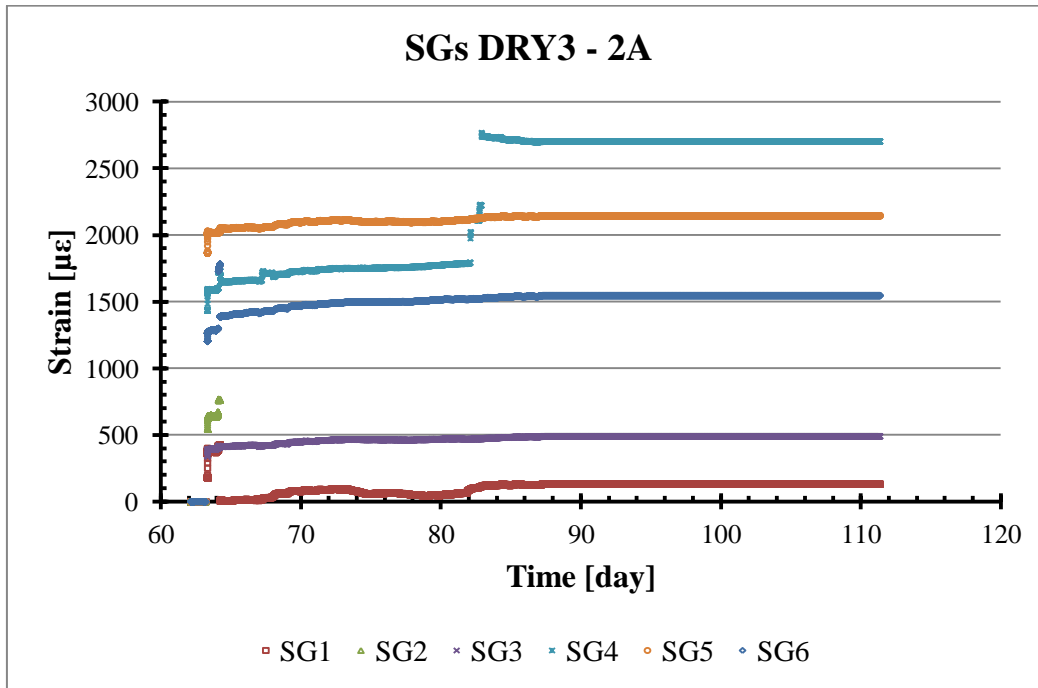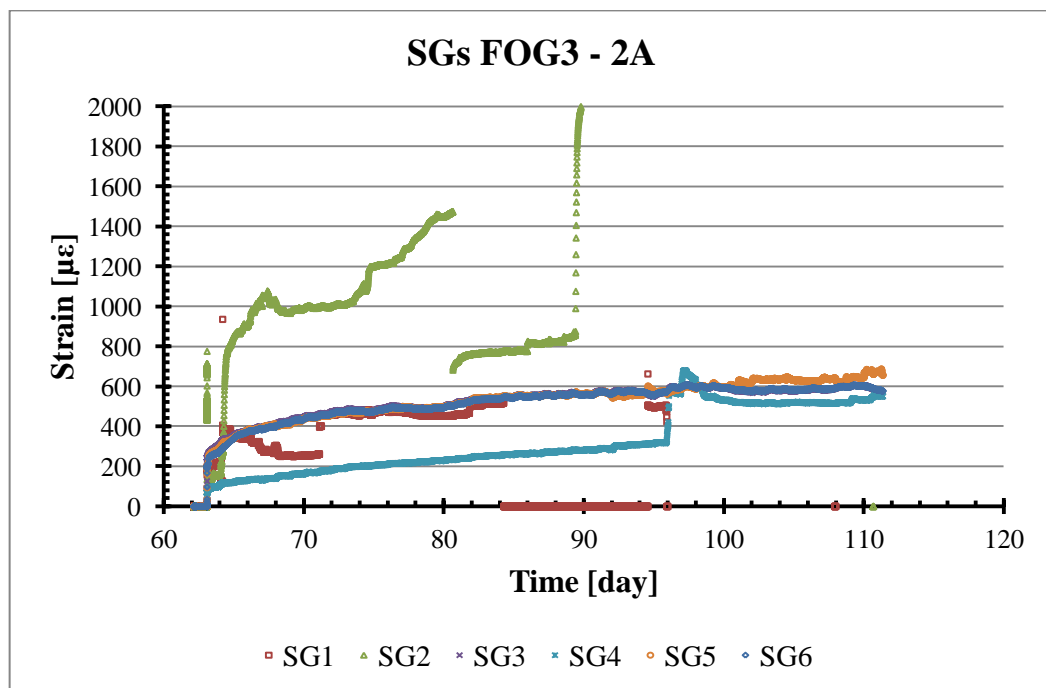

Graph 6.24 – Strain present in the steel bar of sample DRY3 – 2A. For an enlarged graph refer to APPENDIX D

Graph 6.25 – Strain present in the steel bar of sample DRY2 – 3A. For an enlarged graph refer to APPENDIX D

92

Graph 6.26 – Strain present in the steel bar of sample FOG3 – 1A. For an enlarged graph refer to APPENDIX D

Graph 6.27 – Strain present in the steel bar of sample FOG3 – 2A. For an enlarged graph refer to APPENDIX D

6.5.3 Top and bottom displacement

In this paragraph there are the measurements of the displacements of the top and bottom surfaces of the slab, at the mid span cross section. As for the previous cases, the following Graph 6.28, Graph 6.29 and Graph 6.30 are divided according to the load carried by slab, from the biggest to the smallest. In each

graph, there are two series of curve: one with negative displacements and the other with positive ones. They represents, respectively, the top surface (in the top part of the graph) and the bottom surface (in the bottom part of the graph). As the usual convention suggest, positive displacements mean elongation, while negative displacements mean contraction.
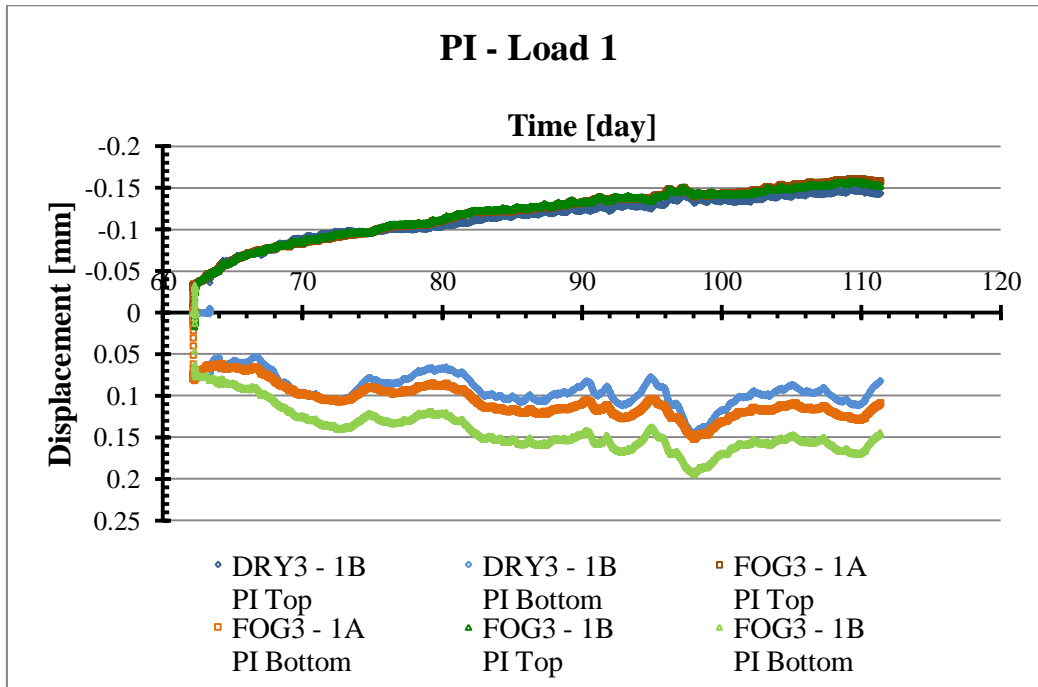
Graph 6.28 - Displacement curves for the samples subjected to Load 1at the top and bottom surfaces. For an enlarged graph refer to APPENDIX D
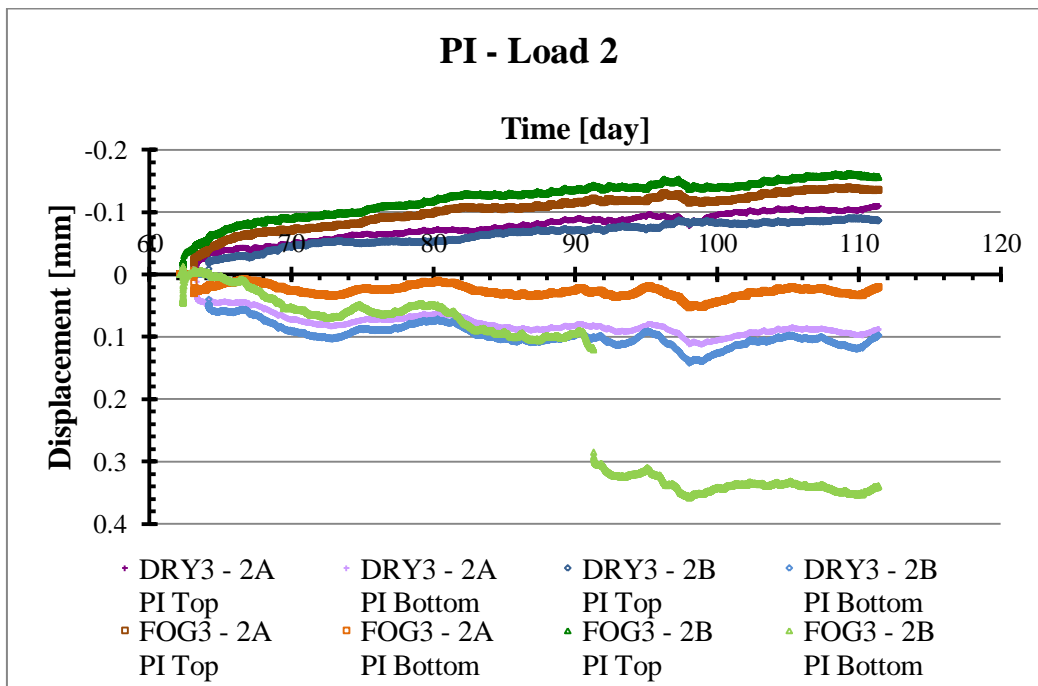
Graph 6.29 - Displacement curves for the samples subjected to Load 2at the top and bottom surfaces. For an enlarged graph refer to APPENDIX D

94
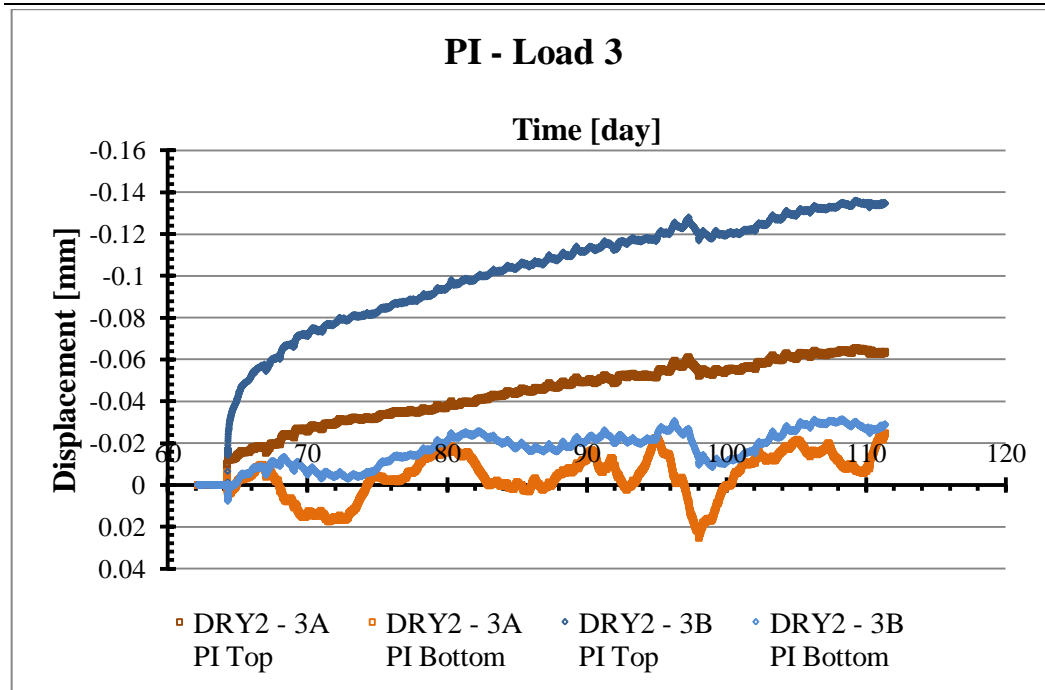
Graph 6.30 - Displacement curves for the samples subjected to Load 3at the top and bottom surfaces. For an enlarged graph refer to APPENDIX D

First of all, a general observation should be done on these three graphs. The results are very consistent and all the curves are similar to the other of the same category. This means that the instrument used to measure these displacements (PI transducer) and its installation on the concrete surface is very reliable.

Looking more deeply in all the graphs, it appears clear how a big contribution to the total displacement is due to the instantaneous displacement. In fact, as already highlighted in the section regarding the deflections, at the time instant in which the slab is loaded, there is a step of around ±0.05 mm, for the Load 1 and Load 2 cases, and a step of around ±0.01 mm for the Load 3 case.

Generally speaking, there is no difference between the "dry" and the "fog" samples. The curves of both samples have the same trend and the same peek in the same time instant. This can be related to the environmental conditions, which are common to all the slabs, more than to the specific creep and shrinkage effects, that, on the other hand, depend on each specific sample.

Another important observation can be done regarding the different trend between top and bottom surfaces. In fact, it can be seen how the top surfaces are subjected to a more linear progression, while the bottom surfaces are more wavy. This is related to the presence of the cracks on the bottom surface, which influence the development of the displacement. It is also nice to observe in Graph 6.29 how there is a huge jump in the specimen FOG3 − 2B (bottom

95

surface) around day 91. This jump is due to a new crack formation on the concrete surface, which increase the displacement from 0.12 to 0.29 mm. This is confirmed by the fact that a new real crack appear on the surface and it is possible to distinguish it by naked eye.

Regarding the slabs subjected to Load 3, the trend can seem quite different between the two specimens. This is due a different response of the slab during the first phase of the test, when the cracks are created. In fact, as it is possible to see from Graph 6.30, the instantaneous response is quite different for the two specimens, while, after that point, their behaviour is pretty much the same.

Chapter 7

Comparison between experimental and analytical deflections

"As far as the laws of mathematics refer to reality, they are not certain; and as far as they are certain, they do not refer to reality".
[Albert Einstein]

7.1   Introduction

This chapter presents the comparison between the first weeks of experimental deflection results and the analogous calculated through the use of the analytical models exposed in Chapter 3. It wants to give to the reader an indication on how reliable are these two models in the calculation of the deflection for cracked cross section.

The numerical models used for this comparison are the Age-adjusted Effective Modulus Method (AEMM) and the Step-by-Step Method (SSM). These two models are implemented in a MATLAB script, following the formulation exposed in Chapter 3. First ,the scripts calculate the curvatures at the mid span and at the supports of the slabs, and then, through the analytical expression provided in paragraph 3.4, the deflection is obtained. The input data to provide to the MATLAB script are the geometric properties of the cross section, the material properties, the applied loads and the information regarding creep and shrinkage.

The deflection value is calculated for each day, starting from the first day in which the test took place up to the last available day recorded. The period under examination is around 45 days long; it is not such a long period, but it is sufficient to understand which is the real experimental trend and which is the analytical one.
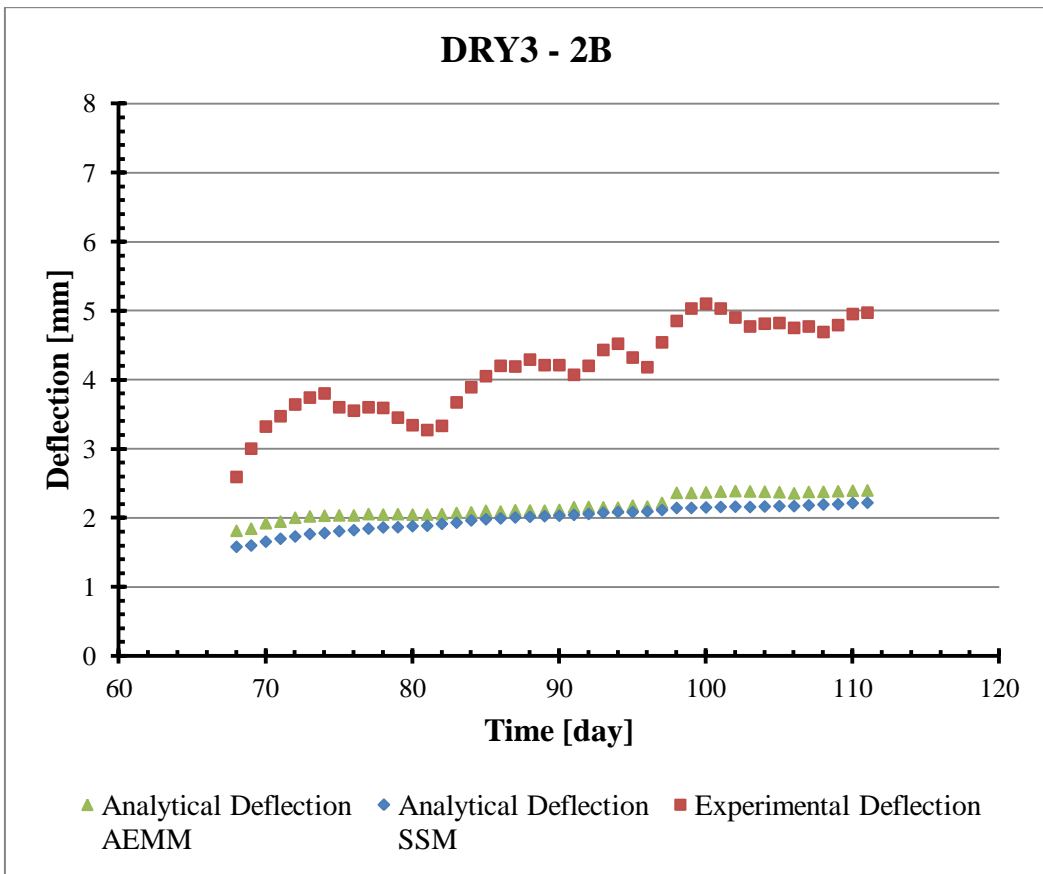
7.2   "Dry" samples comparison

The next five graphs, from Graph 7.1 to Graph 7.5, show the deflection comparison for the "dry" samples. A first general discussion can be done for all the samples; later on, each of them can be examined more in detail.
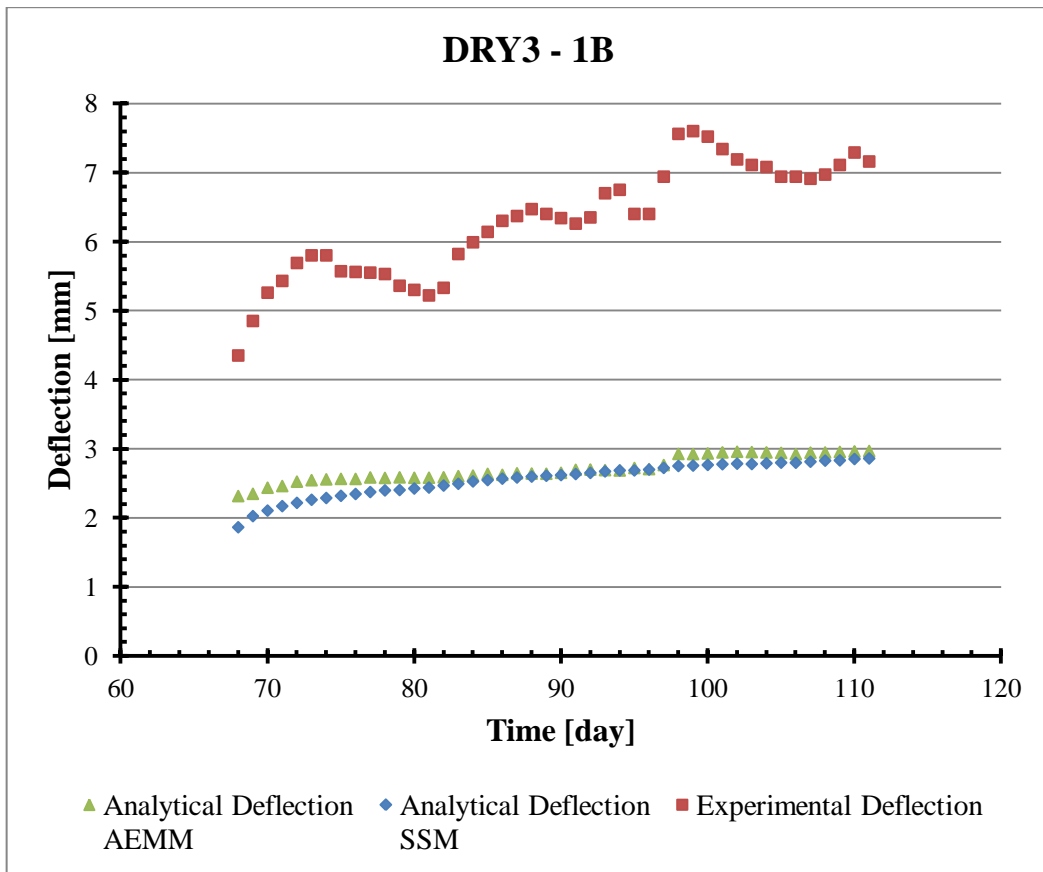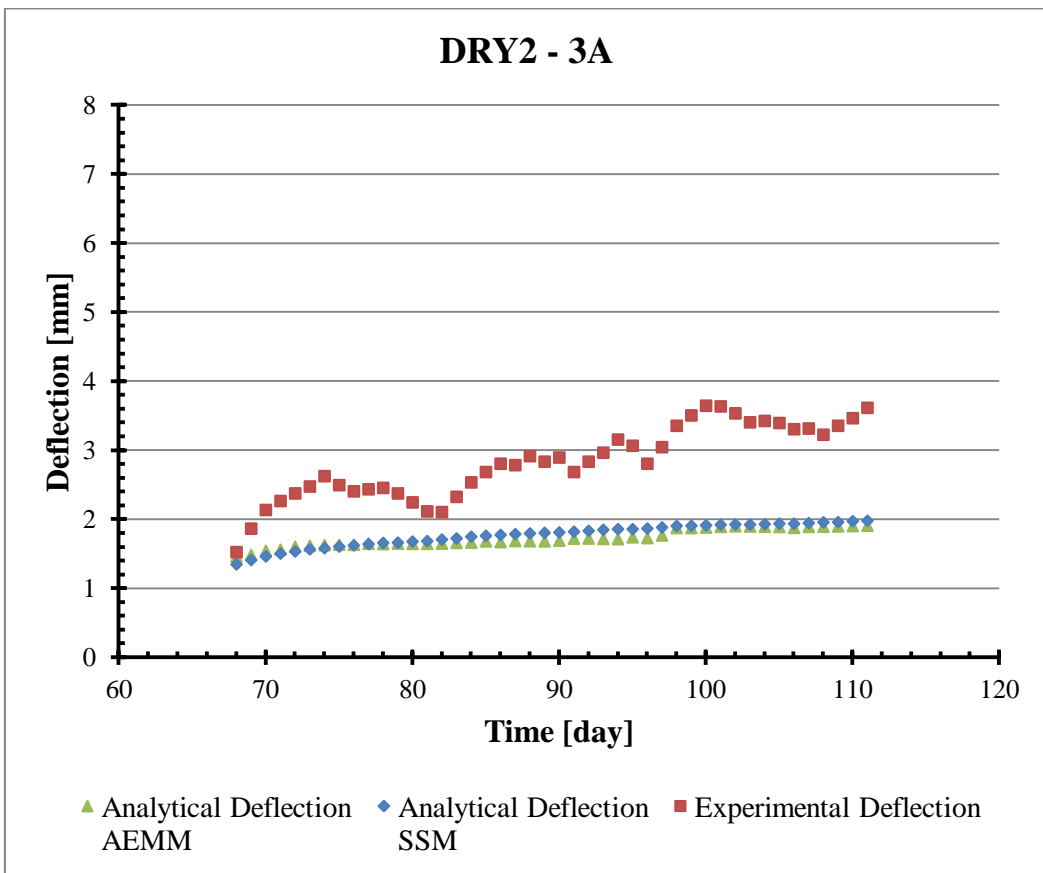
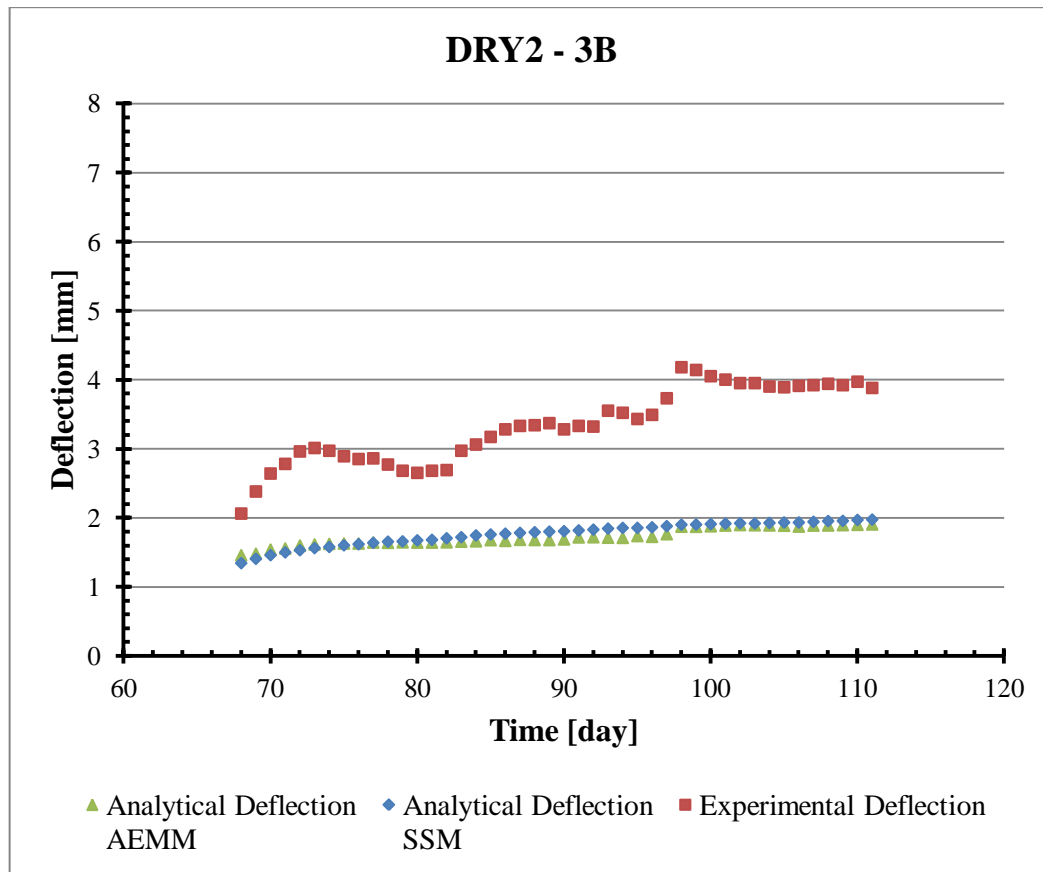**Graph 7.1 – Deflection comparison for specimen "DRY3 – 1B"**
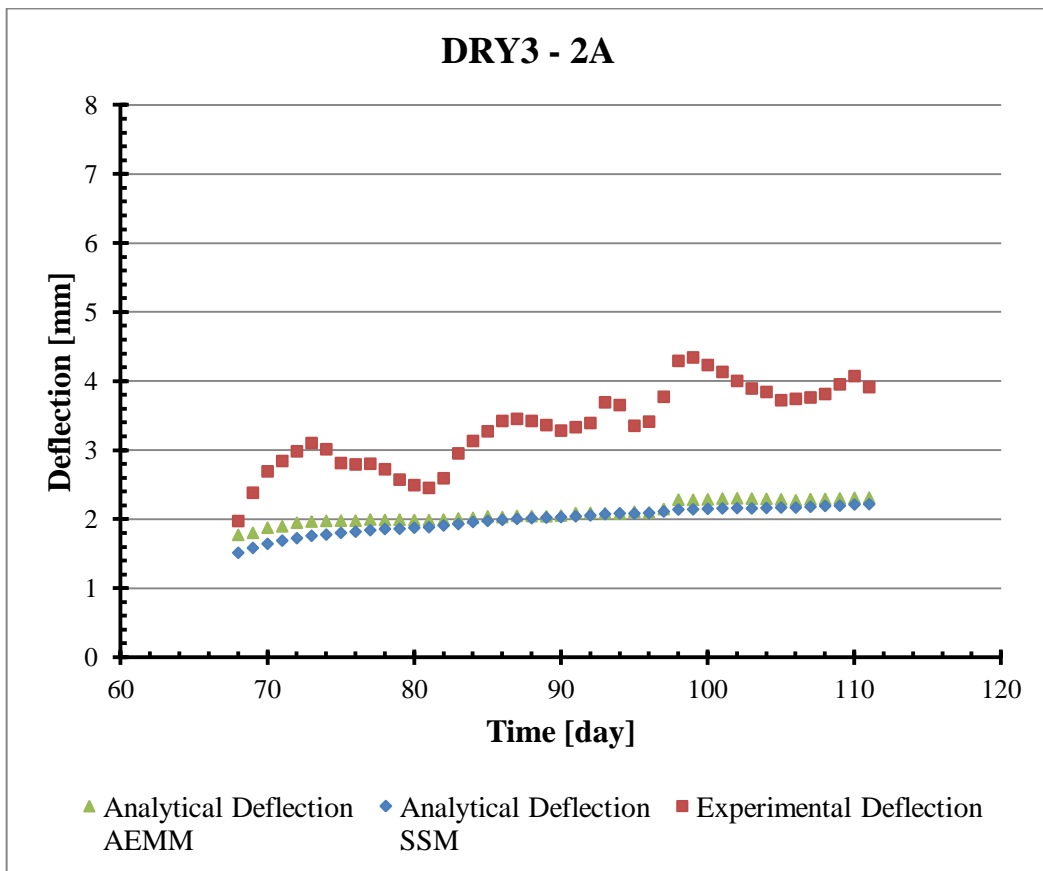
Graph 7.2 - Deflection comparison for specimen "DRY3 – 2A"

Graph 7.3 – Deflection comparison for specimen "DRY3 – 2B"

Graph 7.4 – Deflection comparison for specimen "DRY2 – 3A"

DRY2 - 3B

Graph 7.5 – Deflection comparison for specimen "DRY2 – 3B"

A first, immediate, observation should be done: in all the cases, the analytical models, both the AEMM and the SSM, underestimate the real deflection. The difference between the actual behaviour and the estimated one varies according to the specimen, but on average it varies from a 15% for the instantaneous deflection, to around 50% after around 45 days. This is a huge underestimation and it should be attributed more to the capacity of the models to predict the behaviour of cracked cross sections, than to some mistakes in the models. In fact, as it can be noticed from all these graphs, the estimation provided by the AEMM and the SSM are quite the same. Thus the hypothesis of a possible mistake in the analysis, in my opinion, should not be considered. A possible explanation to such big difference can be explained by the fact that the analysis consider a single cracked cross section, while, in reality, there are at least seven cracks for each slabs. This is a huge limitation of both the analytical models, but, since they are based on the cross sectional analysis, no other possibilities are available. One more reason for such a consideration is the dependence of the such big difference from the internal tension present in the steel bars. As described in the "Design procedure of the load used in the test" (paragraph 5.2.3.1), the slabs subjected to

101

"Load 2" and "Load 3" are less stressed than the one subjected to "Load 1". In fact, as it can be seen from Graph 7.1, the difference between the analytical and the experimental deflections is quite evident; the same cannot be said for the other graphs (Graph 7.2, Graph 7.3, Graph 7.4 and Graph 7.5), in which the slabs are subjected to a lower stress. This difference of internal tension can lead to a different grade of cracking of the cross section, and consequently also, to a different deflection value.

Regarding the different difference between the experimental and the analytical deflections, respectively at the "instantaneous" and at "45 days after" time instants, the problem is related to the slope of the curve. This slope is regulated by the shrinkage coefficients used in the analysis The more higher will be the shrinkage coefficients, the more steep will be the curve. But also in that case, the values used as shrinkage coefficient in the analysis come from the experimental measures recorded during the test and thus the chance of a possible mistake in their calculation should be avoided.

An additional confirmation of the difficulties related to the prediction of the actual deflection is represented by the wavy behaviour of the experimental measures. It clearly appears from the previous graphs how the temperature, and, more in general, all the environmental conditions, affects the real behaviour. This is present as well in the analytical simulations, but in a lower scale. In fact, the analytical curves can be easily associated to a linear expressions, while the experimental one cannot.

A more deep and complicated consideration can be done comparing these results to the ones obtained in the validation proposed in Chapter 4. In those graphs, it was shown how the use of constant shrinkage profile underestimate the real behaviour of the slabs, while the use of a linear shrinkage profile better estimate the experimental deflections. If the hypothesis of a differential shrinkage profile is done also for these cracked reinforced slabs under examination, then the problem can be represented once again. This hypothesis is not so stupid, because the presence of a series of cracks can trigger a differential shrinkage development along the cross section. But to proof this hypothesis more advanced studies must be done.

An additional consideration can be done regarding the effective influence that cracks have in the calculation of the deflections. Comparing Graph 7.4 with

102

Graph 7.5, it appears clear how the difference between experimental and analytical deflections depends from the cracking pattern. Since the two samples are exactly the same, and since the load applied is always the same along all the test (also in the first phase of the test when the cracking pattern is created), the models predict the same behaviour in both the cases, while the actual one is slightly different. This lead to a better or worst interpretation of the comparison results, even if they should be exactly the same. For this reason, it is strongly recommended to have an higher number of samples in order to reduce this problem.

7.3   "Fog" samples comparison

This second series represents the comparison between the experimental and the analytical deflections for the "fog" samples. Most of the general considerations explained in the previous paragraph are valid also for the following Graph 7.6, Graph 7.7, Graph 7.8 and Graph 7.9, but something more can be said and observed.
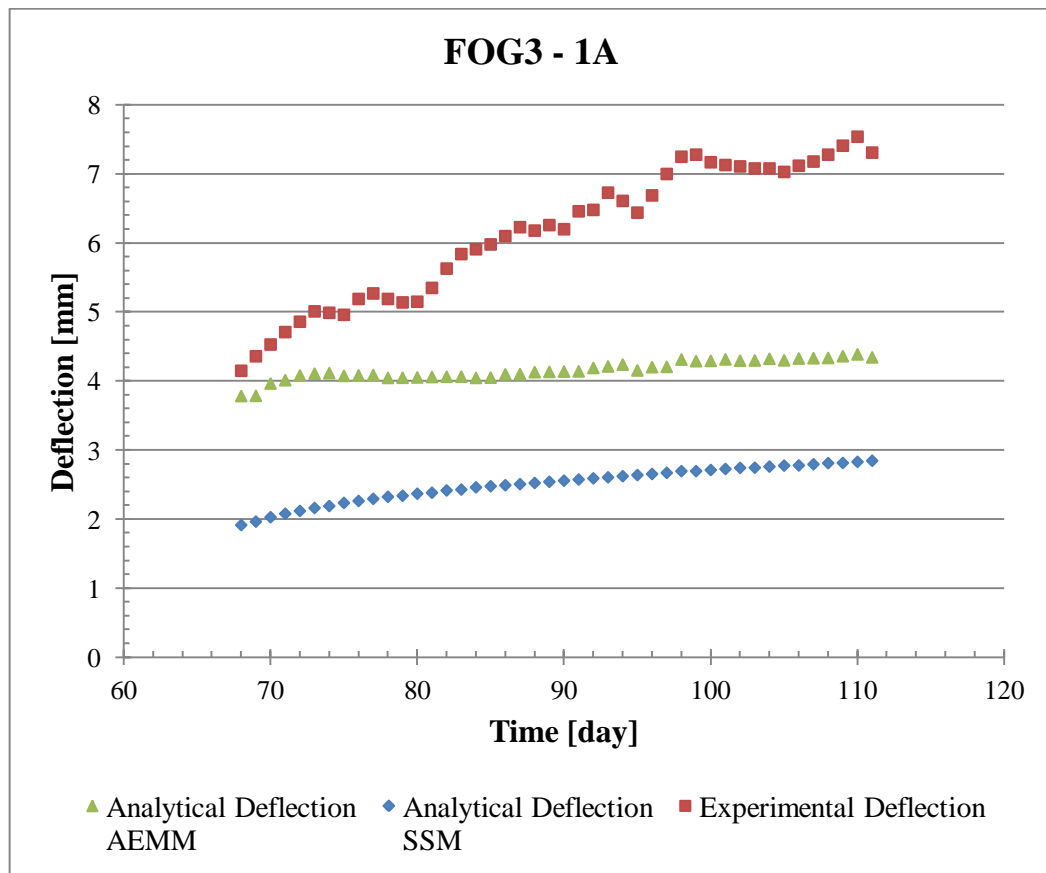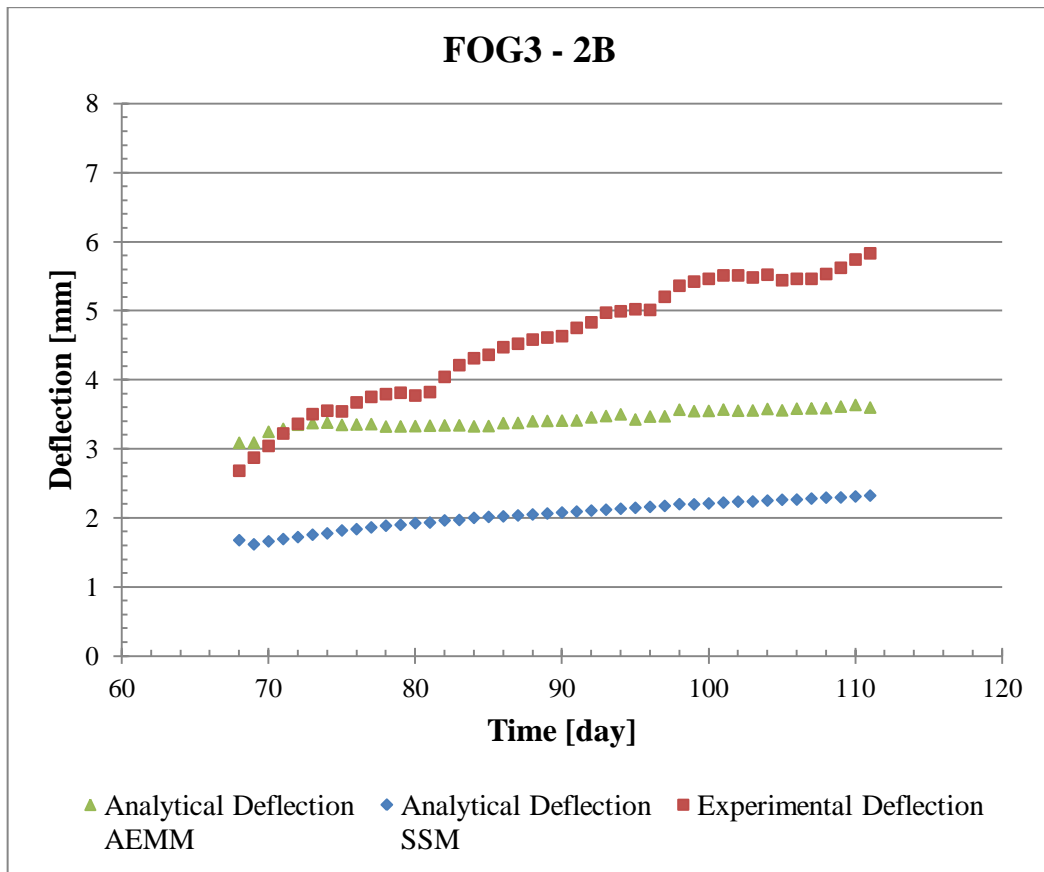

Graph 7.6 – Deflection comparison for specimen "FOG3 – 1A"

103
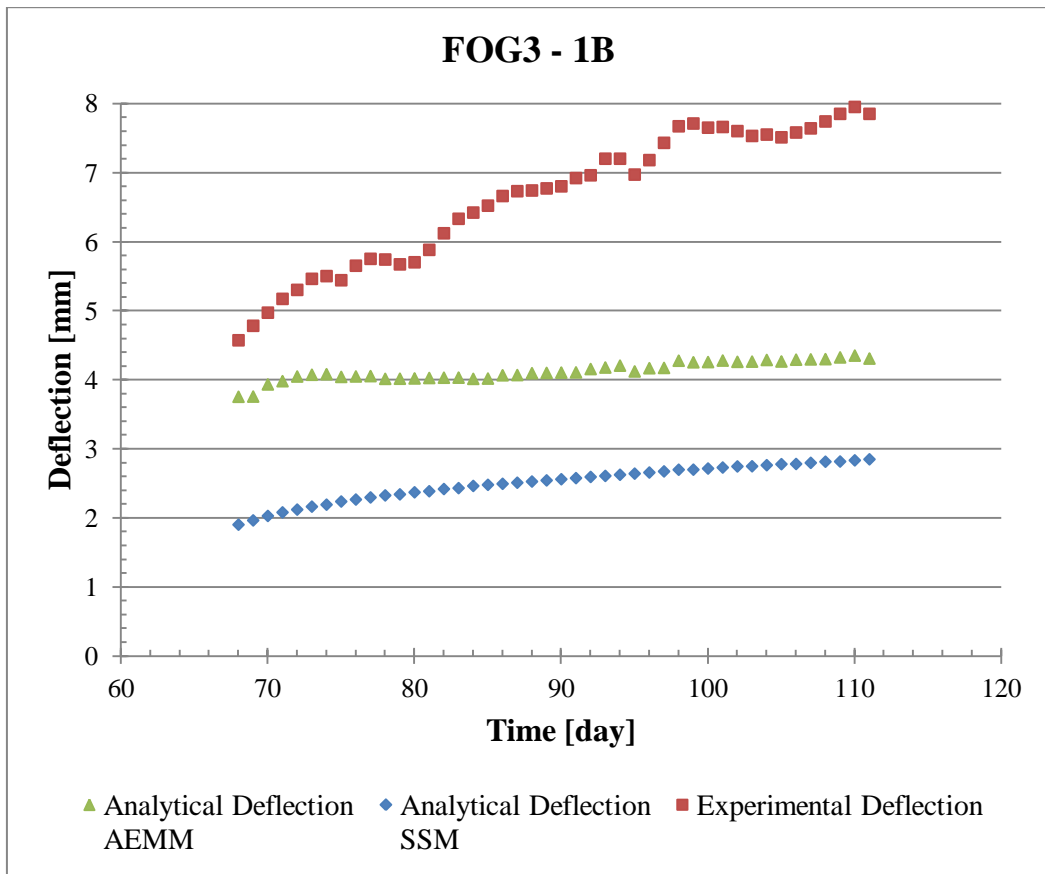
Graph 7.7 – Deflection comparison for specimen "FOG3 – 1B"
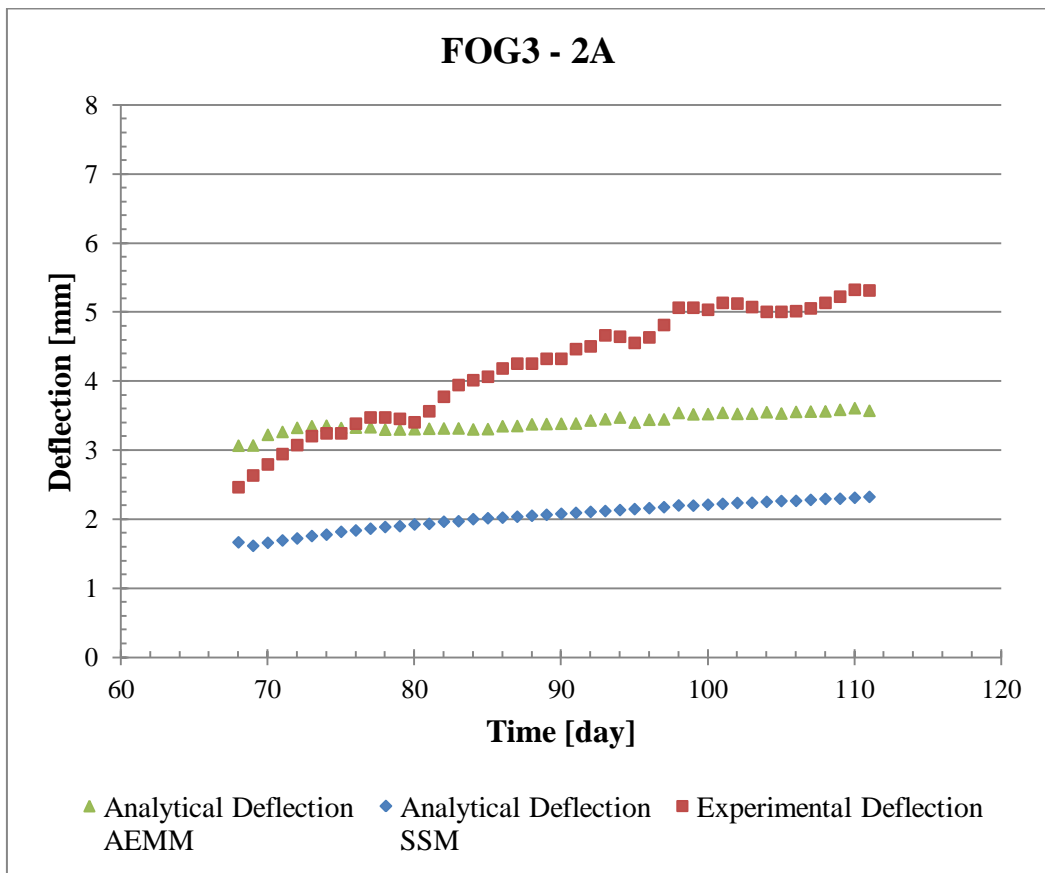
Graph 7.8 – Deflection comparison for specimen "FOG3 – 2A"

FOG3 - 2B

The main bigger difference respect to the previous case of the "dry" samples is that the two analytical models do not provide a similar response, as previously happened. The general trend in the time is always similar, but there is a huge difference in terms of deflection. The two models differ of more than 1mm over a total of 3mm. It is a 30% of difference that cannot be acceptable. In any case, the AEMM seems to better predict the experimental trend, even if the slope of the curve presents the usual problem: the more long the curve goes in time, the more far the analytical prediction is from the experimental curve.

Chapter 8

Conclusions

*"A good scientist is a person
with original ideas. A good
engineer is a person who makes a
design that works with as few
original ideas as possible."*
  [Freeman Dyson]

The aim of this thesis was to investigate the long-term behaviour of reinforced concrete slabs and understand how cracks influence their general comportment, with particular attention to deflections and cracks.

Full-scale tests have been carried out to measure the cracking moment and the long-term response of 10 reinforced concrete slabs. Instantaneous reading has confirmed how the different maturation conditions influence the final strength of the concrete, the cracking moment and the cracking pattern, in addition to the more obvious deflections. The long-term readings, on the other hand, are still not sufficient to draw reliable conclusions, but they are enough to understand how wide and complicated is the topic under examination. The number of factors involved in the test is extremely high and understand how big each influence is represents, probably, the main difficulty.

The use of the room with 100% humidity has given the chance to study more in detail the shrinkage effects and their influence on the slabs. The results have clearly shown how shrinkage cannot be cancel, but simply delayed. Even if this condition cannot be reproduced in the real construction world, it is of fundamental importance for future research study related to shrinkage and long-term effects.

Two theoretical models have been developed to describe this long-term behaviour of the concrete and they have been applied to different concrete floor systems which included post-tensioned composite slabs and reinforced concrete slabs. Even if the validation against the post-tensioned composite slabs was successful, the proposed models do no predict well the experimental response of the long-term tests considered in this study. For sure the main problem is related to the existence of several cracks and how the models take in consideration their presence. Their influence on the shrinkage and creep development is of fundamental importance and the performed validation on the post-tensioned composite slabs was useful to understand how the assumed constant or linear shrinkage profile is fundamental in the evaluation of the deflection and how easy is to underestimate the long-term deflections. The long-term readings in the following months will be very valuable for the calibration of more detailed and complicated numerical models.

Understanding the mechanism through which shrinkage develops in reinforced concrete slab is of fundamental importance for the serviceability

design of such structure. Designers are to be aware that the deflection of a reinforced concrete slab is significantly dependent on shrinkage conditions.

Acknowledgments

I wish to express my deep appreciation and gratitude to my supervisor, Professor Gianluca Ranzi, for his patient supervision, valuable guidance and critical suggestions, continuous support and assistance throughout the course of this research.

I would also like to thanks my parents for their continuous support and incitement to afford this experience. Without their encouragement probably I will not be here to write this sentence. Grazie di cuore.

I wish also to thank Safat for his supervision and continuous help in the endless hours spent together in the laboratory preparing my test.

I would also like to thanks Marco and Andrea for the help and the fellowship expressed during these six months, making me feel more close to Italy than 16400 kilometres!!

Last but not least, I wish to thanks my girlfriend Irene for his patience and love. She is the only one to know how difficult is to be so far away for such a long period. Despite this, she never made me feel bad for my choice to come here in Sydney, but, on the contrary, she always supported it. She also patiently listened to and encouraged me in the worst moment of that long experience.

References

1. **Gilbert, Ian.** Shrinkage, Cracking and Deflection − the Serviceability of Concrete Structures. *Electronic journal of Structural Engineering.* 2001.

2. Australian Standard AS3600. *Concrete structures.* 2009.

3. Eurocode 2: Design of concrete structures - Part 1-1: General rules and rules for building. *UNI EN 1992-1-1.*

4. **American Concrete Institute.** Building Code Requirements for Structural Concrete and Commentary. *ACI 318-11.* 2011.

5. **Taylor, P. J. and Heiman, J. L.** Lon-Term Deflections of Reinforced Concrete Flat Slabs and Plates. *ACI.* November 1977, Vol. 74, pp. 556-561.

6. **Taylor, P. J.** Initial and Long-Term Deflections of a Reinforced Concrete Flat Plate Structure. *Civ. Eng. Trans.* April 1970, Vol. CE12, 1, pp. 14-20.

7. *Deflection as a Design Criterion in Concrete Buildings.* **Blakey, F. A.** September 1963, Vol. CE5, pp. 55-58.

8. **Vanderbilt, M. D.** *Deflections of Reinforced Concrete Floor Slabs.* Department of Civil Engineering, University of Illinois at Urbana-Champaign.

9. *Deflections of Multiple-Panel Reinforced Concrete Floor Slabs.* **Vanderbilt, M. D., Sozen, M. A. and Siess, C. P.** s.l. : ASCE, August 1965, J. Struct. Eng., Vol. 91, pp. 77-101. ST4.

10. *Practical Estimation of Two-Way Slab Deflection.* **Chang, K. -Y. and Hwang, S. -J.** s.l. : ASCE, February 1996, J. Struct. Eng., Vol. 122, pp. 150-159.

11. *Deflections Control of Two-Way Slab Deflection.* **Hwang, S. -J. and Chang, K. -J.** s.l. : ASCE, February 1996, J. Struct. Eng., Vol. 122, pp. 160-168.

12. *Short Term Deflections of Concrete Flat Plates.* **Jofriet, J. C.** s.l. : ASCE, January 1973, J. Struct. Eng., Vol. 99, pp. 167-182.

13. **Timoshenko, S. and Woinowsky-Krieger, S.** *Theory of Plates and Shells.* 2nd. New York : McGraw-Hill, 1959. p. 580.

14. **Brotchie, J. F. and Wynn, A. J.** Elastic Deflections and Moments in an

Internal Panel of a Flat Plate Structure: Design Information. [ed.] Commonwealth Scientific and Industrial Research Organization. Melbourne, Victoria, Australia : Division of Building Research Technical Paper (Second Series), 1975. p. 168.

15. **Gilbert, Ian Raymond and Ranzi, Gianluca.** *TIME DEPENDENT BEHAVIOUR OF CONCRETE STRUCTURES.* s.l. : Spon Press, 2011.

16. Creep (deformation). *Wikipedia.* [Online] 04 October 2011. http://en.wikipedia.org/wiki/Creep_(deformation).

17. *New Model for Practical Prediction of Creep and Shrinkage.* **Bazant, Zdenek P. and Panula, Liisa.** 1 October 1982, Vol. 76, pp. 7-24.

18. **Faber, O.** PLASTIC YIELD, SHRINKAGE, AND OTHER PROBLEMS OF CONCRETE, AND THEIR EFFECT ON DESIGN. *Minutes of the Proceedings.* 1928, Vol. 225, 1928, pp. 27-73.

19. **Ghali, A, Favre, R and Eldbrady, M.** *CONCRETE STRUCTURES Stresses and Deformation - Third Edition.* s.l. : Spon Press, 2002.

20. **Ambrogi, Leonard Diego.** Long-Term Behaviour of Composite Post-tensioned Slabs. Sydney : s.n., 2011.

21. **Trost, H.** Auswirkungen des Superpositionsprinzips auf Kriech- und Relaxations-. *Beton- und Stahlbetonbau.* 1967.

22. Strain Gauge. *Wikipedia.* [Online] 06 11 2011. http://en.wikipedia.org/wiki/Strain_gauge.

Appendices

"We shape our buildings,
thereafter they shape us."
[Winston Churchill]

APPENDIX A - Drawings of the slabs and of the instrumentation
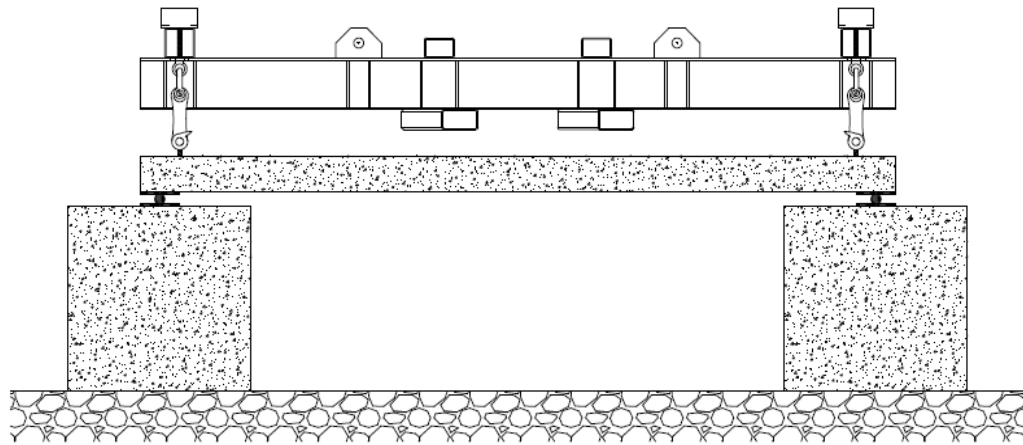
A.1 Handling of the slabs

Figure A.1 – Steel beam used to handling the slabs with the forklift or the crane
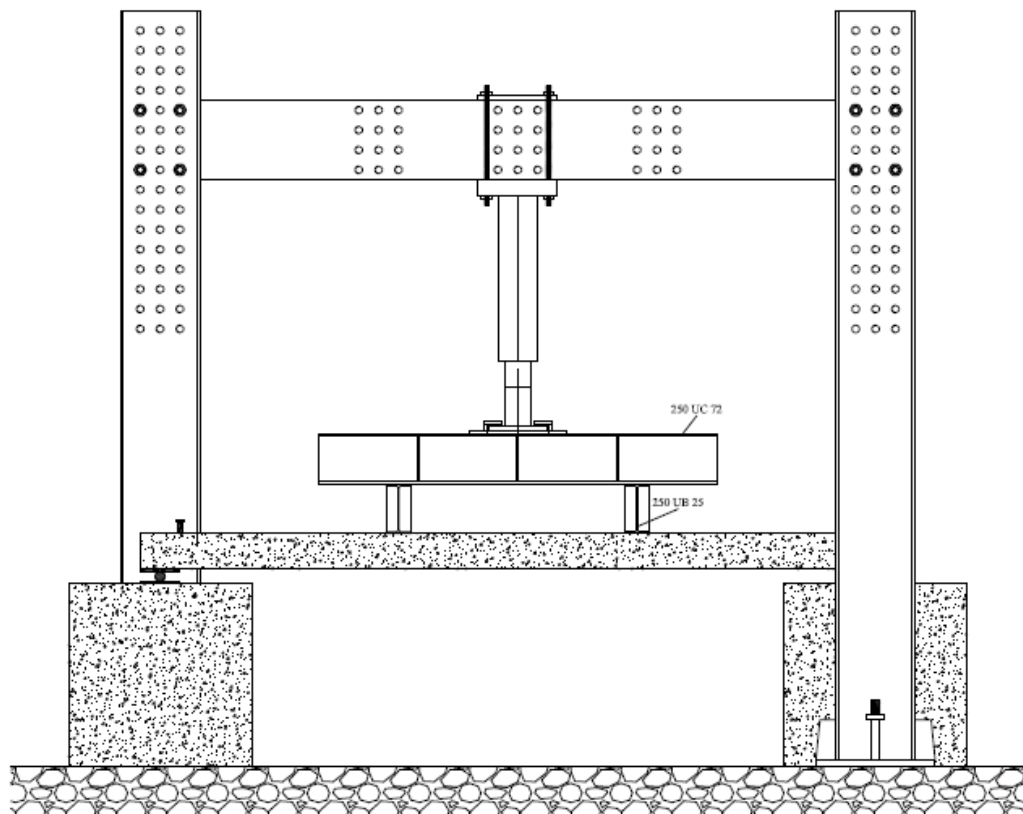
A.2 Experimental test scheme to crack the slabs

Figure A.2 – H-frame scheme used to crack the slabs during the experimental test

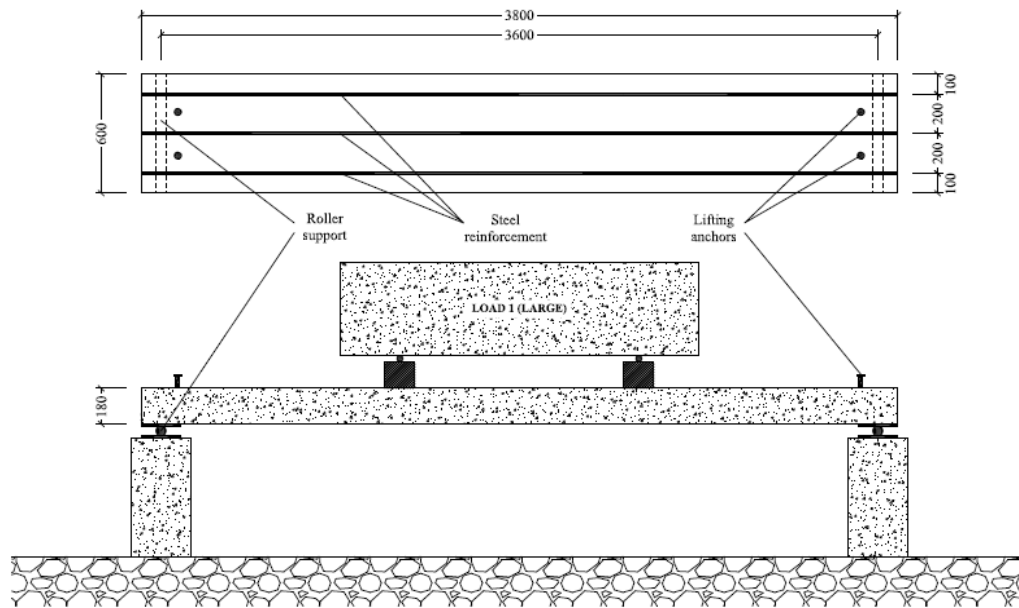## A.3 Slabs with the sustained loads applied after the cracking test

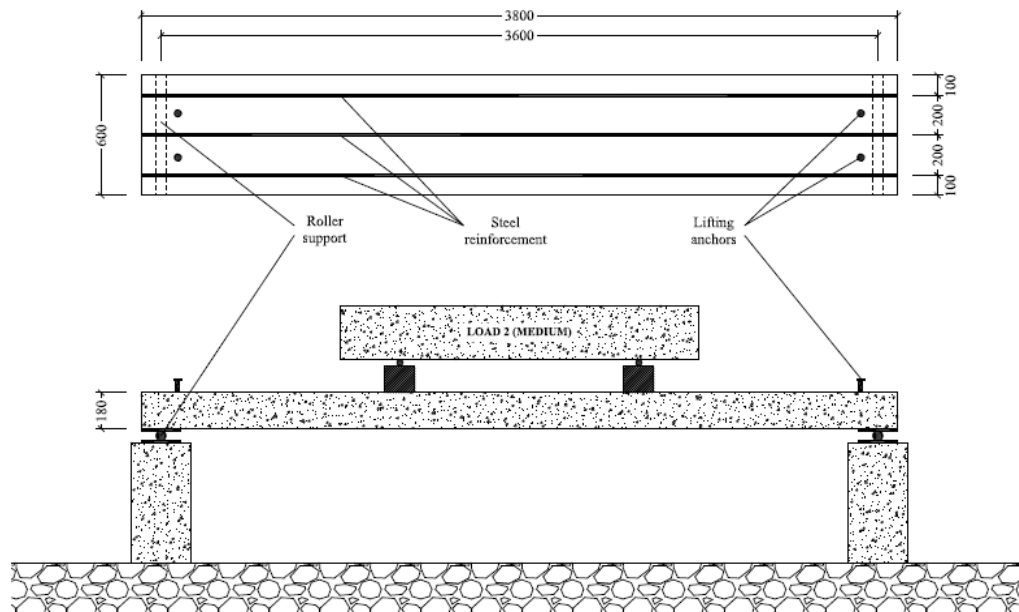**Figure A.3 – Plane view and prospect of the slab subjected to the large sustained load**

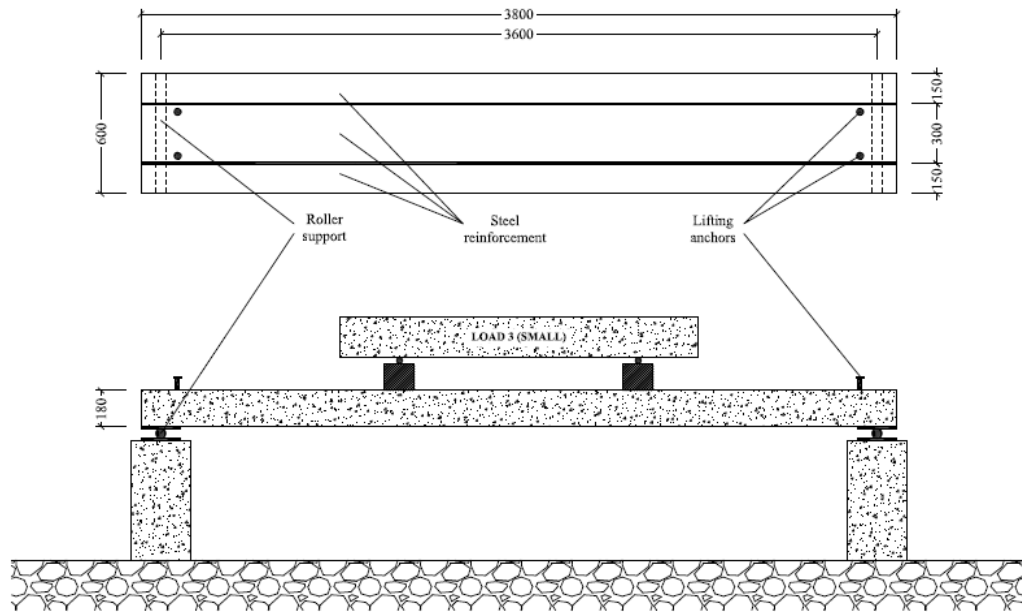**Figure A.4 – Plane view and prospect of the slab subjected to the medium sustained load**

Figure A.5 - Plane view and prospect of the slab subjected to the small sustained load
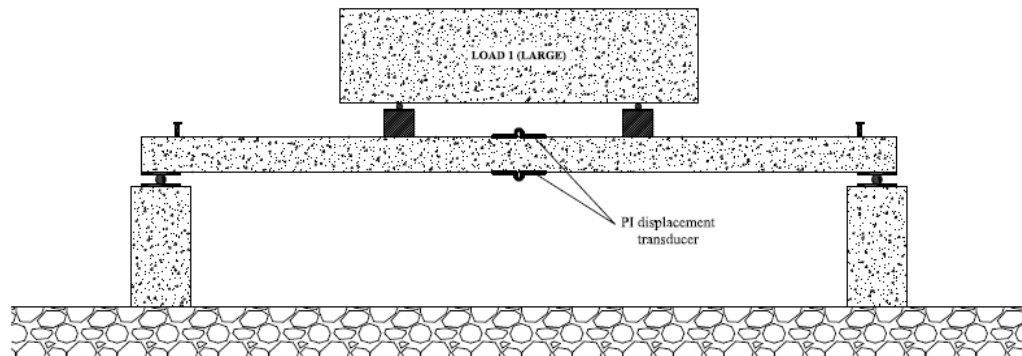
A.4 Instrumentation

Figure A.6 – Prospect of the slab with the PI displacement transducers applied at the mid span on the top and bottom surface
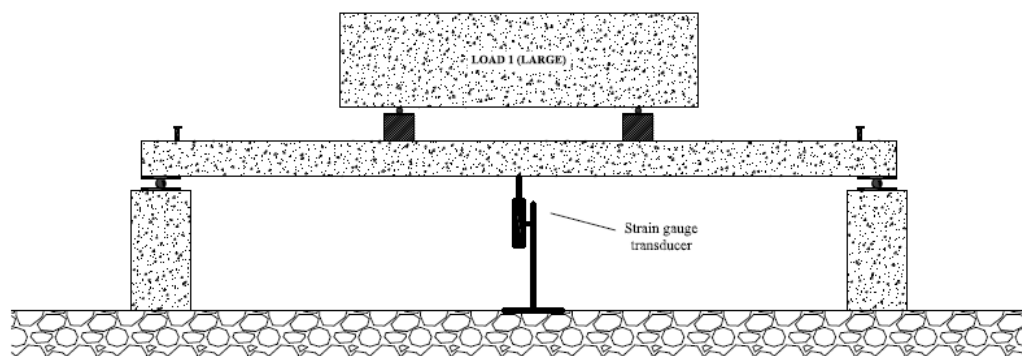

Figure A.7 – Prospect of the slab with the strain gauge transducers applied at the mid span on the bottom surface

APPENDIX B - Strain gauges installation steps

This appendix intends to illustrate all the passages done in the installation of the strain gauge sensor on the steel bar, later used as reinforcement in the slabs. It is a quite detailed and well done installation because these sensors are fundamental for the following measurements.

First of all a plain surface should be created on the steel bar for the allocation of the strain gauge resistance; but after this operation, the surface is not straight plain, instead it presents some furrows due to the machine used, as it can be seen from Figure B.1. For this reason an additional more refined work is required to smooth the surface. First a Dremel drill is used (Figure B.2), and then some sandpaper (Figure B.3). This way, the surface becomes really smooth, as it can be seen from Figure B.4, and the installation of the strain gauge can proceed.

Figure B.1 – Rough steel bar notch for the strain gauge installation

Figure B.2 – First smoothing operation with a Dremel drill

Figure B.3 – Second smoothing operation with a sandpaper

Figure B.4 – Smoothed steel bar notch before the strain gauge installation

Before proceeding in the installation of the strain gauge, the surface should be clean from the dust and all the residues due to the previous process. For this purpose it is used some acetone (Figure B.5) and some rags soaked in acetone

(Figure B.6).

Figure B.6 – Cleaning of the notch with a rag soaked in acetone

Figure B.5 - Acetone

Now the steel bar is ready for the installation of the strain gauge. A strain gauge (Figure B.7) is a resistance which is attached to the investigated object. In this way, when the object deforms, the strain gauge resistance deforms as well and the data recorder transforms this variation in terms of strain and stresses.

The first step, once the strain gauge is outside the plastic protection, is to attached a sticky tape strip on the top surface of the strain gauge (where the resistance is located), as shown in Figure B.8. This operation is required to avoid the contamination of the resistance and, in a second moment when the sticky tape is removed, to check that the strain gauge is really attached to the steel surface. Now a special glue, called CN adhesive (Figure B.9), is put on the bottom surface of the strain gauge, as shown in Figure B.10. As quick as possible, the strain gauge should be reversed and positioned on the steel bar notch (Figure B.11) and then pressed with a protective foil (Figure B.12), in order to avoid sticking the adhesive to the fingers.
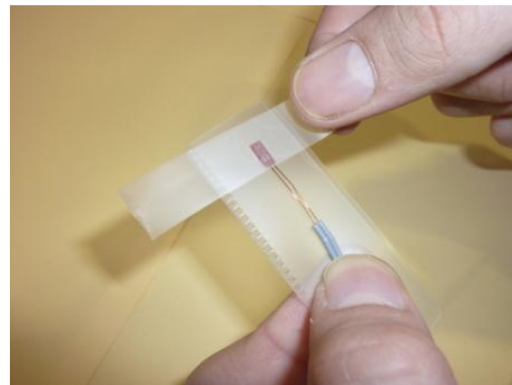
Figure B.7 – Strain gauge

Figure B.8 – Sticky tape on the top surface of the strain gauge

Figure B.9 – CN adhesive

Figure B.10 – CN glue on the bottom surface of the strain gauge

Figure B.11 – Positioning of the strain gauge in the steel bar notch

Figure B.12 – Pressure on the strain gauge to improve attachment with a protective foil

After about 30 seconds of pressure, the sticky tape should be removed as shown in Figure B.13. If some pieces of broken sticky tape remain on the resistance, they must be removed using some tweezers (Figure B.14). Now the

strain gauge is installed and it looks as in Figure B.15, but some protective layers are necessary to avoid damaging it in the future.

Figure B.13 – Removal of the sticky tape

Figure B.14 – Removal of broken sticky tape particles

Figure B.15 – Strain gauge attached

There must be applied several strata of protective material on the strain gauge in order to protect it. The first one is a layer of N-1 (Figure B.16). Before applying it, the copper wire which connects the resistance to the cable should be pulled up, as shown in Figure B.17, in order to avoid that some coating material touches the wires. Then with the help of a brush, it is taken some N-1 from the tube and applied on the strain gauge surface, as shown in Figure B.18. The final configuration, after the strain gauge dries, is reported in Figure B.19. Usually, the N-1 coating material takes at least half a day to dry and thus is advised to proceed in the operation the day after.

Figure B.16 – N-1 coating material

Figure B.17 – Pull up of the strain gauge wire

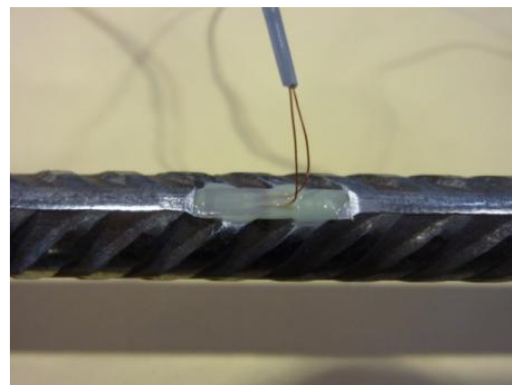Figure B.18 – Application of a N-1 layer on the strain gauge resistance

Figure B.19 – N-1 layer after drying

Once the N-1 is dry, a second protection layer is given. In this case it is used a rubbery material, called SB TAPE (Figure B.20). A thin strip of SB TAPE is cut from the main roll (Figure B.21) and then it is applied on the strain gauge (Figure B.22). At this point, always using a pair of tweezers, adjust and work it in order to cover the entire strain gauge (Figure B.23). After this, with careful, fold the copper wires on the SB TAPE layer just applied (Figure B.24) avoiding that they interweave between them, and apply a second layer of SB TAPE to cover also the wires (Figure B.25). Process the entire packet to be sure that there are no voids and make it smooth. The final packet that is obtained looks similar to the one shown in Figure B.26.

Figure B.20 – SB TAPE

Figure B.21 – Cutting of a thin strip of SB TAPE

Figure B.22 – Application of SB TAPE strip on the strain gauge

Figure B.23 – Processing of the SB TAPE layer

Figure B.24 – Folding of the strain gauge wire

Figure B.25 – Application of a new SB TAPE layer

Figure B.26 – Final configuration of strain gauge packet after SB TAPE application

Now, to make all more rigid and safer, use some super glue (Figure B.27) to attach the plastic coverage of the cable to the steel bar, as shown in Figure B.28. In this way, the possibility that an accidental pull destroys the entire packet is reduced, at least for small strokes.
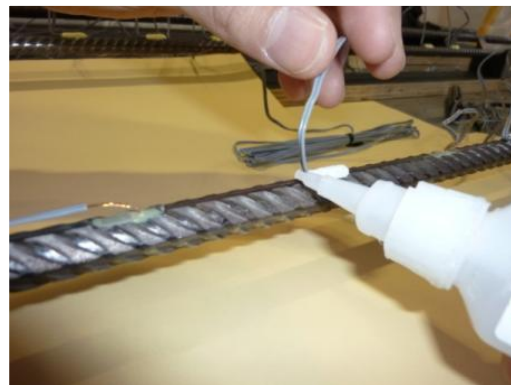

Figure B.28 – Application of the super glue to attach the wire to the steel bar

Figure B.27 – LOCTITE super glue

A last effort is now required to make everything impermeable and safer. To do this, a last layer of N-1 coating material is applied on the SB TAPE strata (Figure B.29). In the end, after the drying of the N-1 layer, the strain gauge is installed and adequately protected, as shown inFigure B.30.

Figure B.29 – New layer of N-1 on the SB TAPE

Figure B.30 – Strain gauge packet installed

APPENDIX C - Photos of the experiment

C.1 Before the pour

Figure C.1 – View of the all prepared samples in the concrete lab for the pour

Figure C.2 – "Dry samples" stored on some timber joist before the pouring operations

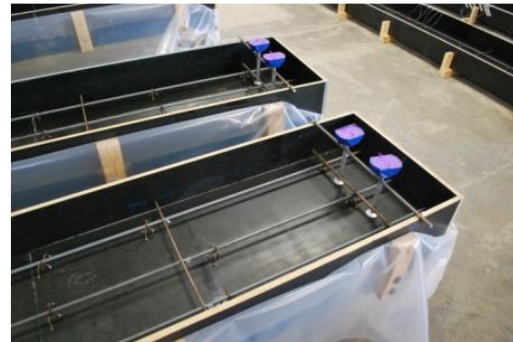**Figure C.3 – "Fog samples" stored on some trolleys before the pouring operations**

Figure C.4 – Detail of the lifting anchors

Figure C.5 – Detail of the strain gauges arrangement

C.2 Poured slab and curing

Figure C.6 – Poured slabs: "dry samples"

Figure C.7 – Poured slabs: "fog samples"

Figure C.8 – Placing of the "blankets" on the "dry samples" to slow down the water evaporation from the samples

Figure C.9 – Curing operation: wetting of the "blanket" to give the concrete mix the required water to develop an higher strength

Figure C.10 – "Dry samples" after the curing operations

Figure C.11 - "Fog samples". No curing operations required because the samples are already stored in a 100% humidity room

C.3 After curing, before cracking test

Figure C.12 – "Dry samples" shrinking before the cracking test

Figure C.13 –"Fog samples" not shrinking before the cracking test

C.4 Movement of the slabs

Figure C.14 – Positioning of the forklift in the right position

Figure C.15 – Lifting of the slab

Figure C.16 – Moving of the sample from the concrete lab to the structural lab

Figure C.17 - Moving of the sample from the concrete lab to the structural lab

Figure C.18 – Drop off the sample on two temporary supports to give the possibility to attach the two targets on the bottom surface of the concrete slab

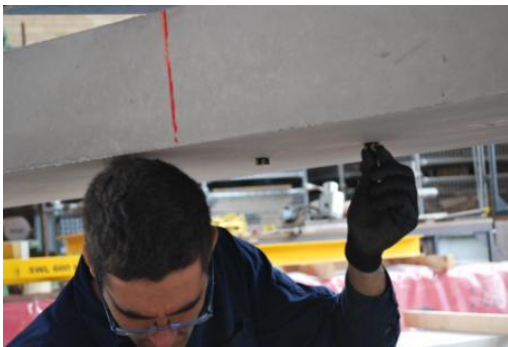**Figure C.19 – Operator attaching the two PI targets on the bottom surface of the concrete slabs**

Figure C.20 – Detail of the operator attaching the two PI targets on the bottom surface of the concrete slabs

Figure C.21 – "Dry samples" stored in the structural lab ready for the following cracking test

C.5 Data logger setup

Figure C.22 – Data logger front view

Figure C.23 –Data logger recorder card

Figure C.24 – Connection of the cable to the data logger

Figure C.25 – Data logger back view

C.6 Test: phase 1

Figure C.26 – Front view of the H-frame

Figure C.27 – Back view of the H-frame

Figure C.28 – Lateral view of the sample and the spreader beam

Figure C.29 – Spreader beam

Figure C.30 – Roller support

Figure C.31 – Cracking pattern at the end of the first phase

C.7 Test: phase 2

Figure C.32 – Sustained load applied on the slab

Figure C.33 – Global view of the laboratory with all the specimen

APPENDIX D – Collection of all the graphs

This appendix collects all the graphs shown in Chapter 6, but in a larger scale, in order to give the chance to see all the details which are hidden by the small dimensions of the previous chapter.

SHRINKAGE - FOG

CREEP + SHRINKAGE - FOG

CREEP - FOG

Deflection - Load 2

SGs DRY3 - 2A

SGs FOG3 - 1A

SGs FOG3 - 2A

PI - Load 1

PI - Load 2

PI - Load 3